METABOLIC AND REGULATORY NETWORK ANALYSIS OF DHA-PRODUCING RECOMBINANT *YARROWIA LIPOLYTICA*

Dissertation

zur Erlangung des Grades

der Doktorin der Naturwissenschaften

der Naturwissenschaftlich-Technischen Fakultät

der Universität des Saarlandes

von

Sofija Jovanović Gašović

Saarbrücken

2023

Tag des Kolloquiums:	07. September 2023
Dekan:	Prof. Dr. Ludger Santen
Berichterstatter:	Prof. Dr. Christoph Wittmann
	Prof. Dr. Andriy Luzhetskyy
Vorsitz:	Dr. Ruth Kiefer
Akademischer Mitarbeiter:	Prof. Dr. Uli Kazmaier

PUBLICATIONS

Partial results of this work have been published in advance authorized by the Institute of Systems Biotechnology (Universität des Saarlandes), represented by Prof. Dr. Christoph Wittmann.

Jovanovic, S., Dietrich, D., Becker, J., Kohlstedt, M., Wittmann, C. 2021. Microbial production of polyunsaturated fatty acids - high-value ingredients for aquafeed, superfoods, and pharmaceuticals. Curr. Opin. Biotechnol. 69, 199-211.

Gläser, L., Kuhl, M., **Jovanovic, S.**, Fritz, M., Vögeli, B., Erb, T. J., Becker, J., Wittmann, C. 2020. A common approach for absolute quantification of short chain CoA thioesters in prokaryotic and eukaryotic microbes. Microb. Cell Fact. 19, 160.

Jovanovic Gasovic, S., Dietrich, D., Gläser, L., Cao, P., Kohlstedt, M., Wittmann, C. 2023. Multiomics view of recombinant *Yarrowia lipolytica*: Enhanced ketogenic amino acid catabolism increases polyketide-synthase-driven docosahexaenoic production to high selectivity at the gram scale. Metabolic Eng. 80, 45-65.

Dietrich, D., **Jovanovic Gasovic, S.**, Cao, P., Kohlstedt, M., Wittmann, C. 2023. Refactoring the genetic architecture of a myxobacterial polyketide gene cluster enables advanced heterologous docosahexaenoic acid production in *Yarrowia lipolytica*. Microb. Cell Fact. 22, 199.

CONFERENCE CONTRIBUTIONS

Jovanovic, S., Kohlstedt, M., Dietrich, D., Gemperlein, K., Wenzel, S., Müller, R., Wittmann, C. 2019. Transcriptome analysis of *Yarrowia lipolytica* for increased production of rare omega-3 fatty acids. HIPS symposium, Saarland University, Saarbrücken, Germany.

Jovanovic, S., Kohlstedt, M., Dietrich, D., Gemperlein, K., Wenzel, S., Müller, R., Wittmann, C. 2019. Transcriptome analysis of *Yarrowia lipolytica* for increased production of rare omega-3 fatty acids. 13th Meeting of the Slovenian Biochemical Society, Dobrna, Slovenia.

ACKNOWLEDGMENT

I would like to express my heartfelt gratitude to my mentor, Prof. Dr. Christoph Wittmann, for his unconditional support and invaluable scientific guidance throughout my research journey. Working under the supervision of such an exceptional scientist has been an absolute pleasure and a source of daily inspiration. His enthusiasm for research has been truly contagious, and, more importantly, his mentorship has made me feel a sense of belonging, bridging the gap that being away from my family can sometimes create.

Many thanks to Prof. Dr. Andriy Luzhetskyy for reviewing this work and providing extremely useful feedback in timely manner. I would also like to thank Prof. Dr. Uli Kazmaier for taking part in my PhD defense as examination chair and to Dr. Ruth Kiefer for diligently fulfilling the role of academic associate.

This research received financial support from the German Ministry for Education and Research (BMBF), for which I am deeply grateful. The opportunity to work on projects "MYXO4PUFA" and "MYXO4PUFA-2" without concerns about financial matters has been immensely appreciated.

Vielen Dank to the entire iSBio team for cultivating an exceptional working atmosphere. The journey towards a PhD has been filled with countless memorable moments, both within and outside the lab. I would like to extend special thanks to Micha, who dedicatedly conducted 14-day long fermentations with me, Susanne, whose support helped resolve administrative challenges over and over again, and Michael, whose maintenance of the machines and expertise in analytics were very helpful.

Additionally, I would like to express my eternal gratitude to the guys from the "monkey office" who provided me with a genuine German/Chinese experience and made my journey much more enjoyable. Demian, thank you for accompanying me in fighting this wild beast over the course of nearly 5 years. To my office colleagues, Muzi, Iza and Julian, I am deeply thankful for many things: the fruitful discussions, shared laughter, tears, continuous knowledge exchange, and unwavering support. My dear Chinese princess, thank you for being a true friend and for demonstrating both strength and emotional depth to the world. Mi niña, gracias por ser siempre tú, pase lo que pase. Que la fuerza te acompañe. Dear Sue, thank you for being a true inspiration and for setting the perfect example of who I should strive to be, both professionally and personally.

Mojim djevama iz-Bosne naročito hvala. Život u Njemačkoj ne bi bio upola zanimljiv niti lak bez vas. Bibi, hvala ti za optimizam, mnogo dobrih fora, putovanja i ideja. Mače, hvala ti što si bila verni prijatelj, naučila me bitnim životnim lekcijama i bila veliki oslonac sve ovo vreme. Hvala za najukusnija jela i najdublje razgovore. Dr. Beganović i Dr. Muhović, čekam vas da pokorimo svet!

Svim mojim prijateljima i članovima porodice, veliko hvala što su bili tu i ostali uz mene. Hvala za podršku i razumevanje, ali i za nezaboravne trenutke kada je bilo potrebno da se napune baterije. Znate vi dobro ko ste!

Na kraju, hvala mom mužu na ogromnoj ljubavi koja mi je dala vetar u leđa i za svaki beg u lepši svet kada je bilo najpotrebnije. Hvala mojoj porodici i životinjama, što su prošli kroz sve ovo sa mnom. Miko i tata, hvala vam na bezuslovnoj ljubavi, na osećaju sigurnosti ma gde bila i na najjačim zagrljajima na aerodromima. Beskrajno hvala mojoj mami što sam baš ja projekat na kome je najduže i najvrednije radila. Hvala za sve neprospavane noći, brigu, požrtvovanost i ljubav. Bez tebe sigurno nikada ne bih došla do ovde. Hvala vam svima što istinski verujete u mene. Volim vas najviše!

Najzad, posvetila bih ovaj rad jednoj maloj naučnici iz Pančeva koja se usudila da krene putem kojim se ređe ide. Hvala ti što oduvek radiš stvari na svoj način i što nisi odustala ni kada je bilo jako teško. Jako sam ponosna na tebe. „*Budi takvo neko čudo što ne ume ništa malo, pa kad kreneš - kreni ludo, ustreptalo, radoznalo. Ko zna šta te tamo čeka u maglama iz daleka. Al' ako se i pozlatiš, il' sve teško, gorko platiš, uvek idi samo napred. Nemoj nikad da se vratiš*.“

TABLE OF CONTENTS

SUMMARY

Heterologous expression of myxobacterial PKS-like PUFA cluster in recently created recombinant *Yarrowia lipolytica* Af4 strain allowed formation of DHA, polyunsaturated fatty acid with significant impact on human health.

The focus of this work was to unravel the complex underlying metabolism of the oleaginous yeast using systems biology tools. Growth-decoupled production of DHA occurred during the stationary phase. The transition triggered drastic changes in global transcription and reduced availability of the two DHA precursors, acetyl and malonyl-CoA up to 98%. Upregulation of genes belonging to PUFA cluster coincided with the activated degradation of lipid bodies and fatty acids and the associated glyoxylate shunt, reactions involved in cellular stress-response, and interestingly, catabolic routes of branched-chain amino acids and L-lysine. This inspired the creation of time-resolved feeding strategies that supplemented the cultures with citrate, L-lysine, L-leucine and L-isoleucine, respectively to provide additional acetyl-CoA. Beneficially, the novel strategy increased DHA production up to 38%. Careful ^{13}C tracer studies then unraveled that the supplemented carbon was significantly incorporated into intracellular CoA-esters, amino acids, and DHA itself. Fed by small amounts of L-lysine, the recombinant producer *Y. lipolytica* Af4 accumulated DHA up to the gram scale in the fed-batch process, and surpassed previous efforts three-fold.

ZUSAMMENFASSUNG

Die heterologe Expression eines myxobakteriellen PUFA-Clusters in dem kürzlich geschaffenen rekombinanten *Yarrowia lipolytica* Af4 ermöglichte die Synthese von DHA, einer mehrfach ungesättigten Fettsäure mit erheblichen Auswirkungen auf die Gesundheit.

Der Schwerpunkt dieser Arbeit lag auf der Aufklärung des komplexen zugrunde liegenden Stoffwechsels der öligen Hefe mit systembiologischen Methoden. Die Produktion von DHA erfolgte wachstumsentkoppelt in der stationären Phase. Der Übergang löste drastische Veränderungen in der globalen Transkription aus und verringerte die Verfügbarkeit der beiden DHA-Vorstufen Acetyl- und Malonyl-CoA um bis zu 98%. Die Hochregulierung des PUFA-Clusters, fiel mit dem aktivierten Abbau von Lipiden und dem damit verbundenen Glyoxylat-Shunt, mit verstärkter Stressreaktion, und interessanterweise auch mit katabolen Wegen von verzweigtkettigen Aminosäuren und L-Lysin zusammen. Dies inspirierte zur Entwicklung von zeitaufgelösten Fütterungsstrategien, bei denen Citrat, L-Lysin, L-Leucin bzw. L-Isoleucin zugeführt wurden, um zusätzliches Acetyl-CoA bereitzustellen. Mit dieser neuen Strategie konnte die DHA-Produktion um bis zu 38% gesteigert werden. ^{13}C-Tracer-Studien ergaben, dass der zugeführte Kohlenstoff in großem Umfang in CoA-Ester, Aminosäuren und DHA eingebaut wurde. Im Fed-Batch-Verfahren produzierte *Y. lipolytica* Af4, der mit geringen Mengen L-Lysin gefüttert wurde, DHA bis in den Grammbereich und übertraf frühere Ansätze um das Dreifache.

1 INTRODUCTION

1.1 General Introduction

Docosahexaenoic acid (DHA) is the one of the two commercially most valuable omega-3 PUFAs. These compounds are naturally synthesized only by selected microorganisms, most notably marine microalgae (Nishshanka et al., 2022) such as *Schizochytrium* sp. (Kujawska et al., 2021; Wang et al., 2021), *Aurantiochytrium* sp. (Bartosova et al., 2021; Hussain et al., 2021), and *Crypthecodinium cohnii* (Pei et al., 2017). DHA itself plays a crucial role in human health, by preventing and intervening in cardiovascular (Swanson et al., 2012) and neurodegenerative diseases, inflammatory (Zhang et al., 2019) and autoimmune disorders, promoting better brain, bone, and eye function and development (Liu et al., 2022; Mun et al., 2019) and demonstrating anti-Alzheimer (Ferreira et al., 2022) and tumor suppressive effects (Aslan et al., 2020; Liu et al., 2021). The history of research on DHA dates back nearly 50 years (Dyerberg et al., 1975), and significant progress has been made in the past decade leading to the growing awareness about the beneficial effects of omega-3 PUFAs. Humans do not possess a comprehensive endogenous biosynthetic pathway, making these PUFAs essential and indispensable for their physiological functions (Madore et al., 2020). To satisfy daily recommendations and keep up with the growing world population, attempts to establish a sustainable source of these molecules rely mostly on biotechnological approaches, including metabolically engineered DHA-enriched crops and seeds as well as the utilization of microbes as DHA-producing cell factories (Jovanovic et al., 2021).

Oleaginous yeasts have emerged as promising heterologous PUFA producers, owing to the excellent ability to accumulate large amounts of lipids and, therefore, fatty acids (Donot et al., 2014). *Y. lipolytica* is a non-conventional dimorphic yeast that has been extensively engineered for this purpose (Jia et al., 2022). Among other fatty acids, the yeast showed great potential in synthesizing PUFAs, including eicosapentaenoic acid (EPA) (Xue et al.,

2013), linoleic acid (CLA) (Imatoukene et al., 2017), α-linolenic acid (ALA) (Cordova and Alper, 2018), arachidonic acid (ARA) (Liu et al., 2019c), and, last not least, DHA (Gemperlein et al., 2019). Noteworthy, the latter strategy used a heterologous PKS-like PUFA-synthase from a terrestrial myxobacterium offering substantially reduced demand for NADPH (Gemperlein et al., 2019). In an optimized fermentation process, the created producer *Y. lipolytica* Af4 accumulated 350 mg L^{-1} of DHA, providing an important proof-of-concept.

1.2 Objectives

The aim of this study was to provide systems-level understanding of the complex metabolic and regulatory networks, associated to the lifestyle of *Y. lipolytica* and their response to heterologous expression of the PUFA gene cluster for DHA overproduction. After establishing a reproducible culture process for the wildtype and the previously generated DHA-overproducer, respectively, and setting-up analytics for the monitoring of substrates and products, systems biology methods should be elaborated. For selected and global transcriptomic analysis, approaches based on qRT-PCR and custom-built DNA-microarrays should be developed and validated, while LC-MS/MS-based analytics should be adapted to allow precise monitoring of intracellular levels of the DHA-precursors acetyl-CoA and malonyl-CoA, and ^{13}C-based fluxomics studies to allow to infer specific pathway fluxes in the yeast. Next, the newly established tools should be used to systematically explore differences between wildtype and producer, the impact of carbon-, nitrogen-, and phosphorus-containing nutrients, and time-dependent dynamics during the production process, respectively. The obtained data should be used to generate a systems biology view on DHA-producing *Y. lipolytica*. Ideally, this should lead to the identification of targets that limit DHA production, and these targets should be evaluated for improved production of DHA.

2 THEORETICAL BACKGROUND

2.1 PUFAs: from poorly understood fats to health angels

Since almost 50 years, polyunsaturated fatty acids (PUFAs) are known as health-promoting active ingredients (Shahidi and Ambigaipalan, 2018). Pioneered by studies on rats (Burr and Burr, 1929), the discovery of PUFA-related health benefits in Greenland Eskimos displayed the starting point of intense research efforts over the past decades which changed the value of these molecules from being only of negligible interest as drying oil constituents into health angels with a multi-billion US$ market (Dyerberg et al., 1975). Revealed by numerous medical studies, PUFAs are indeed indispensable for the brain, nerve (Rey et al., 2019) and eye function (Cholewski et al., 2018; Mun et al., 2019), support fetal development (Valenzuela and Nieto, 2001) prevent neurodegenerative diseases and psychiatric disorders (Bentsen, 2017; Cardoso et al., 2016), and protect against cardiovascular diseases (Adili et al., 2018; Yanai et al., 2018), infection (Calder, 2018; Innes and Calder, 2018), and cancer (Zarate et al., 2017) (**Fig. 1**). Humans (like all vertebrates) cannot synthetize PUFAs *de novo*, making them essential nutrients (Castro et al., 2016).

From a chemical viewpoint, PUFAs are long-chain fatty acids that harbor at least 18 carbon atoms and two or more unsaturated bonds in their hydrocarbon chain. The distance of the first double bond from the end of the acyl chain, i.e. the terminal ω-carbon atom, differs among different PUFAs, allowing us to classify them into omega-6, omega-3 and omega-9 PUFAs (Wiktorowska-Owczarek et al., 2015). The most beneficial (and industrially impacting) PUFAs are omega-3 derivatives, spearheaded by docosahexaenoic acid (DHA, 2:6, ω3), eicosapentaenoic acid (EPA, 20:5, ω3), and α-linolenic acid (ALA, 18:3 ω3) (Harris, 2018). The omega-6 PUFAs form another significant family of dietary PUFAs.

Prominent members such as linoleic acid (LA, 18:2 ω6) and arachidonic acid (ARA, 20:4 ω6), apparently have a more complex role in metabolism (Burns et al., 2018; Zhuang et al.,

2019). On one side, they appear indispensable for important cellular processes, including brain development (Harauma et al., 2017) and function (Tallima and El Ridi, 2018), and development of the infant nerve system (Lien et al., 2018) but can also cause detrimental effects on the other side (DiNicolantonio and O'Keefe, 2018). In addition, different derivatives emerge as new to the market PUFAs due to their increasingly unraveled importance for human health and well-being, including γ-linoleic acid (GLA, 18:3, ω6), stearidonic acid (SDA, 18:4, ω3), dihomo-γ-linoleic acid (DGLA, 20:3, ω6), eicosadienoic acid (EDA, 20:2, ω6), docosapentaenoic acid (DPA, 22:5, ω3), and very long chain (VLC) PUFAs such as tetracosatetraenoic acid (TTA, 24:4, ω6), tetracosapentaenoic acid (TTA, 24:5, ω3), and tetracosahexaenoic acid (THA, 24:6, ω3). PUFAs, headed by DHA and EPA, have reached worldwide attention in recent years due to the increasing awareness of their role in human health (**Fig. 1**).

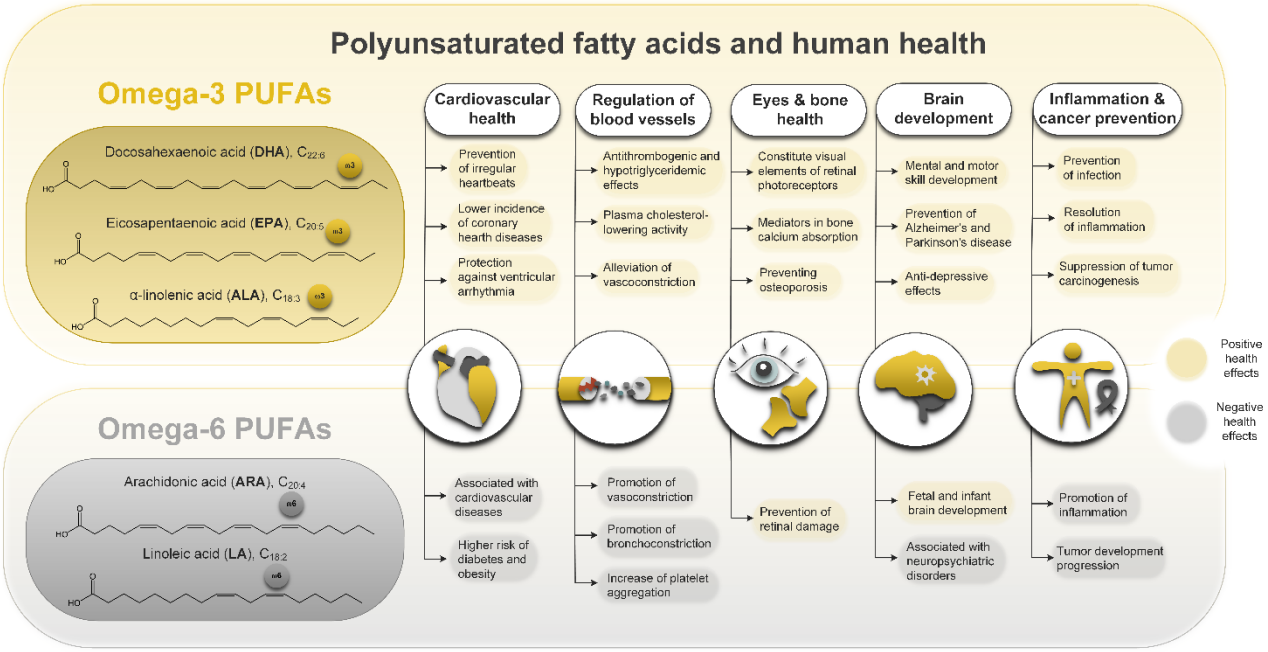

Figure 1. Polyunsaturated fatty acids (PUFAs) and their impact on human health. Involvement of the most prominent omega-3 and omega-6 PUFAs on cardiovascular health (Calder, 2018; Yanai et al., 2018), blood vessel function and control (Adili et al., 2018), eye and bone health (Saini and Keum, 2018), brain development (Harauma et al., 2017), as well as inflammation and cancer (DiNicolantonio and O'Keefe, 2018; Innes and Calder, 2018). Beneficial (yellow) and detrimental (grey) effects are highlighted (Jovanovic et al., 2021).

2.2 PUFA world markets: bridging the gap between supply and demand

Traditionally, the demand for PUFAs is covered by specific PUFA-rich food. Most vegetable oils (e.g., soybean, corn, sunflower oil) are rich in omega-6 PUFAs (**Fig. 2**). Their preferred consumption over animal fats during the past decades has resulted in an increased uptake of omega-6 PUFAs (Saini and Keum, 2018), partially exceeding recommended levels and disturbing the physiological balance between omega-3 and omega-6 PUFAs (Harris, 2018). Flaxseed and chia seed oils and walnuts are a rich source of omega-3 ALA (Saini and Keum, 2018).

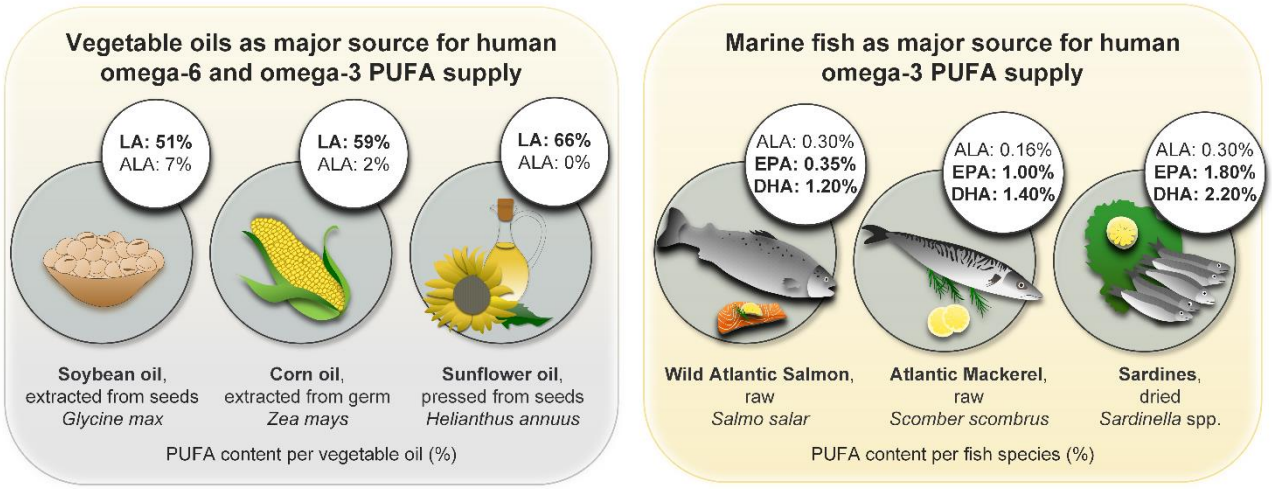

Figure 2. Terrestrial and marine sources of omega-6 and omega-3 PUFAs. The data comprise the current PUFA content in vegetable oils, i.e. soybean, corn and sunflower oil (right), the most prominent sources of LA and ALA and oily fish species, i.e. salmon, mackerel, and sardine (left), the most important food for intake of DHA and EPA (top) (USDA, 2015).

The intake of DHA and EPA, in contrast, relies on marine oily fish such as salmon, sardine, herring, and mackerel (Innes and Calder, 2020) that feed on marine phytoplankton as primary producer of these PUFAs (Sathasivam et al., 2019). That is why the two compounds are also named marine PUFAs. Individual needs for these essential molecules vary depending on age, well-being and overall physical condition, nevertheless, it has been recommended consuming at least two servings of fatty fish per week, which can provide about 500 milligrams of DHA and EPA combined (Racey et al., 2021). Unfortunately, the

supply of DHA and EPA from our oceans is tremendously declining due to overfishing and climate warming (Hixson and Arts, 2016) (**Fig. 3**).

Wild fisheries are not keeping pace with the growing world population, and many are even in decline (Hicks et al., 2019). Aquaculture is meant to provide fish instead but heavily depends on external supply itself and is a major producer and consumer of DHA and EPA at the same time (Tocher et al., 2019). Making this situation even worse, cold-protective PUFA production in primary producing phytoplankton is diminishing due to the increase in global temperature, leading to reduced content of DHA and EPA in caught fish (Mao et al., 2017) (**Fig. 3**).

The resulting picture is dramatic: present predictions for DHA estimate that its availability might decrease to levels, where more than 90% of the world's population will suffer from insufficient supply (Colombo et al., 2020). Notably, we face a serious gap between supply and demand and the deficit has been estimated at over 1 million tons (Salem and Eggersdorfer, 2015). To this end, biotechnological processes for *de novo* production of PUFAs, mainly the marine ones but also others, get more and more into the focus of research. It goes without saying that all developments have excellent market potential and receive high attention from the industry. PUFA enriched oils, meals, and other formulations are sold as food supplement and fish feed in aquaculture (Allen et al., 2019), whereas purified PUFAs display high-price active ingredients of medicals and pharmaceuticals (Finco et al., 2017).

The severe supply deficits have created a multi-billion US$ business: the price of single cell oils is estimated up to 500 US$ kg^{-1} or even higher, depending on the PUFA composition (Gunstone, 2001). In this regard, aquaculture-based and agriculture-based companies team up with single cell oil producers to launch novel products at large scale. Prominent examples are globally leading aquafeed manufacturers such as Skretting (with DSM/Evonik) and Biomar (with Bunge/TerraVia).

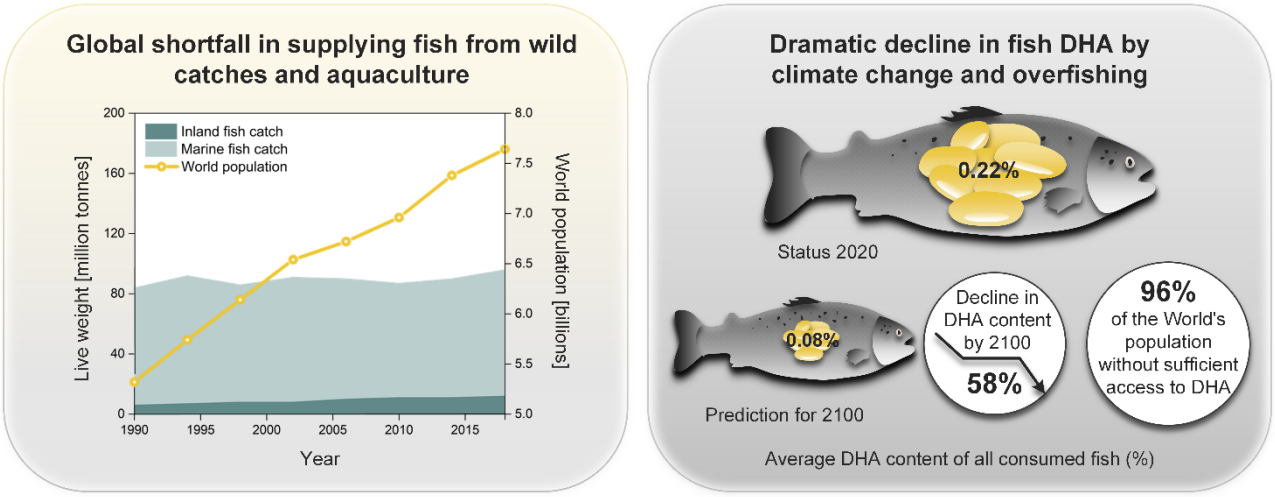

Figure 3. Global view on demand of the marine PUFAs DHA and EPA. The global trend in EPA supply and demand becomes obvious from developments in global aquaculture (inland fish catch) and wild catches (marine fish catch) (FAO, 2020. http://www.fao.org/state-of-fisheries-aquaculture) against the continuous growth of the human population (left). Long-term predictions on the expected shortage of DHA supply from drastically declining DHA content in average fish consumed (right) (Colombo et al., 2020).

Likewise, Cargill recently purchased the Norwegian aquafeed company Ewos, after having developed EPA/DHA-rich canola together with BASF. The world market for omega-3 PUFAs alone is estimated at 13 billion US$ and a calculated annual growth rate (CAGR) of 8%. Among the omega-6 PUFAs, the market size of ARA has been projected to reach 400.000 tons per year, worth of almost 2 billion US$ (Gunstone, 2001). Hence, various strategies have been proposed to enhance production, including the use of natural PUFA producers and metabolically improved mutants derived therefrom plus a range strains, based on conventional microbial workhorses with heterologous expression of PUFA genes and pathways.

2.3 Biosynthesis of DHA and other PUFAs in nature and industry

Only selected organisms synthetize PUFAs naturally, while most cannot (Kabeya et al., 2018). Hereby, nature has evolved two fundamental routes: an aerobic pathway by altering desaturation and elongation reactions (**Fig. 4**) and an anaerobic one *via* enzymes analogues

to polyketide synthases (**Fig. 5**). Henceforth, PUFAs will be directed either to form phospholipids as a part of membrane systems or stored in lipid bodies in the shape of triacylglycerols (TAGs) (Morabito et al., 2019). For some organisms, the incorporation of PUFAs in the cell membrane is regarded crucial for maintaining optimal membrane fluidity and adapting to stress conditions, particularly temperature, UV light and osmotic pressure (Adarme-Vega et al., 2012). Microbial cell factories are regarded as major solution to supply these precious molecules in sufficient amounts to provide PUFA-rich superfoods, aquafeed and medical formulations. In this regard, many attempts have been made to upgrade and streamline microalgae, yeasts, fungi, and bacteria for high level PUFA production and modified PUFA spectrum (Jovanovic et al., 2021).

2.3.1 Aerobic PUFA biosynthesis and producers

The aerobic PUFA biosynthetic pathway is (fully or at least partially) present in animals, selected plants and eukaryotic microorganisms (Qiu et al., 2020). The latter group is quite diverse and, as example, includes the dimorphic fungi and various types of unicellular marine microalgae such as the photosynthetic haptophytes (Bonfanti et al., 2018), dinoflagellates (Chalima et al., 2020), and heterotrophic protists (Zhao and Qiu, 2018). The core of the aerobic route utilizes the canonical fatty acid synthesis (FAS) machinery, which either operates as one large multifunctional polypeptide (type I FAS in animals, yeast, fungi), or as a complex of different mono-functional enzymes (type II FAS in prokaryotes, plants) (Smith et al., 2003). In all cases, acetyl-CoA and malonyl-CoA are the starting precursors to assemble a saturated acyl intermediate in consecutive NADPH-dependent reactions which is then further extended to palmitic acid, a saturated 16-carbon fatty acid (**Fig. 4**). Palmitic acid, *via* chain elongation and desaturation, respectively, serves as precursor for LA. The introduction of a double bond at the ω3 position into the latter forms ALA. The alternating

action of desaturases (oxygen-dependent regioselective introduction of unsaturated bonds) and elongases (chain length extension by two carbon units) modifies and extends the backbone of ALA and LA and yields the omega-3 derivatives EPA and DHA plus the omega-6 derivative ARA, respectively (Li-Beisson et al., 2019). Alternative routes exist for the initial two steps of these conversions: the Δ6-pathway (in protists, fungi, bilaterians, insects, fish, and human) (Mao et al., 2017) and the alternative Δ8-pathway (in the flagellated microalgae *I. galbana*) (Monroig and Kabeya, 2018) (**Fig. 4**). Mammalian cells do not possess desaturases (Δ12 and Δ15) that incorporate double bonds into the ω3 and ω6 positions on the fatty acid backbone, so that they cannot create LA and ALA. Downstream enzymes, required to form longer and more unsaturated PUFAs (including DHA, EPA, and ARA), are present in mammals but their capacity is very weak and regarded insufficient from a medical perspective (Kabeya et al., 2018).

Among the microbes that synthetize PUFAs *via* the aerobic pathway, some species emerged as important specialists. Photosynthetic microalgae such as *Phaeodactylum tricornutum* (Hamilton et al., 2016), *Nannochloropsis oceanica* (Chen et al., 2018; Sirisuk et al., 2018), *Dunaliella salina* (Shi et al., 2018a), *Isochrysis galbana* (Bonfanti et al., 2018) and *Odontella aurita* primarily synthetize EPA (Diao et al., 2020). Other species, including the green algae *Chlorella vulgaris*, mainly store LA and ALA (Norashikin et al., 2018). Henceforth, means of metabolic engineering have been employed to reconstitute and modify existing pathways or express foreign enzymes to produce high level of the most valuable PUFAs (Gong et al., 2014a). Different fermentation strategies, energy supply, and alteration of the microbe's core metabolism are working hand in hand to achieve this goal.

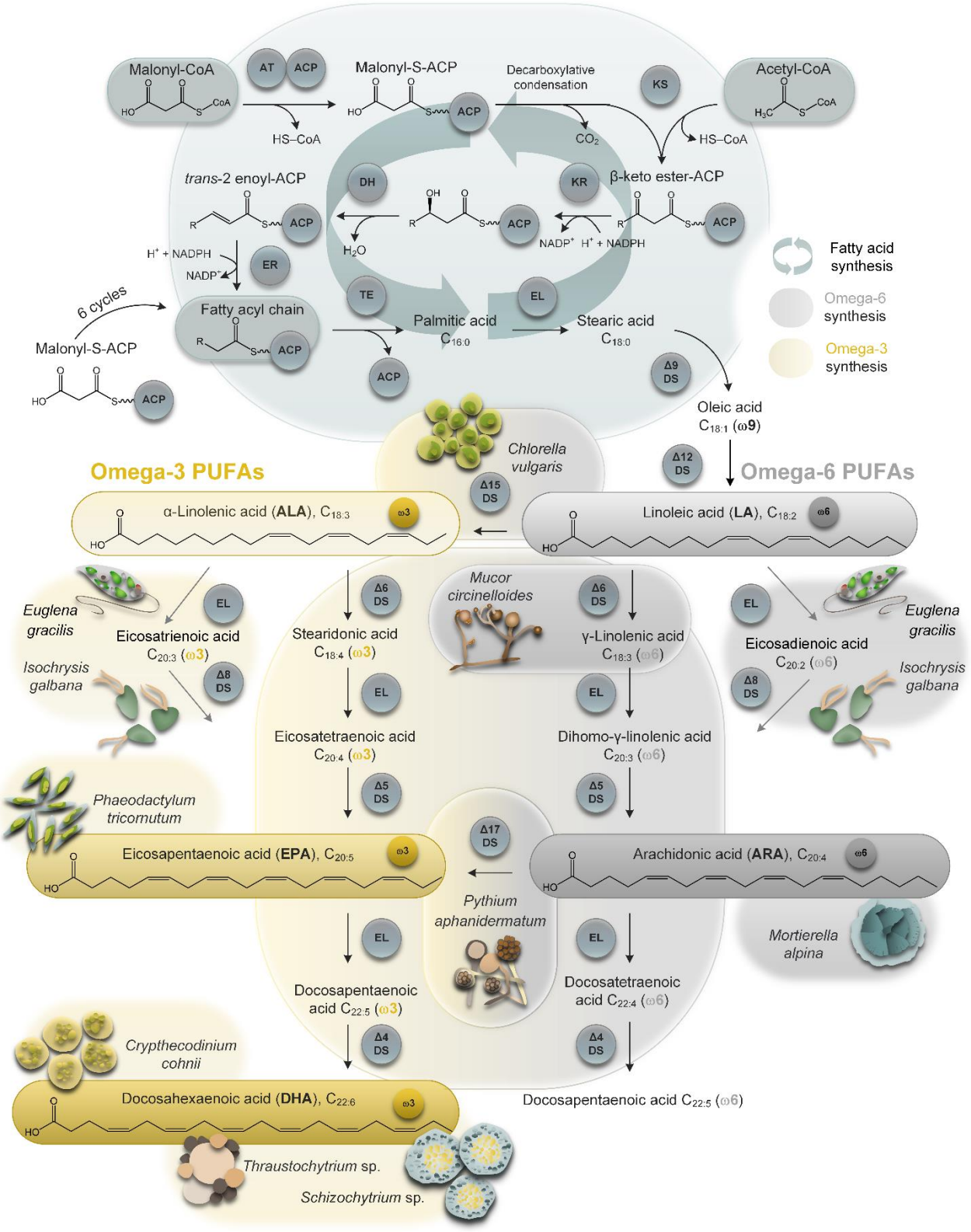

Figure 4. Aerobic pathway for the synthesis of PUFAs in animals, selected plants, and eukaryotic microbes, integrated into the fatty acid synthesis (FAS) machinery. Abbreviations: ER: enoylreductase; KS: ketosynthase; AT: acyltransferase; ACP: acyl carrier protein; KR: ketoreductase; DH: dehydratase; TE: thioesterase; DS: desaturase; EL: elongase.

A promising EPA cell factory, *P. tricornutum,* naturally accumulates up to 36% EPA and traces of DHA in its total fatty acids (Steinrucken et al., 2018). The combined introduction of Δ5-elongase (from marine picoalga) and a glucose transporter, provided a mutant strain which accumulated 36.5% EPA and 23.6% DHA, both as fraction of total fatty acids (TFAs) (Hamilton et al., 2016). As further shown, the overexpression of endogenous Δ6-desaturase increased the selectivity for EPA (Zhu et al., 2017).

Recent engagements to push the natural potential of this diatom and further improve production by means of genetic engineering involved the overexpression of the native gene *AGPAT* (1-acyl-sn-glycerol-3-phosphate acyltransferase) (Balamurugan et al., 2017) and changes to co-produce PUFAs with phytases, important enzymes for applications in aquaculture (**Fig. 6B**) (Pudney et al., 2019).

Mortierella alpina is a filamentous, oil producing zygomycete found in soil, intensively studied due to its outstanding ability to accumulate high levels of the omega-6 PUFA ARA at large scale and potential to broaden PUFA spectrum (Wu et al., 2017). Conversion of ARA into its omega-3 counterpart EPA in this fungus required only one desaturation step (by different heterologous Δ-17 desaturases) which consequently accumulated EPA at gram scale (Ge et al., 2017). Other attempts to further improve ARA production focused on bioprocess engineering aspects and provided a multi-stage fermentation bioprocess (Wu et al., 2017) and co-cultivation with the marine EPA-producing microalga *Nannochloropsis oceanica* (Du et al., 2018).

The dimorphic fungus *Mucor circinelloides*, which grows either yeast-like or forms mycelia, has a remarkable ability to synthesize the omega-6 PUFA GLA. For the purpose of converting the upstream intermediate OA into GLA, native Δ12, Δ6-1 and Δ6-2 desaturases were overexpressed in *M. circinelloides* mutant which exhibited an elevated GLA titer of 180 mg L^{-1} and a GLA content of 43% of TFA (Zhang et al., 2017). Furthermore, heterologous expression of Δ6 elongase from *M. alpina* (**Fig. 6C**) enabled the production of up to 75 mg

L^{-1} DGLA along with 300 mg L^{-1} GLA, suggesting remaining potential to be used in the future (Khan et al., 2019).

2.3.2 Anaerobic PUFA biosynthesis and producers

While marine bacteria, synthetizing EPA and DHA, were known since the 1980s, it was long assumed that they use the common aerobic pathway. Pioneering efforts in cloning EPA biosynthetic genes (Yazawa, 1996) and the subsequent discovery of a novel anaerobic route for bacterial PUFA biosynthesis (Metz et al., 2001) therefore displayed milestones in PUFA research. Biochemically, the anaerobic route is fundamentally different to the aerobic pathway (**Fig. 5**).

It is not integrated with fatty acid biosynthesis but uses a PUFA synthase, i. e. a polyketide synthase (PKS)-like enzyme complex, to synthesize PUFAs *de novo*. The proposed route from acetyl-CoA and malonyl-CoA involves iterative cycles of condensation, dehydration, and keto-reduction (Harwood, 2019). The length of a PUFA molecule, formed by the multidomain complex, is presumably determined by the interaction of ketoacyl synthase, one of the PKS domains with a small regulator, called chain length factor (CLF) (Hayashi et al., 2020). Anaerobic PUFA biosynthesis seems to exclusively exist in microorganisms, such as marine (*Shewanella* spp., *Vibrio* spp.) and terrestrial bacteria (e.g. *Sorangium cellulosum*, *Aetherobacter* spp.) (Gemperlein et al., 2014; Gemperlein et al., 2018), and unicellular microalgae, including *Thraustochytrium* spp., *Schizochytrium* spp., and *Ulkenia* spp. (Allemann and Allen, 2018). The different domains of PUFA synthase are encoded by *pfa* gene clusters. These clusters comprise between 3 to 5 genes, e.g. *pfa123* in *Schizochytrium* spp. and *pfaABCDE* in *Shewanella* spp. (Hayashi et al., 2020). Notably, myxobacterial *pfa* clusters (*pfa123*) encode unique 1-acyl-sn-glycerol-3-phosphate acyltransferases (AGPATs) that incorporate PUFAs into cell glycerophospholipids (Garcia et al., 2016).

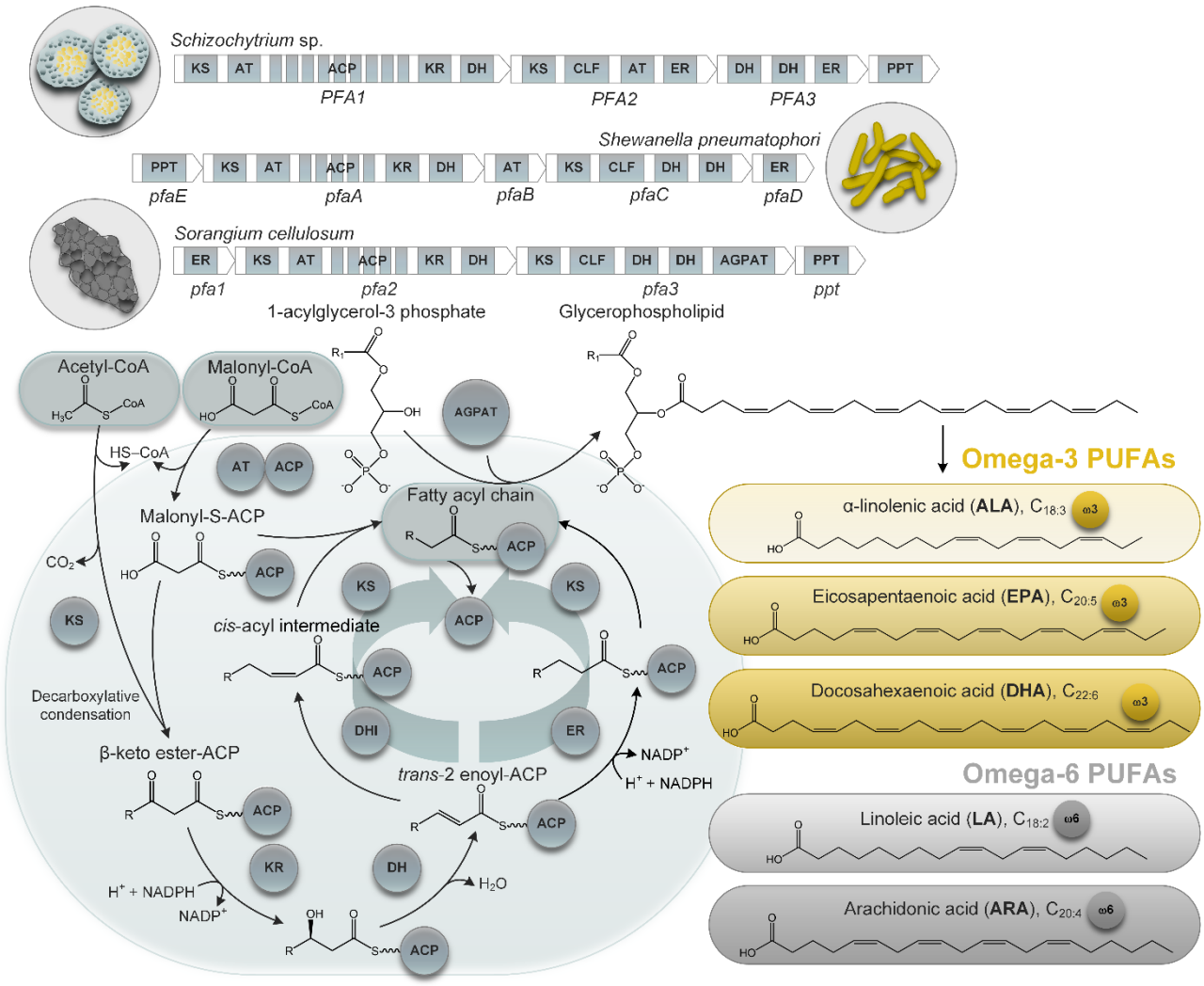

Figure 5. Anaerobic pathway for de-novo synthesis of PUFAs in eukaryotic microalgae and bacteria, using PKS-like PUFA synthases, and corresponding *pfa* gene clusters. Abbreviations: ER: enoylreductase; KS: ketosynthase; AT: acyltransferase; ACP: acyl carrier protein; KR: ketoreductase; DHI: dehydratase/isomerase; CLF: chain length factor; AGPAT: 1-acylglycerol-3-phospatate acyltransferase; PPT: 4′-phosphopantetheinyl transferases.

2.4 Microbial production of DHA

2.4.1 Marine microalgae

Marine microalgae stand out for their capacity to store large amounts of DHA in neutral triacylglycerols and cell membrane lipids. Prominent heterotrophic members, which accumulate high levels of DHA, are marine unicellular thraustochytrids (from the genera *Schizochytrium*, *Aurantiochytrium*, and *Thraustochytrium*) (Chen et al., 2020) and the

dinoflagellate *C. cohnii* (Mendes et al., 2009). Although regarded as microalgae, these microbes have lost photosynthesis and live as saprophytic decomposers in the marine realm (Khozin-Goldberg et al., 2016).

***Schizochytrium* and *Aurantiochytrium* – DHA rich microalgae.** The marine microalgae *Schizochytrium* spp. is the best performing cell factory regarding DHA production. It is used for commercial production of DHA-rich oil (OmegaTech Inc.) and spray-dried biomass (marketed as DHA Gold by Martek Biosciences Corp.) since more than 25 years (Ratledge and Hopkins, 2006). The microbe possesses the aerobic plus the anaerobic PUFA route but lacks Δ12-desaturase so that DHA is presumably formed anaerobically (Ye et al., 2015). Recent studies have provided novel strains and processes with remarkable efficiency. In particular, the oxygen sensitivity of DHA production was tackled. Supplementation with ascorbic acid as an antioxidant decreased the level of intracellular ROS and increased the DHA titer to 38.3 g L^{-1} (Ren et al., 2017). In an alternative approach, adaptive laboratory evolution (ALE) to low temperature and high salinity resulted in the mutant *Schizochytrium* sp. ALE-TF30, which accumulated DHA with a titer of 38.1 g L^{-1}, 57% more than in the parent strain (Sun et al., 2018b). The ALE-TF30 mutant revealed increased expression of polyketide synthases and strongly reduced lipid peroxidation, likely supported by the transcriptionally activated antioxidant defense. In addition, ROS detoxifying enzymes were successfully used to support DHA production. The overexpression of superoxide dismutase (*SOD1*) reduced the ROS level in *Schizochytrium* sp. and resulted in a DHA accumulation of 147 mg (g dry cell weight)$^{-1}$ (Zhang et al., 2018) (**Fig. 6A**). On the bioprocess side, medium optimization identified peptone medium and glycerol as alternative nitrogen and carbon sources (Sahin et al., 2018) and demonstrated DHA production at the 7,000 L scale (Guo et al., 2018).

Notably, mutagenesis and metabolic engineering of *Schizochytrium* sp. has provided the next level of producers with even increased production efficiency for DHA and enhanced

formation of other PUFAs. Atmospheric and room temperature plasma mutagenesis (combined with resistance selection against high levels of malonic acid and zeocin) generated a *Schizochytrium* sp. mutant that produced 14 g L^{-1} DHA, whereby the responsible genetic alterations remain to be elucidated (Zhao et al., 2018). Heterologous expression of malic enzyme (from *C. cohnii*) and C16/18 fatty acid elongase (*ELO3* from *M. alpina*) raised the intracellular levels of NADPH and acetyl-CoA, required for PUFA biosynthesis (Wang et al., 2019a) (**Fig. 6A**). Beneficially this strategy enhanced DHA production.

On the other hand, latest developments are focused on increasing the content of EPA besides DHA, in order to meet the intake recommendations for these fatty acids. An interesting approach refactored the PUFA PKS in *Schizochytrium* sp. (Ren et al., 2018). Replacement of the natural acyltransferase (AT) domain by a homologue from the native EPA-producing bacterium *Shewanella* sp. beneficially changed the lipid composition (**Fig. 6A**). The engineered strain accumulated DHA and EPA at 49.5 and 3.8% of total fatty acids (TFAs), respectively, which was then taken further to produce DHA and EPA up to a level of 28.8 and 2.3 g L^{-1}, respectively (Geng et al., 2019). Furthermore, overexpression of malonyl-CoA ACP transacylase (MAT) in *Schizochytrium* sp. shifted carbon flux towards PUFA synthesis, reaching remarkable levels of 47. 4 g L^{-1} DHA, 11.9 g L^{-1} DPA and 1.6 g L^{-1} EPA (Li et al., 2018). These are promising attempts to derive EPA in strains of *Schizochytrium* sp.

Like its relative *Schizochytrium*, *Aurantiochytrium* (formerly assigned to *Schizochytrium*) contains both PUFA biosynthetic routes, though it is presumed that DHA biosynthesis exclusively depends on PUFA synthase activity. This microbe has been considered more recently, and initial studies mainly addressed fundamental aspects of nutrient and temperature requirement. As example, nutrient starvation stimulated FAS but not PUFA synthase activity in *Aurantiochytrium* sp., which produced 12.5 g L^{-1} and 5.6 g L^{-1} of DHA

under nitrogen and oxygen limitation, respectively (Heggeset et al., 2019). Low temperature (15 °C) altered the lipid composition of a strain of *Aurantiochytrium* sp. (Ma et al., 2015) and fructose could be identified as suitable carbon source to produce DHA (Nazir et al., 2018). Moreover, recent attempts started to unravel the biosynthesis of VC-PUFAs and identified phosphatidylcholine as intermediate prior to incorporation into TAGs (Zhao and Qiu, 2019).

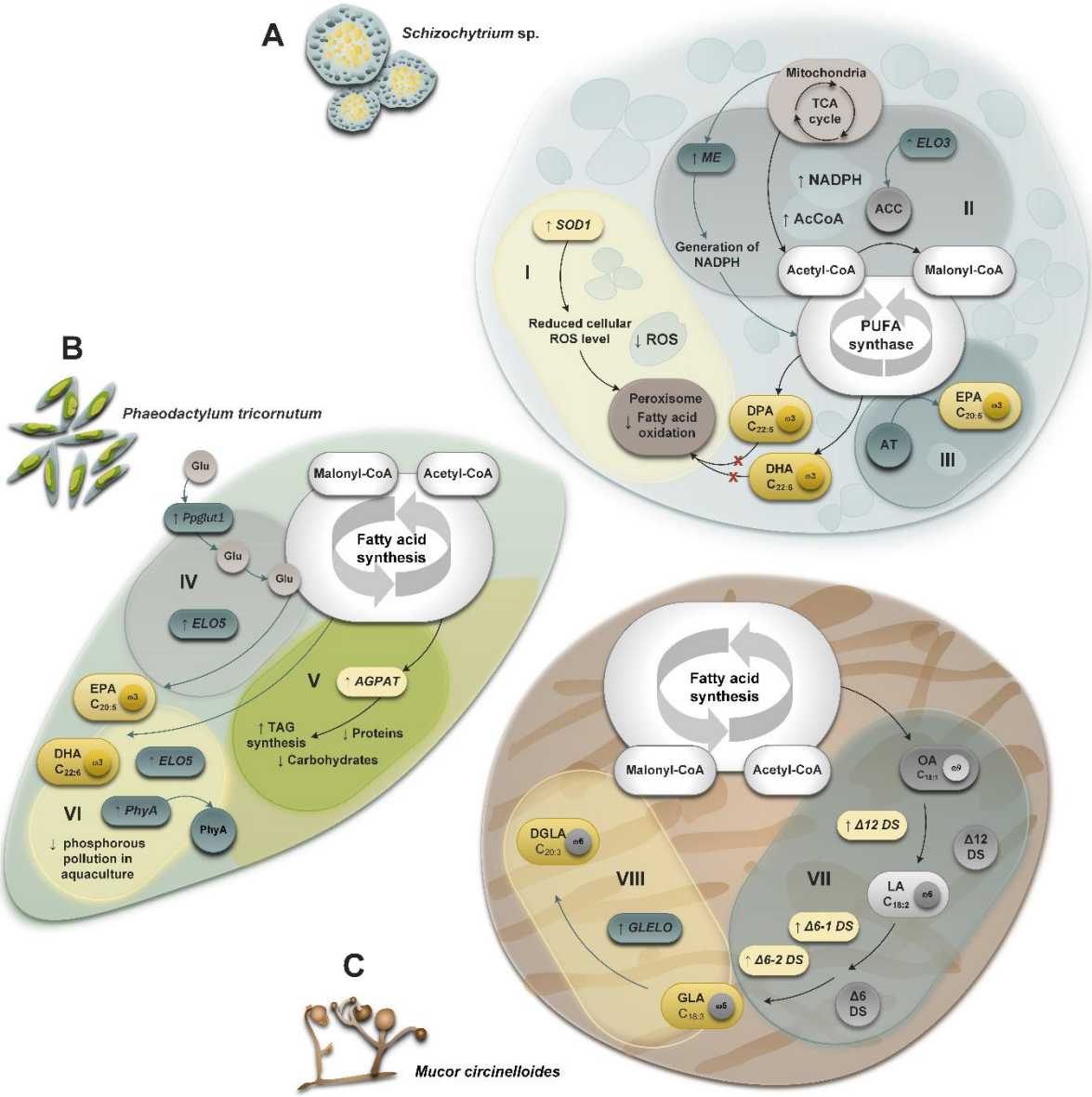

Figure 6. Recent advances in metabolic engineering of microbial PUFA production. The created cell factories include strains of (A) *Schizochytrium* sp. with (i) enhanced redox power and precursor supply (Wang et al., 2019a), (ii) reduced ROS level (Zhang et al., 2018), and (iii) enhanced production of EPA in addition to the major product DHA (Ren et al., 2018), (B) multi-functional *P. tricornutum* (iv) producing EPA and DHA from glucose (Hamilton et al., 2016), (v) exhibiting an increased lipid content with additional lipid droplets in the cytosol and the plastids (Balamurugan et al., 2017), and (vi) co-producing PUFAs together with a fish food phytase (Pudney et al., 2019), and (C) *M. circinelloides* (vii) overexpressing native desaturases (Zhang et al., 2017) and (viii) a heterologous elongase towards enhanced GLA and DGLA formation (Khan et al., 2019).

***Crypthecodinium cohnii* as a newly emerging DHA source.** *C. cohnii* is a red unicellular microalga. The dinoflagellate is obligate heterotrophic and almost exclusively contains DHA in its lipids. An evolved strain of *C. cohnii* was recently derived by chemical modulator-based ALE and found to produce 2.7 g L^{-1} DHA (Diao et al., 2019). DHA production in *C. cohnii* was enhanced to 7.8 g L^{-1} by an increase of oxygen availability (Diao et al., 2018). Likewise, optimized nitrogen feeding was shown to elevate the DHA titer (Liu et al., 2018). A first study recently aimed to infer metabolic fluxes in *C. cohnii*, using the METAFOR approach (Cui et al., 2018). The Emden-Meyerhof-Parnas pathway was identified as a major glycolytic route in the microbe, whereas malic enzyme was suggested as an enzyme involved in the supply of NADPH for lipid accumulation.

2.4.2 Native and heterologous bacteria

Selected bacteria (mainly marine but also terrestrial ones) possess *pfa* gene clusters that encode for PKS-like anaerobic PUFA biosynthesis (**Fig. 5).** The PUFAs obtained help them to thrive in their extreme environments and face cold temperatures, high pressure, and high salt. Likewise, different cyanobacteria form a spectrum of PUFAs, including ALA and SDA (Poole et al., 2020; Santos-Merino et al., 2018; Yoshino et al., 2017). In contrast, leading bacterial cell factories of industrial relevance (e. g. *E. coli, P. putida,* and *C. glutamicum*) can synthetize only saturated and mono-unsaturated fatty acids.

Psychrophilic marine bacteria as natural DHA producers. Recent progress revolves around the discovery of novel species and first attempts to improve PUFA production, admittedly still at a proof-of-concept level. Strains of *Colwellia* are heterotrophs, found in cold environments such as sea ice, polar sediments and deep sea (Techtmann et al., 2016). They anaerobically synthesize DHA up to 17% of TFA (Kusube et al., 2017). The addition of cerulenin (a FAS inhibitor) increased DHA levels to 120 mg L^{-1} at the expense of

monounsaturated fatty acids in strain *C. psychrerythraea* 34H (Wan et al., 2016). Hereby, the cerulenin supplementation study revealed the importance of the PUFA synthase for DHA production in marine bacteria, like in microalgae. Earlier reports revealed that also other marine psychrophiles such as *Psychromonas* spp., *Moritella* spp., *Photobacterium* spp. and *Alteromonas* spp. naturally accumulate higher levels of PUFAs, but lacking efforts over the past few years indicate that these strains have escaped further improvement (Moi et al., 2018).

Natural PUFA production in terrestrial bacteria. Although anerobic PUFA biosynthesis seems mainly present in marine bacteria, selected terrestrial myxobacteria possess *pfa* genes too. Four species of *Aetherobacter* produced all major PUFAs, namely LA, ALA, ARA, EPA, and DHA (Garcia et al., 2016). *Sorangium cellulosum*, a closely related species to *Aetherobacter*, produced only LA, likely related to the fact that its *pfa3* gene lacks the AT domain sequence (Yoshida et al., 2016). Different isolates of the myxobacterium *Phaselicystis flava* were found to be enriched in ARA, whereby strain NOSO-1 (37.5% of TFA) contained threefold more than strain SBKo001 (12.4%), even approaching the high content of *M. alpina* (Garcia et al., 2009).

Heterologous DHA production in *E. coli* and *P. putida*. The common strategy to produce PUFAs in well-established bacterial workhorses implies heterologous expression of PUFA synthase genes from marine bacteria and microalgae. Several studies could prove feasibility but did not surpass the milligram scale so far. Overexpression of the cluster *pfaABCD* from *C. psychrerythraea* and the gene *pfaE* from *S. baltica* resulted in a *E. coli* mutant that produced 2.4 mg L^{-1} DHA, when grown at 15°C in cerulenin-supplemented medium (Peng et al., 2016). Increased performance was achieved by concerted engineering of PUFA biosynthesis and the native fatty acid synthesis in *E. coli*. A recombinant strain that lacked *fabH* and therefore was affected in the first step of short chain fatty acid synthesis, revealed increased DHA production, when additionally expressing the *pfa* gene cluster from *M.*

marina, pointing to a redirection of pathway precursors (Giner-Robles et al., 2018). When additionally supplying the antibiotic cerulenin (inhibiting the other two initiating enzymes FabB and FabF), the mutant accumulated 16.8 mg L^{-1} DHA. Synthesis of marine PUFAs was also demonstrated for lactic acid bacteria to potentially improve the nutritional content of fermented dairy products (Amiri-Jami et al., 2014). The overexpression of the *pfa* cluster from *S. baltica* in *Lactococcus lactis*, resulted in DHA and EPA production with 1.35 mg (g cell dry weight)$^{-1}$ and 0.12 mg (g cell dry weight)$^{-1}$, respectively. A transgenic strain of *Pseudomonas putida* that harbored a myxobacterial gene cluster, was found to produce DPA and DHA (Gemperlein et al., 2016). Several rounds of metabolic engineering, including refactoring and codon optimization of the *pfa* cluster and the alteration of lipid metabolism finally enabled the production of up to 3.0 mg L^{-1} DHA.

2.4.3 Recombinant yeast and fungi

Different yeasts and fungi have emerged as high-efficiency heterologous PUFA producers. Some of them, including dimorphic yeasts and fungi such as *Y. lipolytica*, *M. alpina,* and *M. circinelloides*, benefit from a naturally efficient lipid metabolism which provides PUFA precursors to high level and obviously offers in-built protection against the toxic side-effects of PUFA biosynthesis. It is thus not surprising that mutants of these microbes belong to the world's top class PUFA producers. Even better, the catalogue of producers gets continuously extended. As example, *Ashbya gossypii* (Ledesma-Amaro et al., 2018), *Rhodosporidium toruloides* (Arbter et al., 2019), and other oleaginous yeasts (*Rhodotorula glutinis*, *Trichosporon cutaneum*, *Candida sp.*) have recently revealed promising potential (Kolouchova et al., 2016b).

***S. cerevisiae* is still in its infancy regarding PUFA accumulation.** *S. cerevisiae* produces saturated and monounsaturated fatty acids up to 18 carbons but no PUFAs. Several reports demonstrate recombinant strains of the conventional yeast. Recently, heterologous expression of PUFA elongase *NsFAE* (from *Nannochloropsis* sp.) changed the lipid composition of *S. cerevisiae* and accumulated eicosadienoic acid (EDA), LA and ALA at 5.6%, 3.3% and 2.8% of TFA, respectively (Guo et al., 2019). At present, the achieved performance is far below that of other microbes. *S. cerevisiae* is strongly intoxicated when expressing PUFAs and exhibits low viability and metabolic performance, due to a reduced oxidative stress response, damaged proteins, lipid peroxides and even caspase-mediated cell death (Johansson et al., 2016). It seems that substantial engineering is needed to streamline the yeast for high-level PUFA production, but it would not surprise, given the enormous progress in developing *S. cerevisiae* cell factories for other purposes, to see efficient producers soon.

2.5 *Yarrowia lipolytica*: A fantastic yeast and where to find it

2.5.1 Biochemistry and physiology of an oleaginous lifestyle

To be classified as oleaginous ("*olea*", from Greek ἐλαία/elaía, olive tree), an organism should possess the inherent ability to accumulate lipids to at least 25% of the dry weight (which can account for up to 80% in some species) (Beopoulos et al., 2009). In addition to the necessary amount of lipids for the composition of cellular and intracellular membranes (Thorpe and Ratledge, 1972), these organisms possess unique reserve storage mechanism in discrete lipid bodies. Oleaginous yeasts have been extensively studied for their potential to produce lipids, as a source of biofuels, oleochemicals, and other products (Lamers et al., 2016). The most prominent species include the GRAS-certified dimorphic strain *Yarrowia lipolytica* (Morin et al., 2007), the red-colored yeast *Rhodotorula glutinis* (Kot et al., 2016),

the extremophile *Cryptococcus curvatus* (Gong et al., 2014b; Meesters et al., 1996), and the pathogenic pullulan-producer *Trichosporon pullulan* (Eroshin and Krylova, 1983).

In recent years, *Y. lipolytica* has been intensively utilized in the production of biofuels (Bao et al., 2021) and other products derived from lipids (Darvishi et al., 2017; Lu et al., 2021). *Y. lipolytica* is a non-conventional, ascomycetous yeast (belonging to class *Saccharomycetes*, order *Saccharomycetales*) that attracted attention for its remarkable lipolytic ability, hence earning the title "*lipolytica*" (Madzak, 2021) and encouraging various labs to study its biology (Abdel-Mawgoud et al., 2018) and biotechnological application (Miller and Alper, 2019). Hereby, the yeast has been investigated in various directions, i.e. as a model organism for dimorphism (Morales-Vargas et al., 2012; Pomraning et al., 2018), the study of tolerance under extreme environmental conditions (such as acidic, alkaline, hypersaline, and heavy metal-pollutions) (Mamaev and Zvyagilskaya, 2021), the secretion of recombinant proteins (Celińska and Nicaud, 2019; Korpys-Wozniak et al., 2021; Kubiak et al., 2019), environmental conservation (Bankar et al., 2009). Notably, *Y. lipolytica* received the "Generally regarded as safe" (GRAS) status by the Food and Drug Administration (FDA) (Groenewald et al., 2014). It uses a large array of carbon sources of either hydrophilic (such as glucose, fructose, mannose (Zeng SY et al., 2018), even lactose and xylose, sugar alcohol glycerol, and, to a lesser degree, organic acids and alcohols) (Barth and Gaillardin, 1997) or hydrophobic nature (such as fatty acids, triglycerides and alkanes) (Fickers et al., 2005; Soong et al., 2019). Naturally, *Y. lipolytica* can be found in various natural habitats, such as soil, water, plants, and animals (Barth and Gaillardin, 1997). It is commonly found in environments rich in lipids, such as dairy and alimentary products, oily foods, and lipid-rich waste streams, but also in the digestive tracts of insects and some animals (Sinigaglia et al., 1994).

Yeast can accumulate huge amounts of lipids which are rich in unsaturated fatty acids (namely OA and LA), through a typical aerobic FAS (Fakas, 2017), fundamentally similar to

the ones found in non-oleaginous species, such as *S. cerevisiae* (**Fig. 4**). The total lipid content in oleaginous and non-oleaginous species, however, drastically differs when cultivating them in different nutrient environments (Beopoulos et al., 2009; Ratledge, 2004). A well-known trigger for lipid accumulation in oleaginous microbes is nitrogen limitation in the presence of excess carbon. In contrast, when subjected to nitrogen-limited conditions, non-oleaginous yeasts tend to direct carbon towards the production of different types of polysaccharides (Kolouchova et al., 2016a; Parrou et al., 1999).

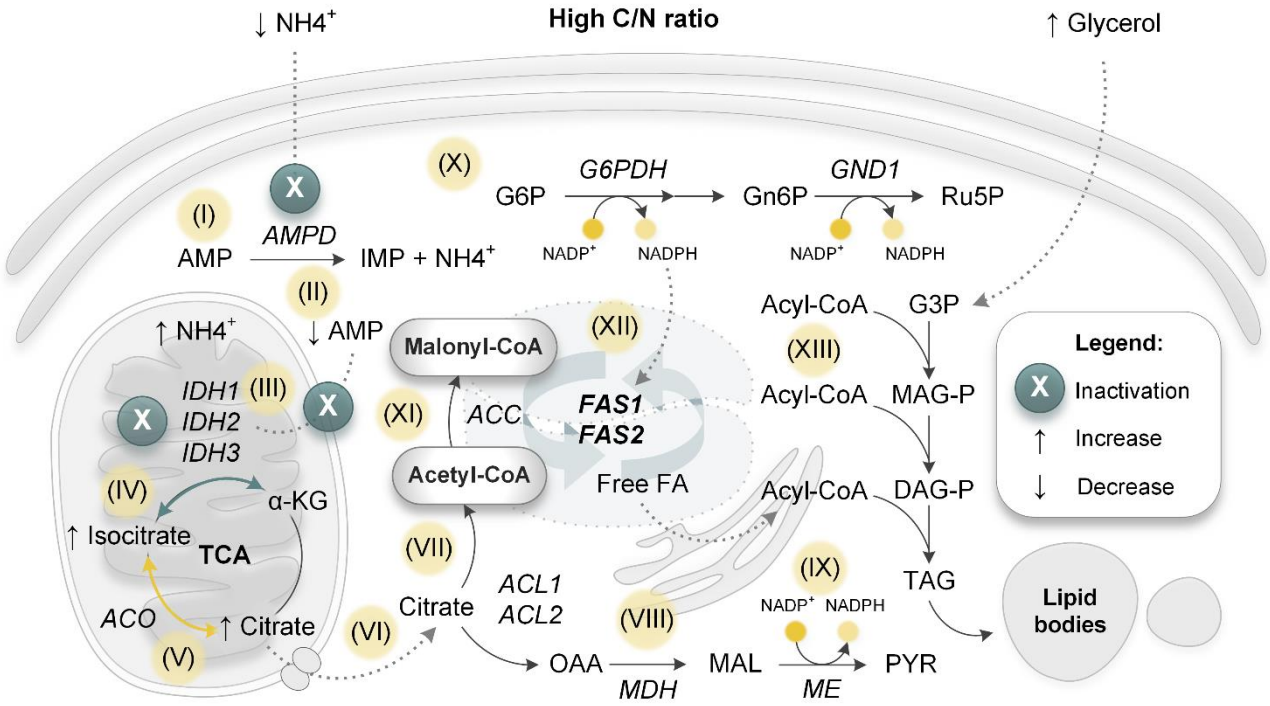

Figure 7. Cascade reactions triggered by nitrogen limitation in *Y. lipolytica.* The scheme highlights cascaded reactions which are induced by low ammonium and high carbon concentrations in the cultivation medium. TCA: tricarboxylic acid cycle; α-KG: α-ketoglutarate; AMP: adenosine monophosphate; IMP: inosine monophosphate; G6P: glucose-6-phosphate; Gn6P: gluconate 6-phosphate; Ru5P: ribulose-5-phosphate; FA: fatty acid; OAA: oxaloacetate; MAL: malate; PYR: pyruvate; G3P: glycerol-3-phosphate; MAG-P: monoacylglycerol phosphate; DAG-P: diacylglycerol phosphate; TAG: triacylglycerol phosphate.

The oleaginous cell adapts to nitrogen limitation in a way that its growth rate slows down while surplus carbon continues to be assimilated and is channeled towards lipid biosynthesis through a cascade of reactions (Moreira et al., 2021) (**Fig. 7**): (i) the allosteric activation of AMP deaminase (*AMPD*) drastically (ii) reduces the intracellular AMP concentration and

triggers the increase of ammonium ions in mitochondria (Morin et al., 2011). Due to its strong reliance on AMP, (iii) isocitrate dehydrogenase (*IDH1, IDH2*, *IDH3*) is inactivated (Morgunov et al., 2004), leading to (iv) isocitrate accumulation and conversion into (v) citrate by aconitase (*ACO*) (Blazeck et al., 2014; Ratledge and Wynn, 2002). Lastly, (vi) citrate is exported into the cytoplasm *via* the citrate shuttle (Yuzbasheva et al., 2019), where it is further (vii) metabolized into acetyl-CoA plus oxaloacetate *via* cytosolic ATP-dependent citrate lyase (*ACL1*, *ACL2*), an enzyme that exclusively exists in oleaginous organisms (Evans et al., 1983). Additionally, (viii) oxaloacetate is converted to malate by malate dehydrogenase (*MDH*) which finally yields (ix) pyruvate *via* the $NADP^+$-dependent malic enzyme (*ME*) (Zhang et al., 2013). In *Y. lipolytica*, however, the primary source of NADPH, required for fatty acid biosynthesis, appears to be the (x) cytoplasmic pentose phosphate (PP) pathway (Wasylenko et al., 2015). Cytosolic acetyl-CoA is carboxylated into malonyl-CoA (xi) through acetyl-CoA carboxylase (*ACC*). The fatty acid precursors plus NADPH are required for *de novo* biosynthesis of fatty acids, mediated by *FAS1* and *FAS2* (xii). Synthesized fatty acids are esterified (xiii) with glycerol-3-phosphate (G3P) into triacylglycerols (TAGs) and finally integrated into lipid droplets (Dulermo and Nicaud, 2011).

Being one of key players, citrate has a pivotal role in the lipid metabolism of oleaginous organisms (Cavallo et al., 2017). The metabolite provides a functional link between catabolic and anabolic reactions in the cell (Bellou et al., 2016) and its growth-decoupled secretion is categorized as a Gaden type II fermentation (Gaden, 1959). Other than through the cytosolic route, citrate is formed from acetyl-CoA and oxaloacetate through citrate synthase (*CS*) in the mitochondria and then transported to the cytoplasm, where it becomes the substrate for *ACL* (Jia et al., 2022). In terms of growth-coupled lipid production, the accumulation of citrate in *Y. lipolytica* is regarded undesired, as it withdraws carbon from lipid synthesis (Papanikolaou et al., 2002a; Qiao et al., 2017; Wang et al., 2013). On the other hand, when degraded, citrate can promote fatty acid biosynthesis (Goncalves et al., 2014), enabling

higher lipid content in citrate-supplemented cultures (Magdouli et al., 2020; Sabra et al., 2017).

2.5.2 A promising heterologous host for PUFA overproduction

In different studies, *Y. lipolytica* was upgraded to produce omega-6 and omega-3 PUFAs, based on using the highly abundant saturated fatty acids OA and LA as starter molecules and obtained the PUFAs of interest through an extension of the native FAS pathway using different combinations of elongases and desaturases. Starting efforts revealed a tremendous tunability of the yeast to provide different PUFAs (**Table 1**).

As example, heterologous expression of Δ6-desaturase from *M. alpina* in *Y. lipolytica* enhanced the GLA level to 6.2% of TFA and yielded 71.6 mg L^{-1} GLA, when cultivating the mutant at lower temperature (Sun et al., 2017). Recombinant *Y. lipolytica*, expressing codon-optimized Δ6-desaturase, Δ5-desaturase, and Δ6-elongase (again from *M. alpina*), produced ARA and its metabolic intermediates DGLA and GLA with 0.4%, 0.8% and 9.0% of TFA, respectively (Liu et al., 2017). Terminal pathway engineering with overexpression of Δ9-elongase and Δ8-desaturase (from *I. galbana*) increased the ARA level to 118.1 mg L^{-1} (Liu et al., 2019c). Moreover, introduction of a bifunctional Δ12/Δ15 desaturase from *Rhodosporidium kratochvilovae* in combination with low temperature fermentation resulted in the accumulation of almost 1.4 g L^{-1} of the omega-3 ALA (Cordova and Alper, 2018).

The milestone in PUFA research in *Y. lipolytica* was the production of EPA at commercial level (Xue et al., 2013) (**Fig. 8A**). For this purpose, various combinations of heterologous enzymes belonging to the alternative aerobic Δ8-pathway (Δ9-elongase, Δ8, Δ5, and Δ17-desaturase) from different native producers (algae, euglenoids, and fungi), such as *Fusarium moniliforme*, *Euglena gracilis*, and *M. alpina* were implemented and tested. The development finally resulted in EPA accumulation up to 56.6% of TFA and 15.0% by cell dry

weight with saturated fatty acids remaining below 5%. Inactivation of peroxisome biogenesis *via* deletion of the *PEX10* gene and improvement of the fermentation process finally boosted EPA 25.0% by weight (Xie et al., 2017).

Table 1. Production of omega-3 and omega-6 PUFAs using different *Yarrowia lipolytica* hosts and strategies. The table summarizes recent omega-3 and omega-6 PUFA production processes in genetically engineered *Y. lipolytica,* implementing different production strategies. EPA: eicosapentaenoic acid; DHA: docosahexaenoic acid; ALA: α-linolenic acid; ARA: arachidonic acid; GLA: γ-linolenic acid; DGLA: dihomo-γ-linolenic acid; TFAs: total fatty acids; CDM: cell dry mass.

[a] – heterologous overexpression of aerobic PUFA pathway(s), [b] – heterologous expression of anaerobic PUFA pathway.

PUFA	Structure	Titer [mg L^{-1}]	Selectivity [% of TFAs]	Yield [mg g_{CDM}^{-1}]	Reference
EPA[a]	C20:5 (**ω3**)	/	56.0	222	(Xie et al., 2017)
DHA[b]	C22:6 (**ω3**)	350	16.8	17	(Gemperlein et al., 2019)
ALA[a]	C18:3 (**ω3**)	1,400	17.0	70	(Cordova and Alper, 2018)
ARA[a]	C20:4 (**ω6**)	120	0.8	12	(Liu et al., 2019c)
GLA[a]	C18:3 (**ω6**)	1,780	9.0	/	(Liu et al., 2017)
DGLA[a]	C20:3 (**ω6**)	160	0.8	/	(Liu et al., 2017)

2.5.3 PKS-like PUFA synthases empower growth-decoupled DHA production

A recent study demonstrated that *Y. lipolytica* can synthetize DHA *de novo* upon heterologous expression of a polyketide synthase-like PUFA synthase (**Fig. 8B**). In brief, the used myxobacterial PKS-like PUFA cluster encoded a PUFA synthase and a phosphopantetheinyl transferase (PPTase), harboring in total 17 subdomains (Gemperlein et al., 2014). The enzymes function as a complex that yields DHA *via* 10 consecutive catalytic cycles (Ye et al., 2015).

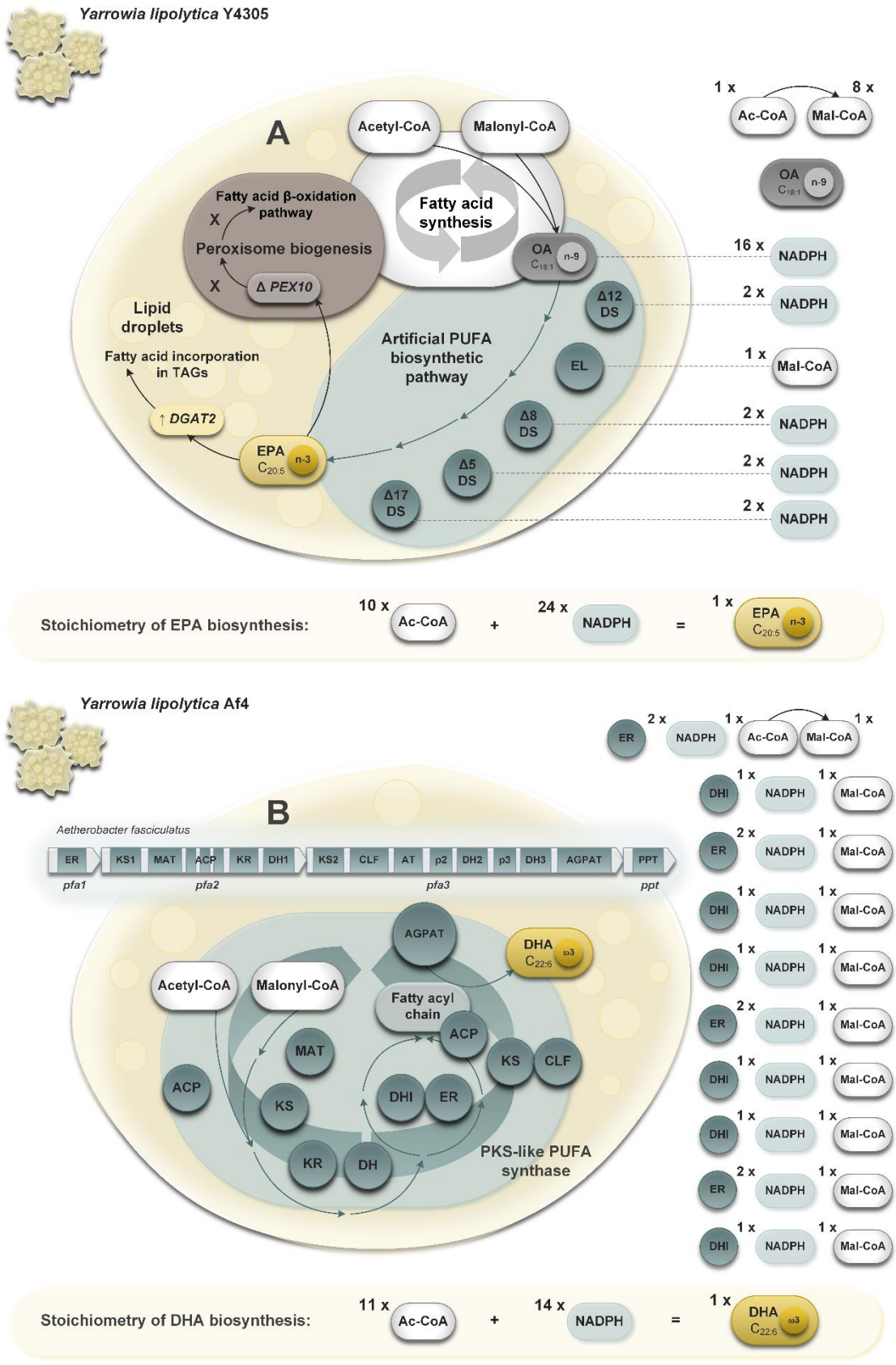

Figure 8. *Yarrowia lipolytica* hosting different genes for the production of marine PUFAs. *Y. lipolytica* Y4305 strain expressing codon-optimized desaturases and elongases from different PUFA producers, enabling NADPH-expensive production of EPA. Further modifications imply altering TAG biosynthesis and peroxisomal biogenesis, by overexpressing *DGAT2* and deleting *PEX10*, respectively (Xie et al., 2017) (A). *Y. lipolytica* Af4 harbors an anaerobic NADPH-efficient PUFA cluster from *A. fasciculatus*, allowing *de novo* synthesis of DHA (Gemperlein et al., 2019).

After genomic insertion of different variants of codon-optimized and refactored/hybrid myxobacterial gene clusters from *Aetherobacter fasciculatus* into *Y. lipolytica* provided a set of mutants with elevated DHA content up to 16.8% of TFA. A specific *pfa* cluster, containing *pfa1*, *pfa2*, *pfa3* and *ppt* domains provided up to 350 mg L^{-1} of DHA, supported by optimized fed-batch fermentation (Gemperlein et al., 2019).The advantage of using PUFA synthases for *de novo* DHA synthesis, as opposed to the classical aerobic pathway, lies in an almost 50% lower demand for NAD(P)H, providing an interesting concept, also for this work. However, due to its high level of dynamic complexity, the optimization of this process presents a significant challenge.

3 MATERIALS AND METHODS

3.1 Strains

The uracil-auxotrophic yeast *Y. lipolytica* Po1h (CLIB 882) and its prototrophic DHA-producing derivative Po1h::SynPfaPptAf4 that expressed a myxobacterial PUFA synthase and a phosphopantetheinyl transferase (PPTase) from the myxobacterium *A. fasciculatus* (SBSr002), respectively, were obtained from previous work (Gemperlein et al., 2019).

3.2 Growth and DHA production media

Different media were used to grow *Y. lipolytica*. Complex YPD medium contained 20 g L^{-1} of glucose, 20 g L^{-1} of peptone (Becton Dickinson, Heidelberg, Germany), and 10 g L^{-1} of yeast extract (Sigma Aldrich, Saint Louis, MO, USA). For YPD plate cultures, 20 g L^{-1} agar was added (Becton & Dickinson). In addition, a minimal medium was used. In its basic composition, it contained 10 g L^{-1} of glycerol, 5 g L^{-1} of $(NH_4)_2SO_4$, and 1.7 g L^{-1} of yeast nitrogen base (YNB) without amino acids and $(NH_4)_2SO_4$ (Sigma Aldrich) in 200 mM MES buffer (pH 6.8). As specified below, the medium formulation was modified as follows throughout this work: (i) replacement of glycerol by glucose, (ii) increased glycerol level, (iii) varied carbon-to-nitrogen (C/N) ratio, and (iv) varied carbon-to-phosphorous (C/P) ratio, respectively (**Table 2**).

Table 2. Variation of the composition of essential nutrients in the growth medium of *Y. lipolytica* and the resulting nutrient ratios (C/N and C/P).

Carbon source		Nitrogen source		Phosphorus source		C/N ratio	C/P ratio
Glucose	10 g L^{-1}	$(NH_4)_2SO_4$	5 g L^{-1}	KH_2PO_4	0.65 g L^{-1}	4.3	41.3
Glycerol	10 g L^{-1}	$(NH_4)_2SO_4$	5 g L^{-1}	KH_2PO_4	0.65 g L^{-1}	4.4	48.7
Glycerol	20 g L^{-1}	$(NH_4)_2SO_4$	5 g L^{-1}	KH_2PO_4	0.65 g L^{-1}	8.6	95.2
Glycerol	20 g L^{-1}	$(NH_4)_2SO_4$	5 g L^{-1}	KH_2PO_4	1.30 g L^{-1}	8.6	41.3
Glycerol	40 g L^{-1}	$(NH_4)_2SO_4$	5 g L^{-1}	KH_2PO_4	0.65 g L^{-1}	17.2	190.4

In further studies that explored different feeding strategies, the minimal medium formulation with 20 g L^{-1} of glycerol, 5 g L^{-1} of $(NH_4)_2SO_4$, and 1.7 g L^{-1} of yeast nitrogen base without amino acids and $(NH_4)_2SO_4$ in 200 mM MES buffer (pH 6.8) was set as reference condition (**Table 2** – marked in grey). In selected experiments, it was supplemented with different nutrients at the beginning of the stationary phase, i.e. citrate (10 mM and 20 mM), L-lysine (10 mM), L-leucine (10 mM), and L-isoleucine (10 mM), respectively. In isotopic tracer studies, ^{13}C-enriched supplements were added instead: 10 mM 99% [$^{13}C_6$] citrate (Sigma Aldrich), 10 mM 99% [$^{13}C_6$] L-lysine (Cambridge Isotope Laboratories, Andover, MA, USA), and 10 mM 99% [$^{13}C_6$] L-leucine (Cambridge Isotope Laboratories), respectively. When growing the wild type, 50 mg L^{-1} of uracil was added to all growth media.

3.3 Batch cultivation in shake flasks

One loopful of cells, propagated on YPD agar for 24 h at 30 °C, was used to inoculate the first preculture (25 mL YPD medium in 250 mL baffled flasks), which was then incubated on a rotary shaker (28 °C, 230 rpm, 75% humidity, Multitron, Infors AG, Bottmingen, Switzerland). After 8 h, cells were harvested (3,000 *x* g, 2 min, 20 °C), resuspended in freshly prepared medium, inoculated to the second preculture (50 mL YNB medium in 500 mL baffled flasks) to an initial OD_{600} = 0.1 and grown overnight under the same conditions. Then, cells were harvested as described above and used to inoculate the main cultures to an initial OD_{600} = 1 (50 mL YNB medium in 500 mL baffled flasks) which were then grown under the same conditions (Dobrowolski and Mironczuk, 2020). All experiments were conducted in biological triplicate. To adjust the biological replicates and avoid artifacts in inoculation due to cell clumping, the inoculum was preferably mixed with 150 mL medium in one big flask (1000 mL non-baffled flask) and divided (into three 50 mL portions in 500 mL baffled flasks) after gentle mixing for around 1 minute.

3.4 DHA production in lab scale bioreactors

The performance of DHA production was evaluated in 1 L lab scale bioreactors. These were monitored and controlled using the DASGIP control software (SR0700ODLS, Eppendorf, Hamburg, Germany). Hereby, different formulations were used as batch medium (500 mL), containing a synthetic mixture of vitamins and trace elements that matched the composition of commercial yeast nitrogen base without amino acids and ammonium sulfate (**Table 3**). Six separate stock solutions (vitamins, trace elements, salts, biotin, folic acid, and ferric chloride) were freshly prepared, sterilized by filtration, and stored at 4°C in the dark for up to 4 weeks. Prior to use, the solutions were mixed.

Table 3. Synthetic formulation of vitamins and trace metals as supplement for growth of *Y. lipolytica*. For each compound, the given concentration reflected the amount contained in yeast nitrogen base (YNB) w/o amino acids and ammonium sulphate, used as a commercial supplement in initial cultivations at a level of 1.7 g L^{-1}. The data comprise the individual compounds, the corresponding formula, the amount in mg required for 1 L of solution, the supplier, and the final concentration. The pH of the trace element and the iron stock was adjusted to 1.0 using 5M HCl respectively.

100 x Vitamin stock solution				
Calcium pantothenate	$C_{18}H_{32}CaN_2O_{10}$	40 mg	Sigma	400 µg L^{-1}
Inositol	$C_6H_{12}O_6$	200 mg	Sigma	2000 µg L^{-1}
Nicotinic acid	$C_6H_5NO_2$	40 mg	Sigma	400 µg L^{-1}
p-Aminobenzoic acid	$C_7H_7NO_2$	20 mg	Sigma	200 µg L^{-1}
Pyridoxine hydrochloride	$C_8H_{12}ClNO_3$	40 mg	Sigma	400 µg L^{-1}
Riboflavin	$C_{17}H_{20}N_4O_6$	20 mg	Sigma	200 µg L^{-1}
Thiamine hydrochloride	$C_{12}H_{18}Cl_2N_4OS$	40 mg	Sigma	400 µg L^{-1}
1000 x Biotin stock solution				
Biotin	$C_{10}H_{16}N_2O_3S$	2 mg	Sigma	2 µg L^{-1}
1000 x Folic acid stock solution				
Folic acid	$C_{19}H_{19}N_7O_6$	2 mg	Sigma	2 µg L^{-1}
100 x Trace element stock solution (pH = 1.9)				
Boric acid	H_3BO_3	50 mg	Sigma	500 µg L^{-1}
Copper sulfate	CuO_4S	4 mg	Sigma	40 µg L^{-1}
Natrium Iodide	NaI	10 mg	Honeywell	100 µg L^{-1}
Manganese sulfate	$MnSO_4 \cdot H_2O$	44.8 mg	Roth	400 µg L^{-1}
Sodium molybdate	$Na_2MoO_4 \cdot 2H_2O$	23.5 mg	Sigma	200 µg L^{-1}
Zinc sulfate	$ZnSO_4 \cdot 7H_2O$	71.2 mg	Sigma	400 µg L^{-1}

1 x Salt solution				
Potassium phosphate monobasic	KH_2PO_4	1000 mg	Honeywell	1 g L^{-1}
Magnesium sulfate	$MgSO_4 \cdot 7H_2O$	1036 mg	Grüssing	500 mg L^{-1}
Sodium chloride	NaCl	100 mg	Grüssing	100 mg L^{-1}
Calcium chloride	$CaCl_2 \cdot 2H_2O$	132 mg	Sigma	100 mg L^{-1}
100 x Ferric chloride stock solution (pH=1.0)				
Ferric chloride	$FeCl_3 \cdot 6H_2O$	33.33 mg	Sigma	200 µg L^{-1}

Six different process configurations were tested, comprising three batch and three fed-batch set-ups. Firstly (reference), containing per liter: 100 g of glycerol, 5 g of $(NH_4)_2SO_4$, 1.04 g MgSO4 · 7 H2O, 1 g of KH_2PO_4, 130 mg $CaCl_2 \cdot 2\ H_2O$, 100 mg NaCl, 33 mg of $FeCl_3 \cdot 6\ H_2O$, 5 mL of a vitamin solution (200 mg L^{-1} inositol, 40 mg L^{-1} calcium pantothenate, 40 mg L^{-1} nicotinic acid, 40 mg L^{-1} pyridoxine · HCl, 39 mg L^{-1} thiamine · HCl, 20 mg L^{-1} aminobenzoic acid, 20 mg L^{-1} riboflavin, 0.2 mg L^{-1} biotin, 0.2 mg L^{-1} folic acid), 5 mL of a trace element solution (71 mg L^{-1} $ZnSO_4 \cdot 7\ H_2O$, 50 mg L^{-1} boric acid, 45 mg L^{-1} $MnSO_4 \cdot H_2O$, 23.5 mg L^{-1} $Na_2MoO_4 \cdot 2\ H_2O$, 10 mg L^{-1} NaCI, 4 mg L^{-1} $CuSO_4$, pH = 1.0) and 200 mM MES buffer (pH 6.5). Secondly (phosphate-enriched) per liter: 100 g of glycerol, 5 g of $(NH_4)_2SO_4$, 2 g of KH_2PO_4, 1.04 g of MgSO4 · 7 H2O, 130 mg of $CaCl_2 \cdot 2\ H_2O$, 100 mg of NaCl, 33 mg of $FeCl_3 \cdot 6\ H_2O$, 5 mL of vitamin stock, 5 mL of trace element stock, and 200 mM MES (pH 6.5). Thirdly (nitrogen-enriched) per liter: 100 g of glycerol, 10 g of $(NH_4)_2SO_4$, 1.04 g MgSO4 · 7 H2O, 1 g of KH_2PO_4, 130 mg of $CaCl_2 \cdot 2\ H_2O$, 100 mg of NaCl, 33 mg of $FeCl_3 \cdot 6\ H_2O$, 5 mL vitamin stock, 5 mL trace element stock, and 200 mM MES (pH 6.5).

The three media were additionally used for the batch phase of three fed-batch processes which additionally included pulse-wise feeding of L-lysine from a concentrated stock (3.0 M), resulting in totally six different conditions (**Table 4**). During the process, antifoam 204 (Sigma Aldrich) was added manually, when needed.

In all cases, one loopful of cells, propagated on YPD agar for 24 h at 30 °C, was used to inoculate the first preculture (3x 50 mL YPD medium in 500 mL baffled flasks), which was

incubated on a rotary shaker (28 °C, 230 rpm, 75% humidity, Multitron, Infors AG, Bottmingen, Switzerland). After 8 h, cells were harvested (3,000 *x* g, 2 min, 20 °C), inoculated to the second preculture (3x 100 mL YNB medium in 1000 mL baffled flasks) to an initial OD_{600} = 0.1, and grown overnight under the same conditions. Then, cells were harvested as described above and used to inoculate the production process. During the process, the temperature was kept at 28 °C ± 0.1 (CWD4 Bioblock, Eppendorf). The pH value was controlled above 3.0 ± 0.1 using a pH probe (405-DPAS-SC-K8S/225, Mettler Toledo, Giessen, Germany) and automatic addition of 6 M NaOH (MP8 pump system, Eppendorf). The level of dissolved oxygen (DO) was monitored using an electrode (Hamilton, Höchst, Germany) and controlled (above 20% saturation during the initial growth phase and above 5% saturation afterwards) by automatic adjustment of the stirrer speed (up to 1,500 rpm) and the aeration rate (up to 1 VVM). Every set-up was conducted in duplicate.

Table 4. Composition of the fermentation medium for testing six different nutrient conditions in lab-scale bioreactors. Abbreviations: C - carbon; N – nitrogen; P – phosphorous.

Designation	C source ●	N source ●	P source ●	C/N ratio	C/P ratio	Feeding ●
C-N-P (●●●)	100 g L^{-1} glycerol	5 g L^{-1} $(NH_4)_2SO_4$	0.65 g L^{-1} KH_2PO_4	43	476	/
C-N-P (●●●) L-Lysine (●●●)	100 g L^{-1} glycerol	5 g L^{-1} $(NH_4)_2SO_4$	0.65 g L^{-1} KH_2PO_4	43	476	150 mM L-Lysine
C-N-2P (●●●●)	100 g L^{-1} glycerol	5 g L^{-1} $(NH_4)_2SO_4$	1.3 g L^{-1} KH_2PO_4	43	238	/
C-N-2P (●●●●) L-Lysine (●●●)	100 g L^{-1} glycerol	5 g L^{-1} $(NH_4)_2SO_4$	1.3 g L^{-1} KH_2PO_4	43	238	150 mM L-Lysine
C-2N-P (●●●●)	100 g L^{-1} glycerol	10 g L^{-1} $(NH_4)_2SO_4$	0.65 g L^{-1} KH_2PO_4	21.5	476	/
C-2N-P (●●●●) L-Lysine (●●)	100 g L^{-1} glycerol	10 g L^{-1} $(NH_4)_2SO_4$	0.65 g L^{-1} KH_2PO_4	21.5	476	100 mM L-Lysine

3.5 Quantification of substrates and products

3.5.1 Cell concentration

The cell concentration was inferred from photometric measurement of the optical density at a wavelength of 600 nm (OD_{600}). In addition, the cell dry mass (CDM) was determined gravimetrically after cell harvest (15,000 × *g*, 4 °C, 10 min), washing of the obtained pellet with 15 mL deionized water, and freeze drying. Systematic parallel measurements provided a linear correlation between CDM and OD_{600} (CDM [g L^{-1}] = 0.424 x OD_{600}) which enabled to infer CDM values from OD_{600} readings.

3.5.2 Glucose, glycerol, citrate and acetate

Culture supernatant was obtained from broth by centrifugation (16,000 x *g*, 3 min, 4 °C). Glucose, glycerol, citrate, and acetate were then quantified by HPLC (Agilent 1200 series, Waldbronn, Germany) using an Aminex HPX-87H column (300 x 7.8 mm, 9 µm, Bio-Rad, Hercules, CA, USA) at 45 °C and elution with 12 mM H_2SO_4 at a flow rate of 0.5 mL min^{-1}. The analytes were detected by refraction index, and external standards were used for quantification.

3.5.3 Phosphate and ammonium

Phosphate and ammonium were quantified by ion exchange chromatography (Dionex Integrion HPIC System, Thermo Fisher Scientific, Waltham, MA, USA). Phosphate was quantified using a Dionex IonPac AS9-HC column at 30 °C (2 × 250 mm, Thermo Fisher Scientific) as stationary phase and 12 mM Na_2CO_3 (0.25 mL min^{-1}) as mobile phase. Ammonium was quantified using a Dionex IonPac CS column at 40 °C (2 x 250 mm, Thermo

Scientific, CA, USA) as stationary phase and 30mM methanesulfonic acid (0.16 mL min^{-1}) as mobile phase. Both ions were detected using suppressed conductivity analysis and quantified *via* external standards.

3.5.4 Fatty acids

A culture volume containing approximately 5 mg of CDM was sampled, centrifuged (12,000 × *g*, 5 min, 4 °C), and dried (Savant DNA120 SpeedVac Concentrator, Thermo Scientific, 60 min, 65 °C). Then, 15 µg of the methyl ester of n-3 heneicosapentaenoic acid (HPA, C22:5) (Cayman Chemical, Ann Arbor, MI, USA) was added as internal standard. Subsequently, transesterification of the fatty acids into the corresponding fatty acid methyl esters (FAMEs) was carried out by adding 300 µL of reagent (50% methanol, 50% toluene, 2% H_2SO_4), and incubating the mixture overnight at 80 °C. Afterwards, 250 µL of a stop solution (0.5 M NH_4HCO_3, 2 M KCl) was added, and the mixture was vortexed for 30 s followed by centrifugation (10,000 × *g*, 5 min, room temperature). After phase separation, the upper phase containing the FAMEs was used for GC-MS analysis. The measurement was carried out on a gas chromatograph (Agilent 6890N, Agilent Technologies, Santa Clara, CA, USA), equipped with an analytical capillary column (Agilent HP-88, 30 m × 250 µm × 0.2 µm, Agilent Technologies), and coupled to a mass-selective detector (5973 Network Mass Selective Detector, Agilent Technologies) (Sahin et al., 2018). Helium 5.0 was used as carrier gas. Initially, the column temperature was kept at 110 °C for 1 min and was then increased by 4 °C min^{-1} up to 240 °C. This temperature was maintained for the rest of the measurement (33.5 min). For analysis, 1 µL sample was injected at a split ratio of 5:1. Furthermore, the following temperature settings were used: inlet 250 °C, MSD transfer line 280 °C, ion source 230 °C, and quadrupole 150 °C. A typical fatty acid methyl ester total ion current (TIC) spectrum of recombinant *Y. lipolytica* is shown in **Figure 9**. As shown, all

analytes could be separated and detected. For quantification, the individual peaks were manually integrated. The obtained peak areas [AUC] and the corresponding mass [µg] of the fatty acid of interest (FA) in the sample was then determined on basis of the used internal standard (IS), as described above HPA (**Eq. 1**).

$$\text{FA [µg]} = \frac{\text{FA [AUC]}}{\text{IS [AUC]}} \text{ x IS [µg]} \qquad \textbf{(Eq. 1)}$$

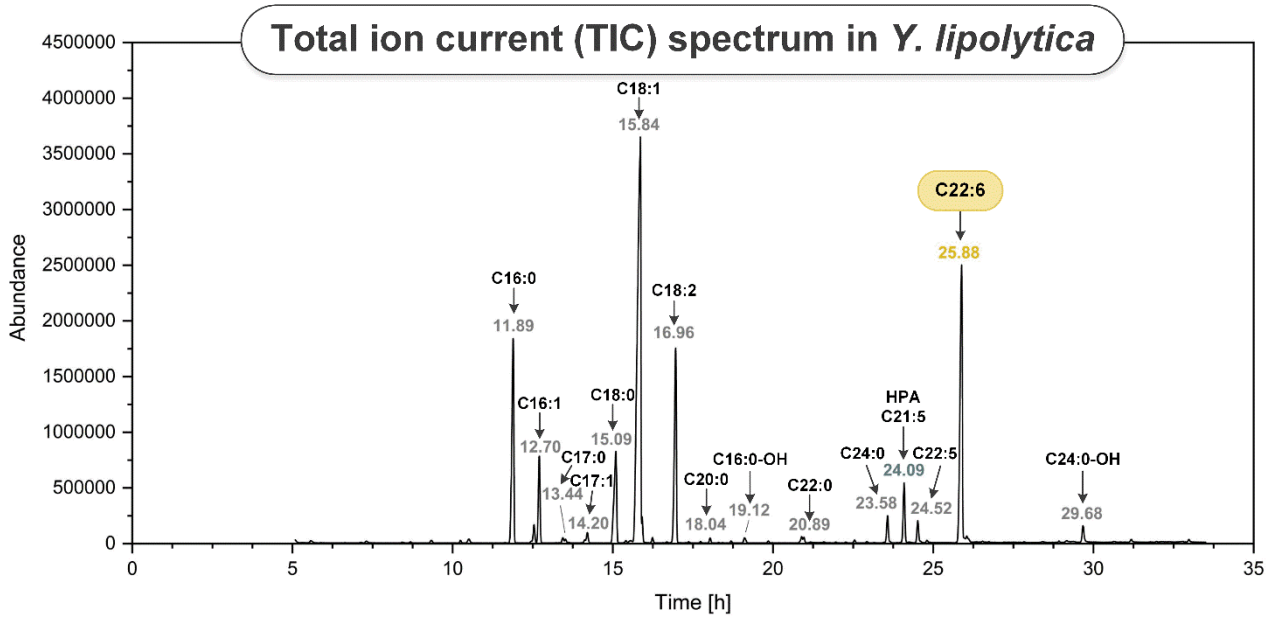

Figure 9. Total ion current (TIC) spectrum in *Y. lipolytica*. Figure displays peaks corresponding to 12 native fatty acid methyl esters (C16:0 – hexadecanoic (palmitic) acid; C16:1 – *9*-hexadecenoic (palmitoleic) acid, C17:0 – heptadecanoic (margaric) acid; C17:1 – *9*-heptadecenoic acid; C18:0 – octadecanoic (stearic) acid; C18:1 – *9*-octadecenoic (oleic) acid; C18:2 – *9,12*-octadecadienoic (linoleic) acid; C20:0 – eicosanoic (arachidic) acid; C16:0-OH – *2*-hydroxyhexadecanoic acid; C22:0 – docosanoic (behenic) acid; C24:0 – tetracosanoic (lignoceric) acid and C24:0-OH – *2*-hydroxytetracosanoic acid), two heterologously synthetized fatty acid methyl esters (C22:5 – *4,7,10,12,16*-docosapentaenoic acid, DPA and C22:6 – *4,7,10,12,16,19*-docosahexaenoic acid, DHA) and internal standard (C21:5 – *6,9,12,15,18*-heneicosapentaenoic acid; HPA).

3.5.5 Amino acids

Amino acids in culture supernatant were quantified by HPLC (Agilent 1200 series, Agilent Technologies) after pre-column derivatization with *o*-phthaldialdehyde and fluorenylmethyloxycarbonyl chloride (Rohles et al., 2018a). The analytes were separated on

a reversed phase column (Gemini 5 µm C18 110 Å, 150 × 4.6 mm, Phenomenex, Aschaffenburg, Germany) at 40 °C using the following gradient of eluent A (20 mM NaH_2PO_4, 0.5 g L^{-1} sodium azide, pH 7.8) and B (45% acetonitrile, 45% methanol, 10% deionized water) at a flow rate of 1 mL min^{-1}: 0 min, 0% B; 0-44.5 min, 0-44.5% B; 44.5-45 min, 44.5-61.0% B; 45-48 min, 61-82% B; 48-48.5 min, 82-100% B; 48.5-51 min, 100-0% B. Fluorescence detection was carried out at 340/450 nm, and α-aminobutyric acid was used as internal standard (Krömer et al., 2005).

3.6 Metabolome analysis

3.6.1 Extraction and quantification of intracellular CoA-thioesters

Absolute quantification of CoA-thioesters was based on LC-ESI-MS/MS, previously validated for different microbes, including *Y. lipolytica* (Gläser et al., 2020). To enable the accurate analysis of samples that exhibited high cell concentrations and partially low abundant analytes of interest, the protocol was adapted as follows. Briefly, cells were collected (5 mg CDM during the exponential growth phase, 20 mg CDM during the stationary phase) and immediately mixed with 500 µL of a ^{13}C-labelled extract (prepared before from cells grown on 99% [$^{13}C_3$] glycerol, Cambridge Isotope Laboratories), and 5 mL ice-cold quenching solution (25 mM formic acid, 95% acetonitrile). The mixture was incubated for 10 min on ice. Cell debris was removed by centrifugation (15,000 × *g*, 4 °C, 10 min), including two washing steps with 10 mL super-cold deionized water (Gläser et al., 2021). The supernatant was frozen in liquid nitrogen, freeze-dried, and resuspended in an acidic buffer (25 mM ammonium formate, 2% MeOH, pH 3.0, 4 °C). The CoA thioesters in the extract were analysed using LC-ESI-MS/MS (QTRAP 6500+, AB Sciex, Darmstadt, Germany), coupled to an HPLC system (Agilent 1290 Infinity System, Agilent). The analytes were separated at 40°C on a reversed phase column (Kinetex XB-C18, 100×2.1 mm, 2.6 µ,

100 Å, Phenomenex, Aschaffenburg, Germany) using the following gradient of eluent A (50 mM formic acid, 25% ammonium hydroxide, pH 8.1) and eluent B (100% methanol) at a flow rate of 300 µL min^{-1}: 0-10% B (0-7 min); 10-100% B (7-10 min); 100% B (10-11 min); 100-0% B (11-12 min); 0% B (12-15). Multiple reaction monitoring (MRM) was used to detect acetyl-CoA, malonyl-CoA, succinyl-CoA, butyryl-CoA, hydroxybutyryl-CoA, 2-metyhl-butyryl-CoA, crotonyl-CoA, propionyl-CoA, isovaleryl-CoA, and hydroxymethyl-glutaryl-CoA (HMG-CoA) (Gläser et al., 2020). Isovaleryl-CoA and 2-metyhl-butyryl-CoA co-eluted while exhibiting identical mass and were therefore determined as lumped pool.

3.6.2 Extraction and quantification of intracellular amino acids

Intracellular amino acids were sampled and extracted using vacuum filtration (Wittmann et al., 2004). The protocol had been previously validated for different yeasts (Bolten and Wittmann, 2008). In brief, 0.5 mL of culture broth was filtered quickly through cellulose nitrate membranes (0.2 µm x 47 mm, Sartorius, Göttingen, Germany), including a washing step with deionized water. The cell-containing filter was transferred into boiling water (containing 220 µM α-aminobutyrate as internal standard) and incubated at 100 °C for 15 min. The obtained extract was cooled down on ice, clarified from debris (16,000 × *g*, 4 °C, 5 min), and the contained amino acids were quantified by HPLC as described above.

3.7 Transcriptome analysis

3.7.1 RNA extraction

In this study, various RNA extraction protocols were evaluated to develop an optimal approach for *Y. lipolytica* based cultures. In short, cells were collected from 2 mL broth (16,000 × *g*, 4 °C, 30 s) and fast-frozen in liquid nitrogen. Total RNA was then extracted and

purified using (i) Direct-zol RNA Microprep Kit (Zymo Research, Freiburg, Germany) (Cervenak et al., 2019); (ii) the NucleoZol and phenol extraction method (Kamineni et al., 2020); (iii) the Qiagen RNeasy Mini Kit (Qiagen, Hilden, Germany) (Ryu and Trinh, 2018); and (iv) the RiboPure RNA Purification Kit (Thermo Fisher Scientific) (Sabra et al., 2017). For the first and second set-up (i, ii), cells were disrupted using NucleoZol (Macherey-Nagel, Lab Supplies, Athens, Greece) and 0.1 mm silica beads (Lysing matrix B, MP Biomedicals, Illkirch-Graffenstaden, France), followed by homogenization in three consecutive cycles (6500 rpm for 20s each), with 1 min breaks on ice in between (Precellys 24, Bertin Technologies, Montignyle-Bretonneux, France). Subsequent RNA extraction and purification was done as previously described.

For the other two protocols (iii, iv), mechanical cell disruption and further preparations for RNA purification were performed as recommended by the manufacturers. In all cases, the obtained purified RNA was thereupon treated with the TURBO DNA-free Kit (Thermo Fisher Scientific) to remove remaining DNA, followed by RNA quantification (NanoDrop 1000 Spectrophotometer, PEQLAB Biotechnology, Erlangen, Germany). A denaturing gel electrophoresis (1% agarose, 1 x TAE buffer, 12% sodium hypochlorite) and a high-resolution microfluidic electrophoresis (RNA 6000 Nano kit, Agilent 2100 Bioanalyzer, Agilent Technologies) were performed to assess the quality and quantity of the extracted RNA in the samples. Hereby, (i) the formation of distinct bands for the ribosomal subunits (26S, 18S, 5 and 5.5S rRNA) of *Y. lipolytica* helped to exclude potential RNA degradation by RNAse activity (Aranda et al., 2012). In addition, the Agilent 2100 Bioanalyzer System software (Plant RNA assay) generated a report that provided information on the RNA integrity number (RIN). In this work, only high-quality samples that exhibited RIN > 8.5 were processed further.

3.7.2 Quantitative real-time PCR

Purified total RNA samples went through another round of DNA digestion (TURBO DNA-free Kit (Thermo Fisher Scientific). The resulting extracts were reverse-transcribed into cDNA (Maxima First Strand cDNA Synthesis Kit for RT-qPCR, Thermo Fisher Scientific). The obtained cDNA samples were then utilized for qPCR using the PowerUp SYBR Green qPCR Master Mix (Thermo Fisher Scientific) and selected primer pairs (**Table 5**) in a final volume of 20 µL (QuantStudio3, Thermo Fisher Scientific).

Table 5. Primers used for qRT-PCR analysis of *Y. lipolytica*. AT: annealing temperature.

Gene ID	Name	Sequence 5'-3'	AT (°C)
YalifMr30	26S_FW	ACACCTCGATGTCGGCTTAC	47
	26S_RV	ACCGTGCTATCTCACAATGC	
YALI0D08272g	ACT_FW	AACTGTTGCCCTCGTTATCG	54
	ACT_RV	GGGCCTCATCACCAACATAG	
YALI0E34793g	ACL1_FW	TCTTGAGTCGCTTCTGATCG	51
	ACL1_RV	GTCGATCTCATGCGATCTTG	
YALI0D24431g	ACL2_FW	AGTCCGGCGCCAAGTTTGTG	56
	ACL2_RV	TTCGCAGCACTCCGTCAATG	
YALI0C11407g	ACC_FW	TGAGGAGGCTCCTGTGACTG	51
	ACC_RV	GAGGATTCAGCTCCAAGAAG	
YALI0B15059g	FAS1_FW	GCCCAGCGAACCCTTAAGTC	52
	FAS1_RV	CCTCATCGGCAAGGTAGTAG	
YALI0B19382g	FAS2_FW	GTCATACCTCGGTAGAAGAC	54
	FAS2_RV	TGAGGACATGAAGGCTAAGG	
YALI0C16797g	ACAD_FW	GGGCGTCGTGGTATTTGTGG	50
	ACAD_RV	AACTCTCCCGAATCTCTGTG	
YALI0E32035g	TGL_FW	TATGGTCACTGCTGCTCTTG	48
	TGL_RV	CAGATGCTGTCTACTCTACC	
pfa1_ER	pfa1_ER_FW	AGCGACGAGCCGGAGAATAC	54
	pfa1_ER_RV	AATCGAACGCCGTGGACCTC	
pfa2_ACP$_2$	pfa2_ACP2_FW	CTGCCGAGATGCTCGGAATG	54
	pfa2_ACP2_RV	AACGACCTCGGGCAGGTTAG	
pfa3_CLF	pfa3_CLF_FW	CCCTATTGCCGTGATCTCCC	55
	pfa3_CLF_RV	CAGGGTTTGCTCCAGATCTC	

The used primers were designed as 20bp sequences of the target genes of interest. Their efficiency was validated in separate amplification reactions prior to application, using different concentrations of primer and genomic DNA. All primers used in this study exhibited a proven efficiency between 0.9 and 1.2. After validation, we used the 26S rDNA as endogenous control for data normalization (Borkowska et al., 2020; Rodriguez et al., 2016; Theron et al., 2020). The qRT-PCR cycles were conducted using the following parameters: hold stage (50 °C, 2 min; 95 °C, 2 min), 40 PCR cycles (95 °C, 15 s; 60 °C, 15 s; 72 °C, 1 min); melt curve stage (96 °C, 15 s; 60°C, 1 min; 95 °C, 15 s). The obtained data were processed by the QuantStudio Design & Analysis Software (Thermo Fisher Scientific), using the in-built standard curve method. All samples were assessed *via* three biological replicates, each analyzed in three technical replicates, respectively.

3.7.3 Global gene expression profiling

Global gene expression profiling involved RNA reverse-transcription into cDNA, hybridization to a custom-made DNA microarray, and scanning (Pauli et al., 2023). Briefly, the layout of the microarray (SurePrint G3 Custom GE8 × 60K) was designed from target transcripts using the eArray online tool (Agilent Technologies) (Christmann et al., 2023). The created probes covered the entire genome of *Y. lipolytica* CLIB122 (assembly ASM252v1 CDS, GCA 000002525.1) (Dujon et al., 2004), functionally annotated using splicing site predictions and similarity searches *via* UniProtKB, BLAST and MycoCosm (Grigoriev et al., 2014), plus the integrated myxobacterial PUFA cluster genes, encoding for 17 enzymatic domains (Gemperlein et al., 2019).The array covered native genes of the yeast plus the genes of heterologous PUFA cluster, in total 6472 targets. For the latter, we designed 17 separated targets that were each specific to one of the 17 enzyme subunits of the PKS, encoded by the four genes *pfa1, pfa2, pfa3* and *ppt*. Three probes per target gene were

designed in sense orientation with a length of 60 bp and a melting temperature (T_m) of 80 °C, using Base Composition Methodology method. Each probe was randomized to different locations on the slide using SurePrint technology (Agilent Technologies), making in total 19276 probes and 1319 Agilent Controls. All were applied as 3 biological replicates resulting in 62976 total Features.

Prior to analysis, 50 ng of pre-purified total RNA was clarified from remaining DNA (TURBO DNA-free Kit (Thermo Fisher Scientific), and reverse-transcribed into fluorescent cDNA (Low Input Quick Amp WT Labeling One-Color Kit, Agilent Technologies, RNA Spike-In One-Color Kit, Agilent Technologies, and RNeasy Mini Kit, Qiagen).

A total of 600 ng of labelled cRNA was hybridized onto the microarray (Gene Expression Hybridization Kit, hybridization gasket slides, SureHyb chamber, hybridization oven, Agilent Technologies). Subsequently, the hybridized slides were washed (Gene Expression Wash Buffer Kit, Agilent Technologies) and scanned by the SureScan Microarray Scanner (G4900DA, SureScan Microarray Scanner Control Software, Version 9.1.11.13, Agilent Technologies). Afterwards, the scans were processed, and transcriptomics data extraction was performed with Feature Extraction Software (Version 12.1.1.1.1, Agilent Technologies).

The obtained raw data were analyzed and further evaluated with the GeneSpring GX Software (Version 14.9, Agilent Technologies). To minimize systematic non-biological differences, the data were normalized using the Percentile Shift method. Statistical evaluation of the data was based on the 3-way ANOVA test. The fold change cut-off and the *P* value were set to 2 and ≤ 0.05, respectively (Kohlstedt et al., 2022). The total obtained 64 raw data sets are accessible from the Gene Expression Omnibus (GEO) Database (GEO 224529). Each sample was analyzed as biological triplicate.

3.8 Fluxome analysis

3.8.1 GC-MS for ^{13}C-labeling analysis of intracellular amino acids

The protocol for analysis of the ^{13}C labelling pattern of free intracellular amino acids was based on previous work with a related yeast (Schwechheimer et al., 2018a). In short, cells were sampled, and amino acids were extracted in boiling water, as described above. Then, the obtained extract was dried under nitrogen. For derivatization of the contained amino acids, 50 µL *N*,*N*-dimethylformamide (1% pyridine) and 50 µL MBDSTFA (*N*-(tert-butyldimethylsilyl)-*N*-methyltrifluoroacetamide, Macherey-Nagel, Düren, Germany) was added. The mixture was incubated for 35 min at 80 °C. Afterwards, it was cooled down, clarified from debris (16,000 x *g*, 5 min, 4 °C), and analyzed by GC-MS (GC 7890A, MSD 5975C, Agilent Technologies) using an HP-5MS column (30 m, 250 µm × 0.25 µm, Agilent Technologies) with helium 5.0 as carrier gas (1.7 mL min^{-1}). Initially, samples were analyzed in scan mode to exclude undesired isobaric matrix effects for the ion clusters to be used for the labelling analysis (Wittmann, 2007). Afterwards, the mass isotopomer distribution (MID) of validated amino acids of interest was assessed using selective ion monitoring (SIM), including all mass isotopomer from the monoisotopic (m) to the fully ^{13}C-enriched (m+x) variant (**Table 6**). The selected ions [M-57], [M-85] and [M-159], resulting from well-known fragmentation events by the imposed electron impact ionization (Schwechheimer et al., 2018b), were successfully used before in ^{13}C experiments of other yeasts (Frick and Wittmann, 2005; Schwechheimer et al., 2018a). They contained all carbon atoms of the amino acid of interest [M-57] and all carbons except the C1 [M-159] and [M-85], respectively. In this work, samples of naturally labelled *Y. lipolytica* cultures were used to validate that, in each case, the measured ^{13}C labelling pattern matched the theoretical value inferred from natural isotope abundance (Kohlstedt and Wittmann, 2019). Histidine and tryptophan did not yield suitable signals and were therefore not considered further. The obtained MIDs were corrected for natural isotopes (van Winden et al., 2002).

Table 6. GC-MS analysis of the ^{13}C labelling pattern of free intracellular amino acids in *Y. lipolytica*. For each amino acid, the individual mass isotopomer of one selected ion cluster was measured by selective ion monitoring (SIM).

Amino acid	Fragment	m [*m/z*]	m+x [*m/z*]	Carbon atoms
L-Alanine	[M-57]	260	263	C1-C3
Glycine	[M-57]	246	248	C1-C2
L-Valine	[M-57]	288	293	C1-C5
L-Leucine	[M-159]	200	205	C2-C6
L-Isoleucine	[M-159]	200	205	C2-C6
L-Proline	[M-85]	258	262	C2-C5
L-Methionine	[M-57]	320	325	C1-C5
L-Serine	[M-57]	390	393	C1-C3
L-Threonine	[M-57]	404	408	C1-C4
L-Phenylalanine	[M-57]	336	345	C1-C9
L-Aspartate	[M-57]	418	422	C1-C4
L-Cysteine	[M-57]	406	409	C1-C3
L-Glutamate	[M-57]	432	437	C1-C5
L-Asparagine	[M-57]	417	421	C1-C4
L-Lysine	[M-57]	431	437	C1-C6
L-Glutamine	[M-57]	431	436	C1-C5
L-Arginine	[M-57]	442	448	C1-C6
L-Histidine	[M-57]	440	446	C1-C6
L-Tyrosine	[M-57]	466	475	C1-C9
L-Tryptophan	[M-57]	489	500	C1-C11

3.8.2 LC-MS/MS for ^{13}C-labeling analysis of intracellular CoA thioesters

Prior to ^{13}C analysis, 2 mL of cell broth was quenched in 10 mL ice-cold quenching solution (25 mM formic acid, 95% acetonitrile) and extracted. Then, the ^{13}C labelling pattern of selected CoA esters (acetyl-CoA, malonyl-CoA, succinyl-CoA) was assessed by LC-MS/MS analysis of ion clusters that allowed a clean quantification of the ^{13}C labelling in the contained acyl-residue using the MRM mode. On one hand, each CoA ester yielded a fragment at *m/z*

428 that corresponded to its adenosine-3,5-diphosphate-containing backbone but lacked the acyl group. The analysis of the mass isotopomer distribution of this ion cluster (*m*, 428; *m*+1, 429; *m*+2, 430; *m*+3, 431) delivered information about the ^{13}C enrichment of the *de novo* synthetized backbone. It turned out that this fragment was not enriched in ^{13}C for any of the CoA esters that was analyzed within 48 hours after the ^{13}C tracer had been supplied. This revealed that *de novo* synthesis of the CoA ester backbone was insignificant during the studied time. However, significant ^{13}C enrichment was detectable in the molecular ion $[M+H]^+$, which contained the (non-^{13}C-enriched) backbone plus the acyl residue. Therefore, analysis of the molecular ion allowed to specifically infer the ^{13}C labelling pattern of the acyl-group of each CoA ester. To this end, we analyzed the corresponding $[M+H]^+$ proton adducts (*m/z* 810-812 for acetyl-CoA, *m/z* 854-857 for malonyl-CoA, and *m/z* 868-872 for succinyl-CoA) using MRM. The output was corrected for natural isotopes (van Winden et al., 2002).

3.8.3 GC-MS for ^{13}C-labeling analysis of intracellular fatty acids

Fatty acid methyl esters, extracted and derivatized as described above, were measured in scan mode (*m/z* 50 – 850) to evaluate signal quality and exclude isobaric overlay of the sample matrix with analyzed ion clusters (Wittmann, 2007). For native fatty acids (including C16:0, C18:0, C18:1, C18:2) the molecular ion (M^+) yielded a clean, prominent signal which matched the expected theoretical mass isotopomer distribution for non-enriched samples. This ion was therefore used to derive the corresponding MIDs. For DHA, the molecular ion was of too low quality and intensity to be used. Here, the *m/z* 313 ion fragment ($C_{21}H_{29}O_2$, formed upon loss of $–CH_3CH_2$ and containing carbons 3 to 22 of DHA) (Wang et al., 2019b) was used for analysis after successful validation with non-labeled samples. Selected ion monitoring was in all cases performed to infer ^{13}C labelling patterns. All outputs were corrected for natural isotopes (van Winden et al., 2002).

3.8.4 ^{13}C isotope experiments data processing

The output of the isotope correction (van Winden et al., 2002) represented the mass isotopomer fractions of an analyte's carbon skeleton of (MID_{corr}). They were used to derive its total ^{13}C enrichment, termed summed fractional labeling (SFL) (Schwechheimer et al., 2018b), according to **Eq. (2)**. The data are given in percent, whereby 100% represents a fully ^{13}C labeled carbon backbone, with *n* being the number carbon atoms and *i* representing the number of ^{13}C atoms of an isotopomer.

$$SFL = \sum_{i=1}^{n+1} \frac{i * MID_{i,corr}}{n} * 100 \qquad \textbf{(Eq. 2)}$$

4 RESULTS AND DISCUSSION

4.1 Adaptation of quantitative systems biology tools for *Y. lipolytica*

In order to obtain precise quantitative insights into the complex metabolic processes associated to DHA production in the oleaginous yeast, the first step was the adaptation and refinement of omics technologies for transcriptomics, metabolomics and ^{13}C-based fluxomics in *Y. lipolytica*.

4.1.1 Transcriptome analysis

The isolation of high-quality RNA is a crucial step prior to valid and accurate transcriptional measurements. To this end, initial efforts aimed at precise RNA extraction protocols and appropriate methods to estimate the quality and the quantity of the extracted RNA. For qRT-PCR analysis, the experiments additionally investigated several candidates as housekeeping genes for data normalization. Finally, all developed workflows were thoroughly validated for statistical quality and uniformity between biological replicates.

Four different RNA extraction protocols were tested. As shown, they provided different amounts of extracted RNA (**Fig. 10A**). Phenol extraction was found rather inefficient (i, ii) (Krebs et al., 2009), while commercial kits yielded to highly concentrated RNA (iii, iv). The 260/280-ratio, one value to evaluate the purity of extracted RNA was acceptable for all protocols. The 260/230-ratio, a second measure to evaluate RNA purity was, however, lower than 2.0 as expected for pure RNA (Cortes-Maldonado et al., 2020; Sasidharan et al., 2012), when using first two protocols, demonstrating the presence of contaminants. Furthermore, denaturing gel electrophoresis (**Fig. 10B**) showed ambiguous ribosomal RNA bands that resulted from the first protocol, while second protocol offered much clearer bands that

corresponded to 26, 18, 5 and 5.5S rRNA. The integrity of the isolated RNA samples was tested using the Bioanalyzer (Fleige and Pfaffl, 2006; Schroeder et al., 2006).

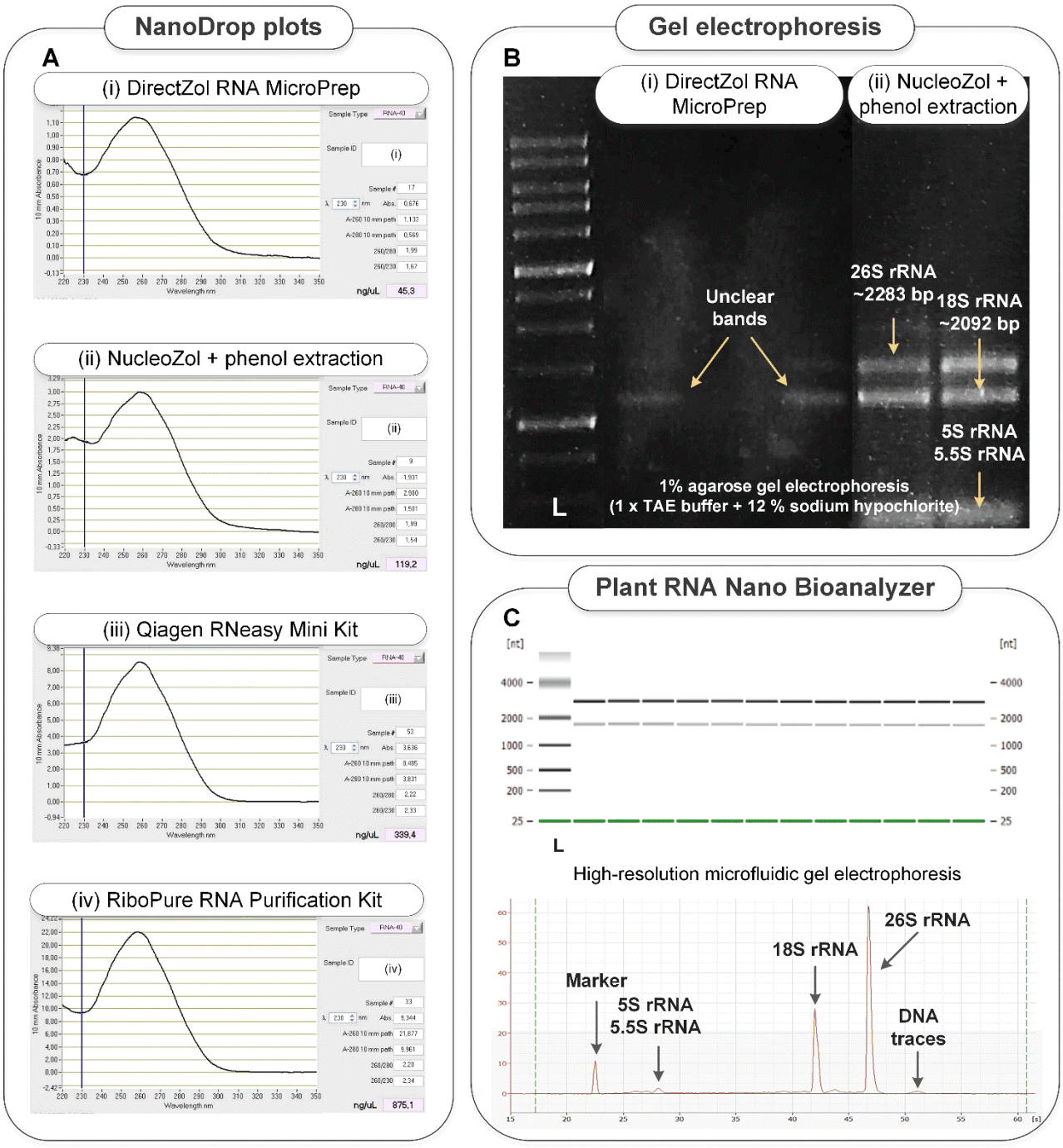

Figure 10. RNA extraction method development. Figure demonstrates different RNA extraction protocols and tools for quality and quantity assessment: NanoDrop measurement (A) indicated different RNA concentrations, while the 230/260 and 260/280 ratios were used to infer the purity of the RNA samples. The methods compared included DirectZol RNA MicroPrep (i), NucleoZol and phenol extraction (ii), the Quiagen RNeasy Mini Kit (iii) and the RiboPure RNA Purification Kit (iv); denaturing gel electrophoresis (B) showed recognizable 26S, 18S, 5.5 and 5S rRNA bands for samples isolated with (ii) NucleoZol extraction and an ambiguous pattern for the DirectZol extraction method (i); gel electrophoresis and electrophoreogram using the Bioanalyzer system (C) revealed high RNA quality displayed after extraction with the RiboPure RNA Purification Kit from the presence

of two rRNA bands (upper plot) and the presence of several peaks that indicated stable and intact RNA, including a the marker peak (~23s), small rRNA peaks (~28s), the 18S rRNA peak (~42s), the 26S rRNA peak (~47s) and only traces of DNA (~51s). The results were obtained using the Plant RNA Nano Software. L – ladder.

The obtained RIN number, and the associated gel and electropherograms (**Fig. 10C**) revealed that the RiboPure RNA Purification kit yielded the best quality RNA and displayed the most efficient extraction method. It was used in all further experiments. The Plant RNA Nano Software (Johnson et al., 2012) was chosen among other existing protocols as the most suitable tool to determine the RIN of yeast RNA.

The subsequent steps aimed to develop a qPCR method, to provide high-precision insights into the transcriptional dynamics of selected genes and give a more comprehensive understanding of the intricate regulatory processes at play (Ganger et al., 2017). A critical aspect in ensuring accurate gene expression analysis was the selection of a suitable internal control, typically a housekeeping gene, that exhibits consistent expression across all compared experimental conditions. Previously, the β-actin gene had been widely used for qRT-PCR normalization in *Y. lipolytica* (Borkowska et al., 2020; Rodriguez et al., 2016; Theron et al., 2020). However, in the context of this study, the gene was found unsuitable as an internal control due to significant variations in its expression level across different process phases, including the exponential phase (10h), the early stationary phase (48h), and the late stationary phase (96h) (**Fig. 11A**).

As an alternative candidate, the 26S rRNA gene could be identified as a suitable reference, owing to its stable expression throughout the cultivation process (Jacob et al., 2013), visualized by the high agreement in the Ct value across different time points. Hence, this gene was selected for normalization further on. When evaluating both controls, the relative gene expression of the genes of interest (here three genes in the PUFA cluster, namely, *ER*, *ACP* and *CLF*) differed strongly (**Fig. 11BC**).

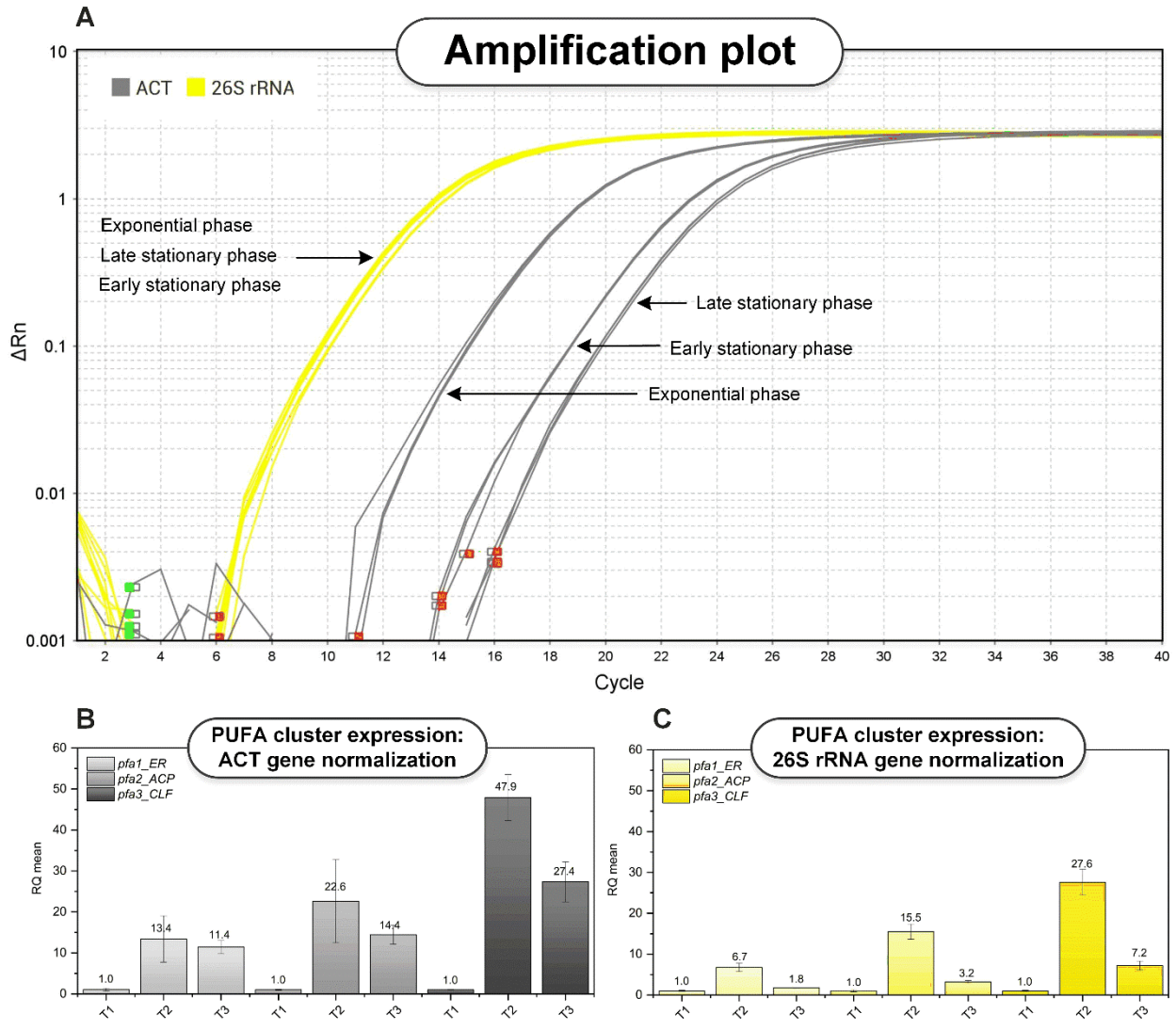

Figure 11. Validation of the endogenous control gene for qRT-PCR analysis. The data show amplification plots of β-actin gene (*ACT*) and 26S rRNA gene (A) in 3 different phases – T1: exponential phase (10h), T2: early stationary phase (48h) and T3: late stationary phase (96h). Phases reflect time points during cultivation shown in **Fig. 15B**. Relative gene expression changes using *ACT* (B) and 26S rRNA gene (C), data are normalized to the gene expression levels of T1; RQ – relative quantification, ER – enoyl reductase, ACP – acyl carrier protein, CLF – chain length factor.

In order to obtain global transcriptome pictures of *Y. lipolytica*, a custom-made DNA array was designed (see chapter **3.7.3**). A total dataset of 48 transcriptomic samples, obtained from different cultures and process time points, was used to evaluate data quality. Principal Component Analysis (PCA) was used to analyze the high-throughput datasets (unprocessed scanned features). The analysis revealed excellent agreement of three biological replicates (**Fig. 12**).

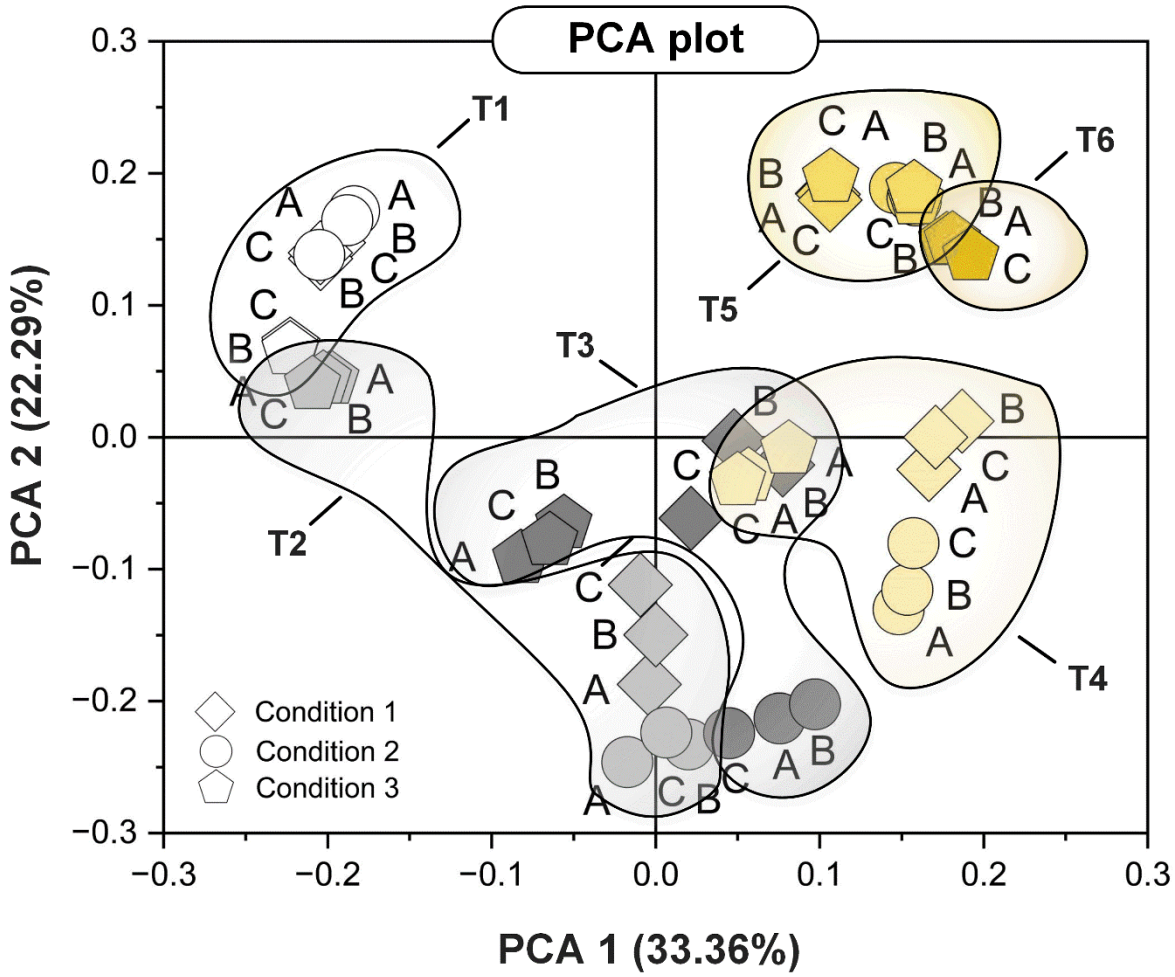

Figure 12. Statistical evaluation of the global gene expression profiling in Y. *lipolytica*. Principal component analysis (PCA) of the raw data obtained from custom-made DNA microarray analysis revealed statistical differences and similarities in gene expression between the DHA producer *Y. lipolytica* Af4 cultivated in three different conditions (shown on **Fig. 21**) at different stages of cultivation (T1 – 10h, T2 – 24h, T3 – 48h, 208 T4 – 72h, T5 – 96h, T6 – 120h), whereby all three biological replicates are shown.

4.1.2 Metabolome and fluxome analysis

To obtain metabolic insights into DHA-producing *Y. lipolytica*, different methods for the quantification of intracellular CoA thioesters (Chapter **3.6.1**) and fatty acids (Chapter **3.5.4**), as well as analytical tools for ^{13}C-labeling analysis (Chapters **3.8.2** and **3.8.3**) were optimized and evaluated.

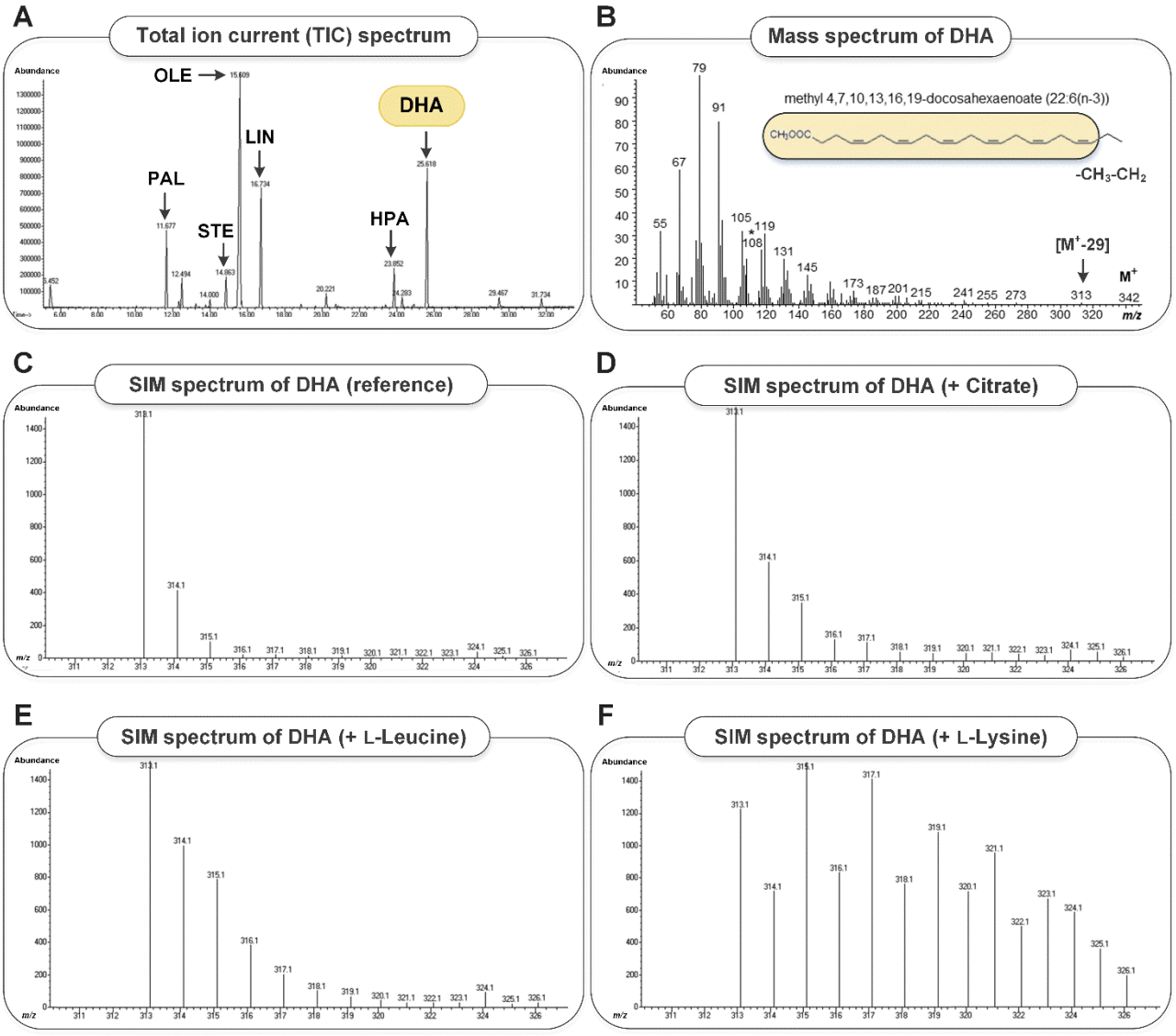

Figure 13. GC-MS analysis of the intracellular fatty acids in *Y. lipolytica* after derivatization into the corresponding fatty acid methyl esters (FAMEs). The data comprise the total ion current (TIC) spectrum of DHA-producing *Y. lipolytica* after 180h of cultivation, including HPA (heneicosapentaenoic acid) as internal standard (A); the mass spectrum of methyl docosahexaenoate (B, after 180 h); selected DHA fragment ion (*m/z* = 313) in non-labelled culture samples (C, after 72h); culture supplemented with [$^{13}C_6$] citrate (D, after 72 h), [$^{13}C_6$] L-leucine (E, after 72 h), and [$^{13}C_6$] L-lysine (F, after 72 h). PAL: palmitic acid; OLE: oleic acid; STE: stearic acid; LIN: linoleic acid; HPA: heneicosapentaenoic acid; DHA: docosahexaenoic acid.

GC-MS analysis revealed intracellular spectrum of fatty acids after derivatization into the corresponding fatty acid methyl esters (FAMEs) (**Fig. 13A**). The example shown reflects total ion current (TIC) spectrum from glycerol-grown *Y. lipolytica*, after 180h of cultivation (**Fig. 15B**). The spectrum comprised of nine native fatty acids, heterologously synthesized DHA, and HPA, added as internal standard. The mass spectrum of methyl-

docosahexaenoate (methyl-DHA) (**Fig. 13B**, after 180 h) included the fragment ions *alpha* (*m/z* = 152) and *omega* (*m/z* = 108), characteristic for unsaturated fatty acids, and, furthermore, the presence of the McLafferty ion (*m/z* = 74), typically observed for fatty acids (Yang et al., 2007). These ions, however, exhibited strong isobaric overlay with the sample matrix, excluding their use to precisely determine the ^{13}C-enrichment of the analyte. The signal of the molecular ion (*m/z* = 424) was too weak and therefore did not enable a clean ^{13}C labelling analysis of DHA, either. We therefore selected the fragment ion (*m/z* = 313) for labelling analysis, that corresponded to a loss of $-CH_2-CH_3$ (Wang et al., 2019b). This ion was found suitable when validated with non-labelled culture samples (**Fig. 13C**, after 72 h). As shown, it allowed to precisely monitor the incorporation of ^{13}C in isotopic tracer studies with [$^{13}C_6$] citrate (**Fig. 13D**, after 72 h), [$^{13}C_6$] L-leucine (**Fig. 13E**, after 72 h), and [$^{13}C_6$] L-lysine (**Fig. 13F**, after 72 h). For the native fatty acids PAL, OLE, LIN, and STE, respectively, the corresponding molecular ion was found of sufficient quality and intensity after validation with non-labelled standards and culture samples. It was then used for the ^{13}C labelling analysis of these metabolites.

The traceability and quantification of the thioesters of coenzyme A, particularly the DHA building blocks acetyl-CoA and malonyl-CoA, was regarded important in this study. Additionally, the quantification of other CoA thioesters, which contribute to approximately 5% of enzymatic reactions, promised to provide valuable insights into the metabolic state of the cell (Gläser et al., 2020). After method optimization, various CoA-esters could be separated using LC-MS/MS 10minutes. The coupling to an MS/MS detector allowed their differentiation based on distinct mass-to-charge (*m/z*) ratios (**Fig. 14AB**). Furthermore, the ^{13}C labelling pattern of selected CoA esters (acetyl-CoA, malonyl-CoA, succinyl-CoA) was assessed by LC-MS/MS using the MRM mode. The obtained spectrum showed significant differences in observed ion clusters when using non-labelled substrate [$^{12}C_3$] glycerol (**Fig. 14C** - up) and 6h after supplementation with [$^{13}C_6$] L-lysine (**Fig. 14C** - down).

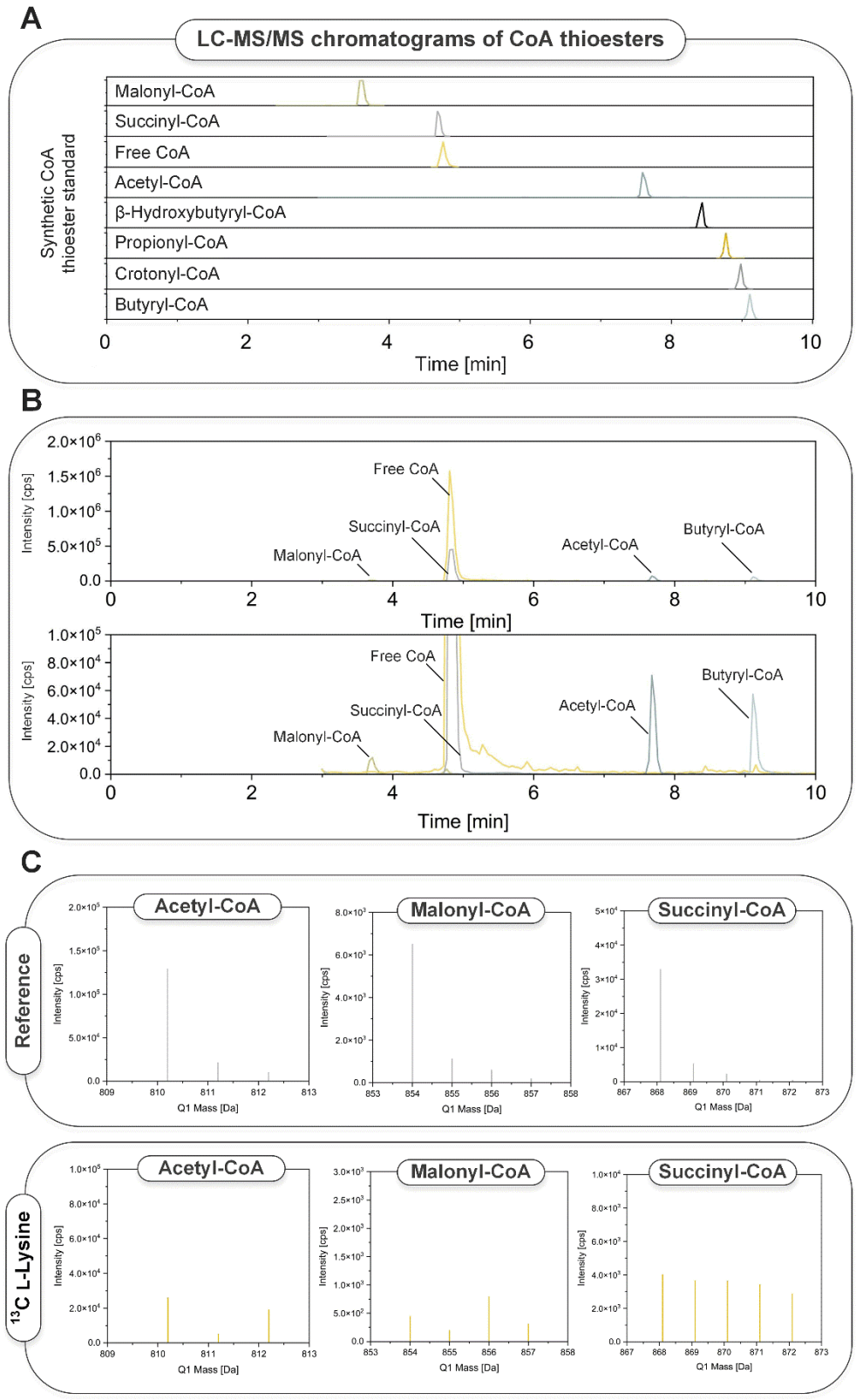

Figure 14. LC-MS/MS chromatogram and related mass spectra of CoA thioesters. Figure represents chromatogram of a synthetic CoA thioester standard sorted by the retention time of each analyte (A); LC–MS/ MS chromatogram of the extracted intracellular CoA thioesters in *Y. lipolytica* (B), present in high (up) and low abundance (down); molecular ion cluster $[M+H]^+$ of acetyl (*m/z* 810-812), malonyl (*m/z* 854-857) and succinyl-CoA thioesters (*m/z* 868-872), containing the non-enriched CoA-backbone (*m/z* 428) plus the acyl-residue (C) from reference culture (non-labelled) (up) and from culture supplemented with [$^{13}C_6$] L-lysine, 6h after addition.

4.2 A systems view into growth-decoupled DHA production in *Y. lipolytica*

The metabolically engineered *Y. lipolytica* strain Af4 was recently shown to overproduce DHA upon expression of a biosynthetic gene cluster from the myxobacterium *Aetherobacter fasciculatus* (SBSr002) (**Fig. 15A**) (Gemperlein et al., 2019), a PUFA with multiple health benefits and recognized commercial value (Jovanovic et al., 2021). Here, we aimed to improve its production performance.

4.2.1 Growth and DHA production dynamics

As a starting point to better understand the molecular processes that controlled (and eventually limited) the formation of DHA, we analyzed the growth and production dynamics of the engineered yeast in glycerol-based cultures (**Fig. 15B**). The cells used up the carbon source (225 mM) within 24 h, while accumulating a small amount of citrate (2.8 mM) and acetate (1.9 mM) as a result of metabolic overflow (Cavallo et al., 2017; Sabra et al., 2017). A biomass concentration of 14.3 g L^{-1} was reached at the end of the growth phase. The formed cells contained a substantial amount of native lipids, including saturated, mono- and di-unsaturated 18-carbon and 16-carbon fatty acids, mainly oleic acid (C18:1) and linoleic acid (C18:2), and, to a lower extent, stearic acid (C18:0), and palmitic acid (C16:0). In addition, traces of longer saturated fatty acids were present (C22:0, C24:0, C26:0) (**Fig. 15D**), overall revealing the typical profile of *Y. lipolytica* under these conditions (Carsanba et al., 2020). DHA was not detectable during this initial process stage. The product started to visibly form only after 48 h, when glycerol had been consumed and cell growth had ended. During the following stationary phase, the DHA pool was constantly built up. At the end of the process, a final titer of 102 mg L^{-1} DHA was achieved. In this regard, synthesis of DHA occurred growth decoupled. The formation of the PUFA coincided with the re-consumption of extracellular citrate and the degradation of native intracellular lipids (**Fig. 15BD**). In this

regard, the PKS-driven strain exhibited a production mode that largely differed from previous strategies (Kujawska et al., 2021; Nazir et al., 2018) which, in fact, employed desaturases and elongases to derive PUFAs in *Y. lipolytica* during growth through an artificially extended native fatty acid biosynthesis (Xue et al., 2013). The simultaneous breakdown of native fatty acids and the buildup of DHA enabled a continuous increase of product selectivity over time, so that, finally, DHA accounted for 17% of the total fatty acid pool (**Fig. 15D**). This seemed an advantage compared to growth-coupled production strategies, where the formation of DHA competes with native fatty acid biosynthesis and requires the use of expensive supplements such as cerulenin (Wan et al., 2016) and other biochemical stimulants (Hussain et al., 2021) to suppress the latter.

4.2.2 Assessment of the growth dynamics and lipid accumulation of the wild type

Compared to the producer, the wild type exhibited a similar behavior in growth, glycerol consumption, and citric acid production (**Fig. 15C**) but markedly differed in the extent of intracellular lipid degradation during the stationary phase. On a quantitative basis, the wild type degraded 20% less native fatty acids (200 mg L^{-1}) than the engineered strain (250 mg L^{-1}) and, therefore, contained 17% more of them at the end of the process (687 mg L^{-1}) (**Fig. 15E**). When additionally considering DHA, which was exclusively synthetized in the producer, the level of total fatty acids, however, was almost the same in both strains. *Y. lipolytica,* due to its oleaginous nature, catabolizes intracellular lipid bodies during carbon starvation, suggesting that the newly formed DHA was, at least partially, synthesized from the native lipid pool through recycling processes (Liu et al., 2020; Shaigani et al., 2021).

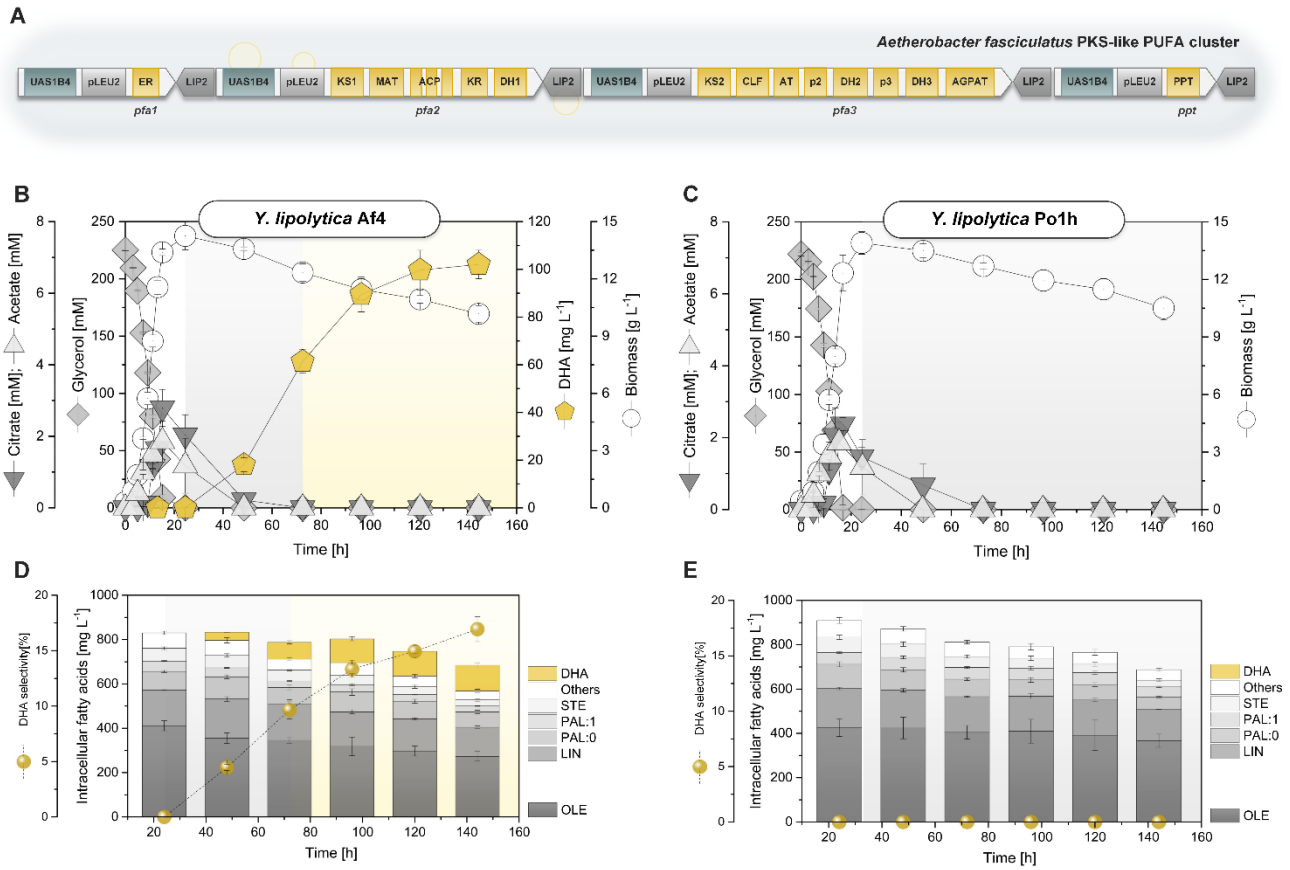

Figure 15. Production of docosahexaenoic acid (DHA) in recombinant *Y. lipolytica* Af4 expressing a polyketide-synthase like complex-encoding gene cluster from the myxobacterium *A. fasciculatus* and characterization of the wild type. The data represent architecture of the heterologously expressed PUFA cluster (A); the cultivation profile using a minimal medium with 20 g L^{-1} (220 mM) of glycerol as the sole carbon source (B) and changes in the intracellular content of native fatty acids and DHA over time (D). The process exhibited three phases of exponential growth, early DHA production, and late DHA production, indicated by the background color. The corresponding data for the non-producing parent wildtype *Y. lipolytica* are shown for comparison (C, E). PAL:0, palmitic acid (C16:0); PAL:1, palmitoleic acid (C16:1); STE, stearic acid (C18:0); OLE, oleic acid (C18:1); LIN, linoleic acid (C18:2); DHA, docosahexaenoic acid (C22:5). Other native fatty acids occurring in low amount such as docosanoic acid (C22:0), tetracosanoic acid (C24:0), and hexacosanoic acid (C26:0) are given as summed fraction. The data display means and standard errors from three biological replicates.

4.3 Linking DHA precursor availability to the transcriptional picture

As shown, the production process exhibited three phases: (i) exponential growth on glycerol with native fatty acid, citrate, and acetate accumulation, (ii) early DHA production with parallel degradation of citrate, acetate, and native fatty acids, and (iii) a late (weaker) DHA production with degradation of native fatty acids alone (**Table 7**).

Table 7. Dynamics of DHA production in recombinant *Y. lipolytica* Af4. The data display the specific rates related to the metabolism of citrate, acetate, DHA, and native fatty acids (FA) during the three phases of glycerol-based batch cultures, highlighted in **Fig. 15B**. Positive values indicate formation, while negative values indicate consumption. The data displays the average values and standard errors from three biological replicates. CDM: cell dry mass.

Exponential growth phase [mg g_{CDM}^{-1} d^{-1}]		**Early DHA production phase [mg g_{CDM}^{-1} d^{-1}]**		**Late DHA production phase [mg g_{CDM}^{-1} d^{-1}]**	
Citrate	124 ± 12	Citrate	-15 ± 4	Citrate	0 ± 0
Acetate	88 ± 7	Acetate	-6 ± 1	Acetate	0 ± 0
DHA	0 ± 0	DHA	2 ± 0	DHA	0.2 ± 0
Native FA	172 ± 8	Native FA	4 ± 1	Native FA	-8 ± 1

4.3.1 Availability of intracellular CoA thioesters

For a closer insight, we analyzed the intracellular pools of CoA esters that were closely linked to the metabolism of citrate and native fatty acids, respectively, on one hand and to the formation of DHA on the other hand, namely acetyl-CoA, malonyl-CoA, and succinyl-CoA. During the initial growth phase, acetyl-CoA (650 nmol g^{-1}) was the most abundant CoA ester in *Y. lipolytica*, followed by succinyl-CoA (74 nmol g^{-1}), free CoA (72 nmol g^{-1}) and malonyl-CoA (17 nmol g^{-1}). Remarkably, the CoA ester pools largely disappeared when the cells entered the stationary phase and started the production of DHA (**Fig. 16**). The level of acetyl-CoA, the DHA starter unit, decreased by 96%. Malonyl-CoA, of which even 10 molecules are required to synthesize one DHA molecule, dropped by as much as 98% into the picomolar range (54.6 pmol g^{-1}). Sufficient precursor availability is known as a key requirement for metabolite overproduction (Lange et al., 2017; Rohles et al., 2022; Rohles et al., 2018b) so that the collapsing precursor levels at the on-set of DHA production pointed to a potential bottleneck. Furthermore, the initially high abundance of the two CoA esters excluded the absence of DHA formation during the exponential phase resulted from missing precursors.

4.3.2 Transcriptional changes of CoA-associated genes

In view of these changes, we studied relevant reactions around the supply and withdrawal of the two CoA esters, on the level of transcription. For this purpose, we used q-RT-PCR, considering the 26S rRNA gene for normalization (**Fig. 11**). ATP citrate lyase was analyzed due to its significance in catalyzing the formation of cytosolic acetyl-CoA for fatty acid biosynthesis (Beopoulos et al., 2012). The expression of the two encoding genes *ACL1* and *ACL2* was high during the exponential growth phase but dropped 6-fold and 15-fold (log_2-fold changes of -2.6 and -3.9) with the entry into the stationary phase, and even further towards the end of the process (log_2-fold changes of -3.2 and -4.8) (**Fig. 16**). *Aspergillus niger* mutants that lack citrate lyase, exhibit a significant decrease of acetyl-CoA (Chen et al., 2014) suggesting that the reduced expression of *ACL1* and *ACL2* contributed to the low abundance of this metabolite during the stationary phase, even though citrate was available up to 48 h (**Fig. 15B**). The expression levels of *TAGL*, encoding triglyceride lipase, and *ACAD*, encoding acyl-CoA dehydrogenase, increased (log_2-fold increase of 1.7 and 2.5) when the cells entered the stationary phase and behaved similarly in the late phase (log_2-fold increase of 3.0 and 1.8). Both enzymes are involved in lipid degradation. At the same time, fatty acid synthase, responsible for *de novo* lipogenesis and encoded by *FAS1* and *FAS2*, respectively (Liu et al., 2019c), was down regulated (log_2-fold changes of -1.6 and -0.9 at the onset of production and -2.4 and -1.9 in the late production phase, respectively).

The strongly increased expression of *pfa1* (log_2-fold changes of 3.8 in early production phase and 3.5 in late production phase), *pfa2* (log_2-fold changes of 4.6 and 3.8), and *pfa3* (log_2-fold changes of 5.6 and 4.8), revealed strong upregulation of the PKS cluster during the stationary phase. On the contrary, *ACC*, encoding acetyl-CoA carboxylase as exclusive source for cytosolic malonyl CoA (Santin and Moncalian, 2018) was found down regulated (log_2-fold changes of -1.5 and -2.1 throughout the two production phases), likely contributing to the limited abundance of the precursor during later phases of the cultivation process. In

this regard, the production of DHA was embedded into complex metabolic and transcriptional dynamics, linked to the cellular adaptation upon the shift from the growth to the stationary phase. Notably, the metabolomic and transcriptomic analysis discovered a temporal mismatch between the expression of the heterologous pathway (stationary phase) and sufficient availability of the primer and chain extender precursors, acetyl-CoA, and malonyl-CoA (exponential phase).

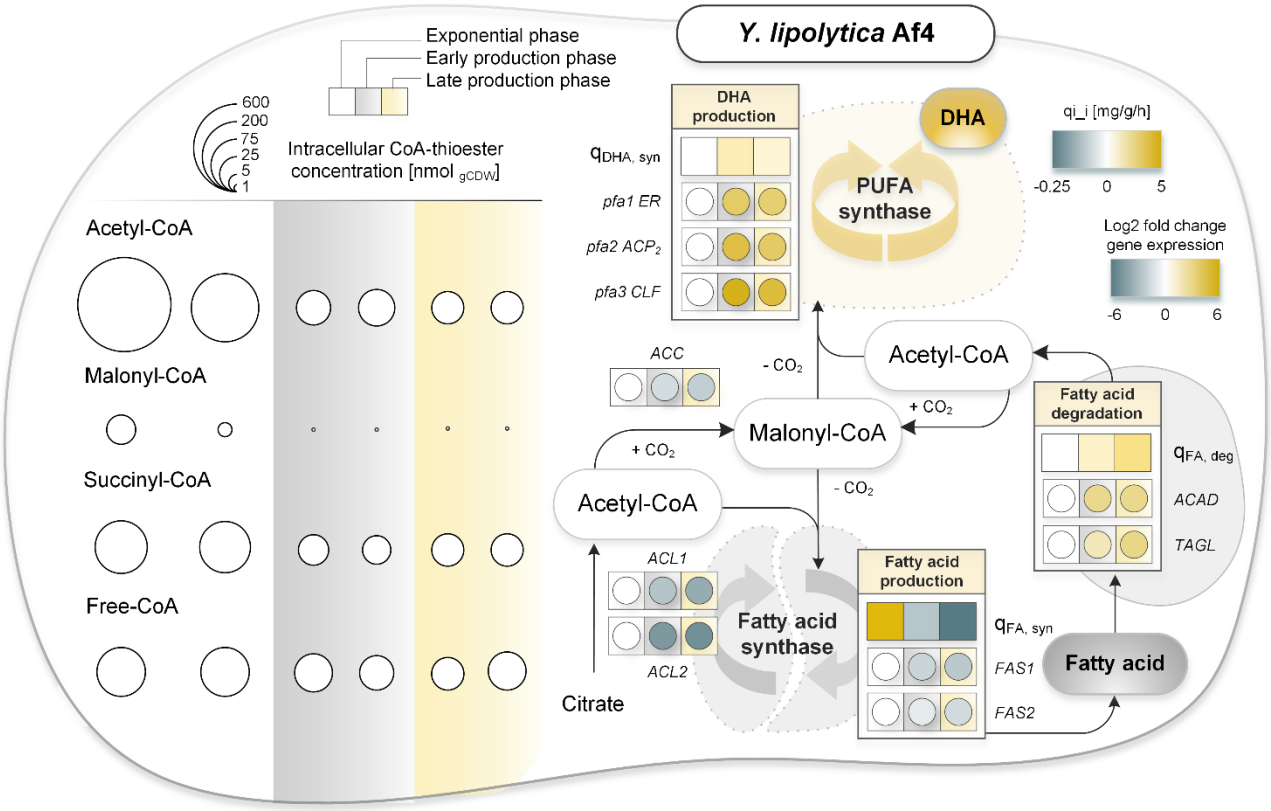

Figure 16. Multi-omics profiling of DHA-producing *Y. lipolytica* Af4. The data comprise the levels of intracellular acetyl CoA, malonyl-CoA, succinyl CoA, and free CoA assessed by LC-MS/MS, using a ^{13}C labelled extract from cells grown on [$^{13}C_6$] glycerol for absolute quantification (Gläser et al., 2020). The concentrations were assessed at different time points during the cultivation: exponential growth phase (6h, 10h), early stationary phase (24h, 48h) and late stationary phase (72 h, 96 h) (**Fig. 15B**). In addition, the expression of selected genes was quantified using q-RT-PCR. The data refer to samples taken after 10 h, 48 h, and 96 h, respectively. In addition, the corresponding specific rates for DHA synthesis ($q_{DHA,syn}$), native fatty acid synthesis ($q_{FA,syn}$), and native fatty acid degradation ($q_{FA,deg}$) for each of the three process phases are displayed (**Table 7**). *ACL1, ACL2*, ATP-dependent citrate lyase (Beopoulos et al., 2012); *ACC*, acetyl-CoA carboxylase (Santin and Moncalian, 2018); *pfa1 ER* – enoyl reductase; *pfa2 ACP*$_2$ – acyl carrier protein; *pfa3 CLF* – chain length factor, (Gemperlein et al., 2019). *FAS1, FAS2* – fatty acid synthase (Liu et al., 2019c); *ACAD* – acyl-CoA dehydrogenase (Haddouche et al., 2011; Mlickova et al., 2004); *TAGL* – triglyceride lipase (Dulermo and Nicaud, 2011).

4.3.3 Analysis of the CoA thioesters metabolism in the wild type

A similar pattern was observed upon detailed examination of the non-producing *Y. lipolytica* Po1h strain (**Fig. 17**). Transcriptional changes demonstrated a similar trend, indicating that even in the absence of DHA synthesis, the stationary phase cells still exhibit a suppression of the fatty acid synthesis machinery through downregulation of *ACC*, *ACL1*, and *ACL2*, while simultaneously promoting fatty acid degradation *via* upregulation of *ACAD* and *TAGL*. These transcriptional changes were followed by alterations in the concentrations of intracellular CoA thioesters.

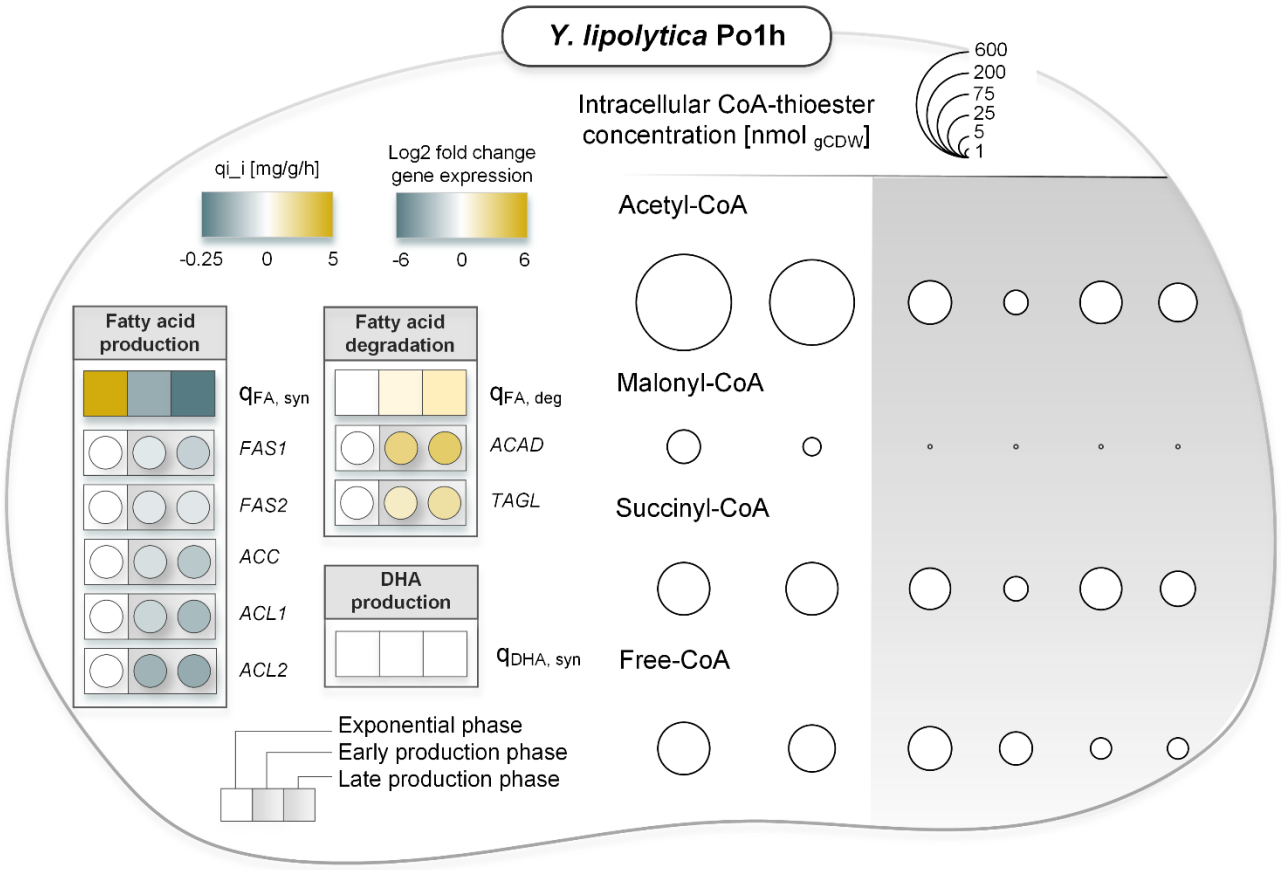

Figure 17. Multi-omics profiling of wild type strain *Y. lipolytica* Po1h. The dataset includes measurements of intracellular levels of acetyl-CoA, malonyl-CoA, succinyl-CoA, and free-CoA. These concentrations were evaluated at various time points during the cultivation process, including the exponential growth phase (6h, 10h), early stationary phase (24h, 48h), and late stationary phase (72h, 96h) (**Fig. 15C**). Furthermore, the expression levels of specific genes were quantified using quantitative real-time PCR (qRT-PCR). The gene expression data corresponds to samples obtained at 10h, 48h, and 96h time points. *ACL1, ACL2*, ATP-dependent citrate lyase, *ACC*, acetyl-CoA carboxylase; *pfa1 ER* – enoyl reductase; *pfa2 ACP*$_2$ – acyl carrier protein; *pfa3 CLF* – chain length factor; *FAS1, FAS2* – fatty acid synthase; *ACAD* – acyl-CoA dehydrogenase; *TAGL* – triglyceride lipase.

During the initial growth phase, levels of the most prominent intracellular CoA thioesters, acetyl (530 nmol g^{-1}), malonyl (14 nmol g^{-1}), succinyl (60 nmol g^{-1}) and free-CoA (63 nmol g^{-1}) showed a slight decrease compared to the measured CoA levels in the DHA-producing strain (**Fig. 16**).

At the onset of the stationary phase, a significant reduction in the levels of available CoA esters was also revealed in the wild type, suggesting a robust core metabolic activity of the yeast to utilize most of the available precursors during the growth phase and accumulate substantial amounts of native lipids (**Fig. 15E**).

4.3.4 Impact of the carbon source: glycerol versus glucose

When using glucose as a substrate instead of glycerol (both in concentration of 10 g L^{-1}), the overall characteristics of growth and production were found to be similar (**Table 9, Fig. 18**) (Papanikolaou et al., 2009). Intracellular CoA thioesters repertoire, as well as the intracellular fatty acids repertoire in glucose-based medium (**Fig. 18CE**) resembled the one measured from glycerol-based culture condition (**Fig. 18DF**).

Table 9. Impact of the carbon source on the formation of biomass, citrate, docosahexaenoic acid (DHA) and native fatty acids in Y. lipolytica Af4. The cultivations were performed in minimal medium, composed of 10 g L^{-1} of glucose or glycerol, 5 g L^{-1} of $(NH_4)_2SO_4$, and 1.7 g L^{-1} of yeast nitrogen base without amino acids and ammonium sulfate in 200mM MES buffer (pH 6.8). The maximum level of biomass and citrate was observed after 24h, whereas the given maximum concentration of native fatty acids was obtained after 36h. Final DHA titers, yields and contents correspond to the 180h time point (**Fig. 18**).

Carbon source [10 g L^{-1}]	Max biomass [g L^{-1}]	Max citrate [mM]	Max native FA [mg L^{-1}]	DHA titer [mg L^{-1}]	DHA yield [mg g_{CDM}^{-1}]	DHA content [%]
Glucose	6.3 ± 0.2	0.3 ± 0.1	321 ± 9	36 ± 1.3	9 ± 0.4	16 ± 1
Glycerol	**6.6** ± 0.1	0.7 ± 0.0	329 ± 7	**44** ± 2.6	11 ± 0.6	18 ± 1

Obviously, the growth-decoupled DHA production behavior was carbon source independent, even though the final DHA titer on glucose was 14.3% lower, eventually caused by the weaker accumulation of citric acid (**Table 9**) (Sabra et al., 2017). The preference for glycerol could come from the nature of the carbon source, mainly because glycerol serve as a backbone for TAG synthesis and therefore is one of the key molecules in the lipogenesis (Workman et al., 2013).

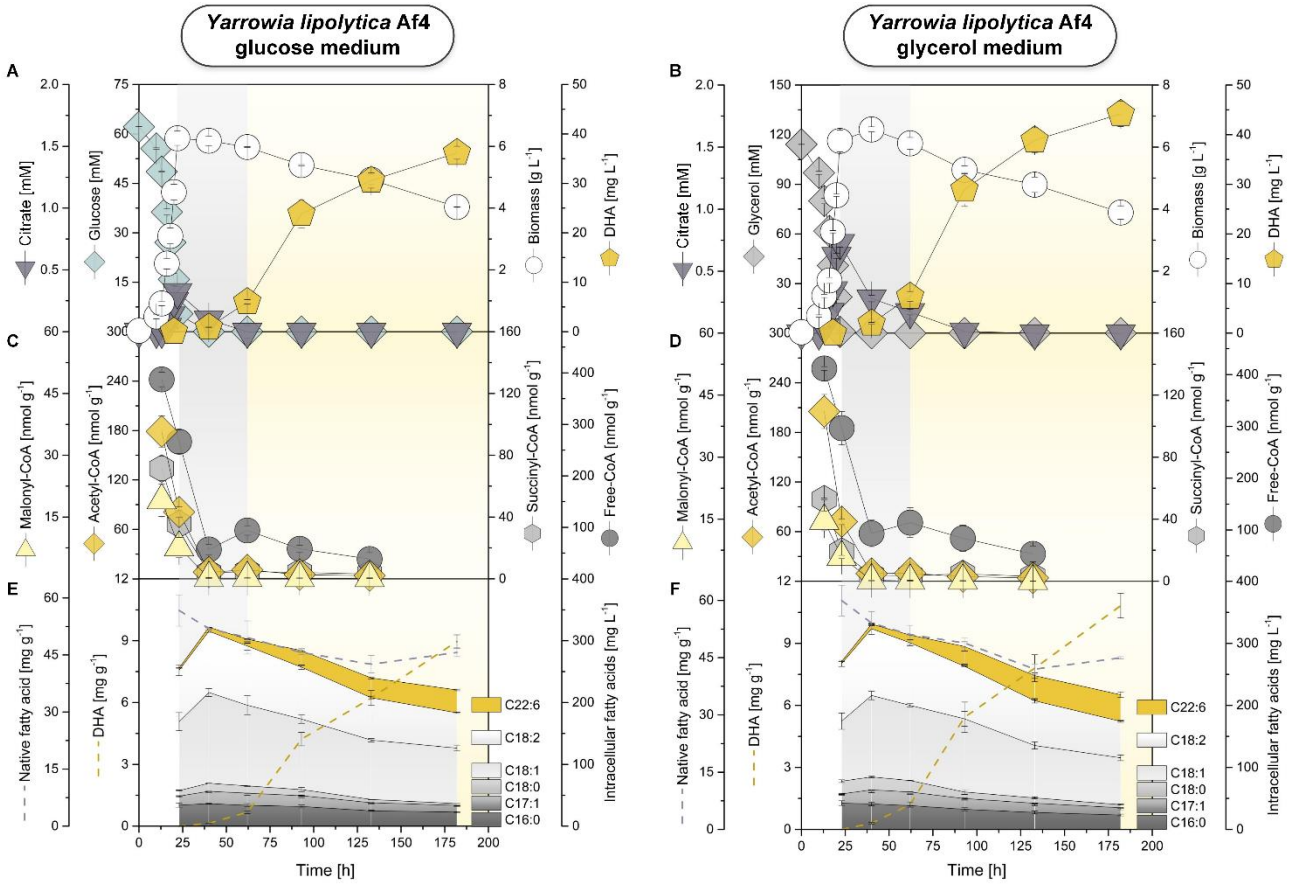

Figure 18. *Yarrowia lipolytica* Af4 cultivation profiles (A, B), CoA-thioester levels (C, D) and fatty acid concentrations (E, F) in glucose and glycerol-based medium, respectively. Both mediums contained 10 g L^{-1} of carbon source and other components of the reference minimal medium: 5 g L^{-1} of $(NH_4)_2SO_4$, and 1.7 g L^{-1} of yeast nitrogen base without amino acids and ammonium sulfate in 200mM MES buffer (pH 6.8). Final titers are present in **Table 7**. C16:0: palmitic acid, C17:1: margaric acid, C18:0: stearic acid, C18:1: oleic acid, C18:2: linoleic acid, C22:6: docosahexaenoic acid.

4.4 Global transcriptome profiling of DHA-producing *Y. lipolytica*

For a wider insight into cellular dynamics, we conducted a time series of global transcriptome analyses. The analysis, based on a custom-made microarray, provided a high level of agreement with qRT-PCR in temporal expression behavior and the magnitude of changes, underlining the consistency of both methods (**Fig. 11**). PCA analysis of 24 wild-type and overproducer transcriptome data sets from different cultivation time points revealed generally high reproducibility between biological replicates (**Fig. 19**). In addition, the PCA data revealed fundamental changes in global gene expression over time. Both strains showed a continuous shift of the transcriptome that resulted in a different expression pattern in each of the three process stages.

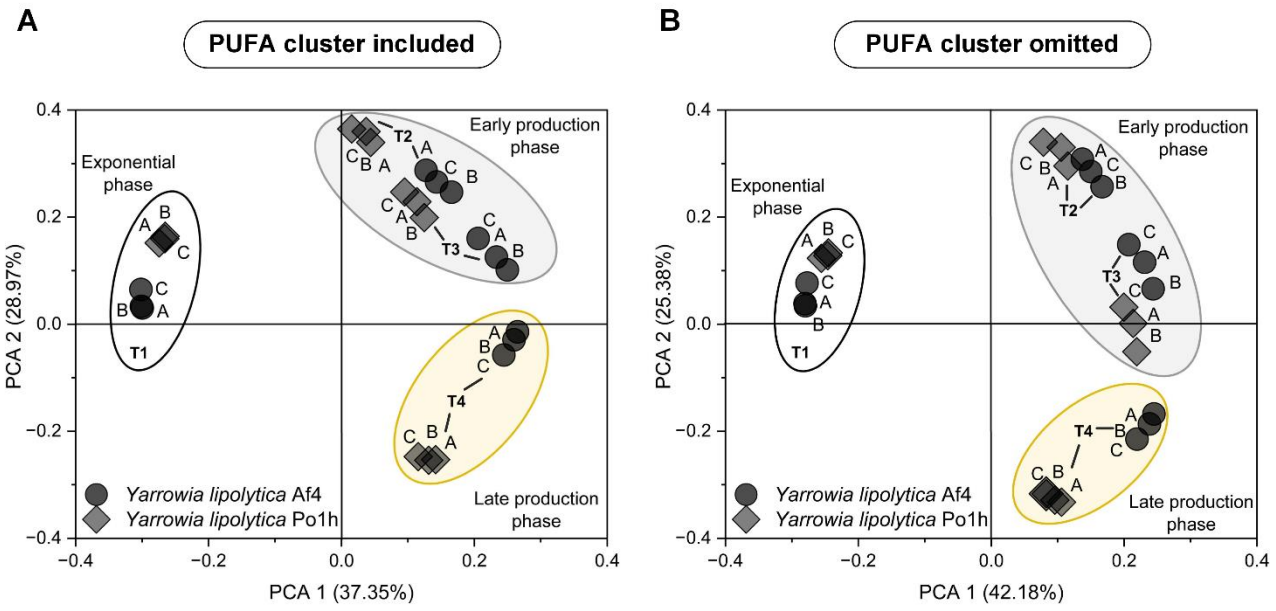

Figure 19. Statistical evaluation of the global gene expression profiling in *Y. lipolytica*. Principal component analysis (PCA) of the raw data obtained from custom-made DNA microarray analysis revealed statistical differences and similarities in gene expression between the DHA producer *Y. lipolytica* Af4 and the wild type Po1h at different stages of cultivation. In one scenario, the PCA considered all probes on the array to infer the overall similarity between the two strains (A), whereas, in another scenario, the PUFA cluster genes were excluded from the analysis to identify similarities in the native genes (B). The given points refer to the cultivation profiles in **Fig. 15B** and **Fig. 15C** (T1 – 10h, T2 – 24h, T3 – 48h, T4 – 72h), whereby all three biological replicates are shown.

Differences in expression were hereby observed for key genes around DHA biosynthesis, citrate, and fatty acid metabolism, so that we kept the division of the process in three phases in the following (**Appendix Fig. 30**). Interestingly, wild-type and overproducer exhibited a high concordance in global gene expression during exponential growth and early DHA production (**Appendix Fig. 31**). Towards the end of the process, the two strains drifted further apart, revealing a stronger impact of the heterologous pathway during this phase (**Appendix Table 12**).

4.4.1 Regulatory network dynamics around myxobacterial gene cluster

To further elucidate the transcriptome changes, we evaluated the data based on the three process phases: exponential phase, early DHA production phase, and late DHA production phase. In numbers, the recombinant DHA-producer changed the expression of 5,323 genes (82% of its genetic repertoire) upon the shift from growth to early DHA production: 3,286 genes were upregulated, and 2,037 genes were downregulated. In comparison, 2,118 genes were upregulated, and 3,205 genes were downregulated in the late DHA production phase, compared to the growth phase. For inspection of the transcriptional changes in central carbon metabolism, we selected a subset of approximately 200 genes. These encoded for biochemical reactions and pathways that were associated to glycerol, citrate and acetate metabolism, Emden-Meyerhof-Parnas (EMP) pathway, pentose phosphate (PP) pathway, TCA cycle, glyoxylate shunt, CoA ester metabolism, intercompartmental transport, lipid synthesis, lipid breakdown, DHA formation, and stress defense (**Fig. 20**).

Prominently, the coding sequences for the previously identified 17 subdomains of the PKS-like PUFA synthase (Gemperlein et al., 2014) were strongly and evenly up regulated, suggesting efficient and streamlined transcription of the entire enzyme complex upon the on-set of DHA production.

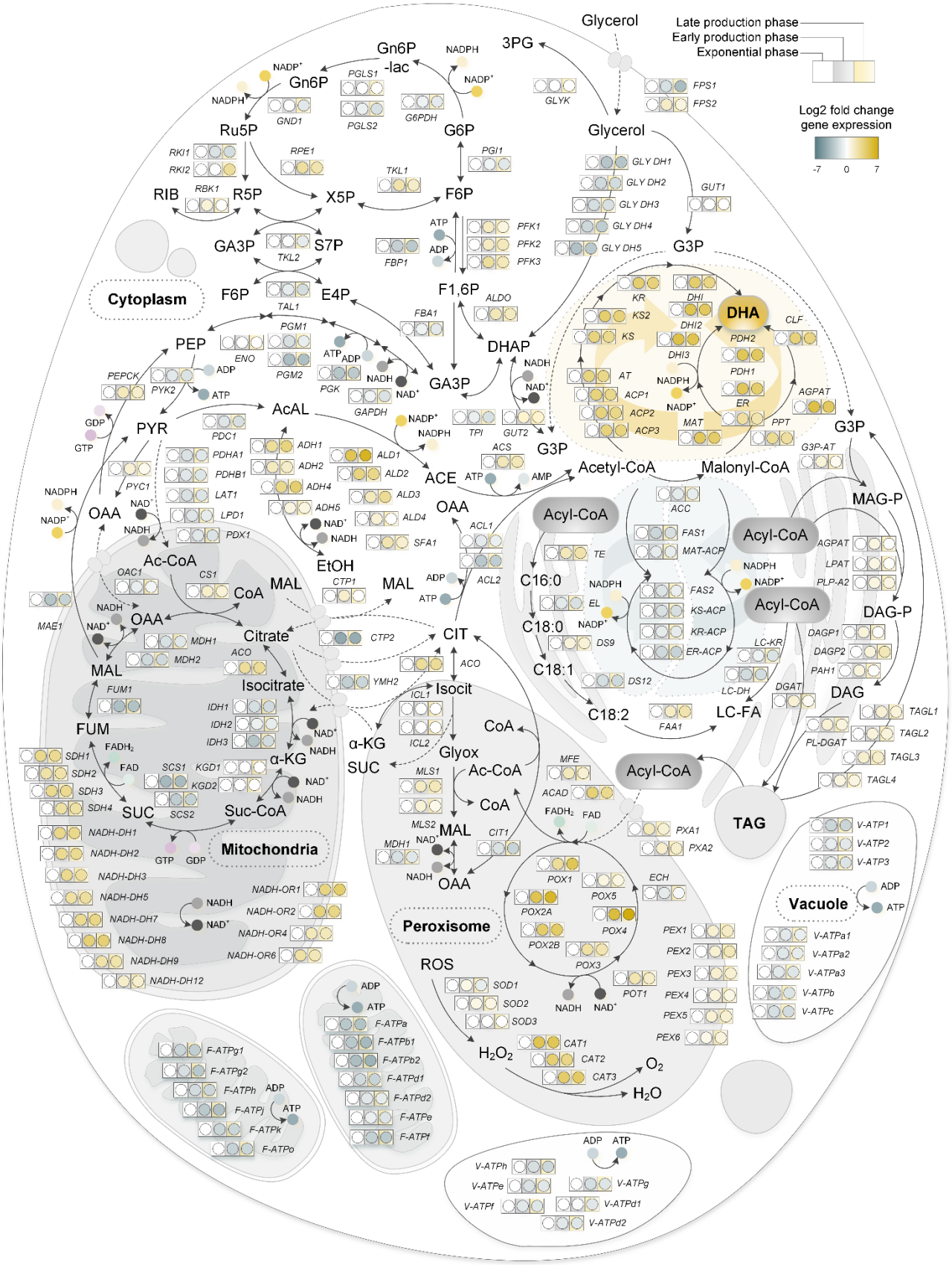

Figure 20. Transcriptional dynamics within the carbon metabolism of *Y. lipolytica* Af4 expressing a myxobacterial PKS-like synthase for production of DHA from glycerol.

The data reflect the gene expression at three different time points during the process, representing the exponential growth phase (10 h), the early stationary phase (48 h), and the late stationary phase (96 h) (**Fig. 15**). They display average values from three biological replicates, normalized to expression at 10 h for comparison. The complete raw and processed data sets are available at the Gene Expression Omnibus Database (GEO 224529). The presented (approximately 200) genes encode the core metabolic machinery of the yeast, including glycerol utilization, citrate and acetate metabolism, Emden-Meyerhof-Parnas (EMP) pathway, pentose phosphate (PP) pathway, TCA cycle, glyoxylate shunt, CoA ester metabolism, intercompartmental transport, lipid synthesis, lipid breakdown, DHA formation, and stress defense. The genes encode glycerol uptake *via* aquaglyceroporin, *FPS1*, *FPS2* *GLYDH*, glycerol dehydrogenase, *GUT1*, glycerol kinase, *GUT2*, G3P dehydrogenase (Erian et al., 2022; Lubuta et al., 2019); the PP pathway (Wasylenko et al., 2015; Yuzbasheva et al., 2017); the EMP pathway (Bian et al., 2018); *ADH*, alcohol dehydrogenase, *ALD*, aldehyde dehydrogenase (Liu et al., 2019a); the pyruvate dehydrogenase complex (*PDHA1, PDHB1, LAT1, LPD1, PDX1*) (Guo et al., 2014); *ACS*, acetyl-CoA synthetase (Gatter et al., 2016); the mitochondrial TCA cycle (da Silva et al., 2020); the peroxisomal glyoxylate shunt (Liu et al., 2019a; Liu et al., 2016); transporters for intercompartmental metabolite exchange, i.e. *OAC* (transport of oxaloacetate) (Luevano et al., 2010), *CTP1* (citrate/malate exchange), *CTP2* (transport of citrate), *YMH2* (citrate/α-ketoglutarate exchange) (Yuzbasheva et al., 2019), *PXA1,* PXA2, (transport of acyl-CoA) (Dulermo et al., 2015); *ACL1*, *ACL2*, ATP-dependent citrate lyase (Beopoulos et al., 2012); *ACC*, cytosolic acetyl-CoA carboxylase (Santin and Moncalian, 2018); *FAS1*, *FAS2,* fatty acid synthase (Liu et al., 2019c); *ACP*, acyl carrier protein, *TE*, thioesterase, *EL*, elongase, *DS9*, desaturase, DS12, desaturase, FAA1, long chain fatty acid synthase (Wang et al., 2022); *AGPAT*, 1-acylglycerol-3-phosphate O-acyltransferase, *DAGP*, diacylglycerol diphosphate phosphatase, *DGAT*, acyl-CoA: diacylglycerol acyltransferase (Qiao et al., 2015), *TAGL1-4*, triglyceride lipase isoenzymes (Dulermo and Nicaud, 2011); *ACAD*, acyl-CoA dehydrogenase*, POX1*-6, peroxisomal acyl-CoA oxidase, *MFE*, multifunctional β-oxidation enzyme, *POT1*, ketoacyl thiolase (Haddouche et al., 2011; Mlickova et al., 2004); *PEX1-6*, assembly proteins for peroxisomal genesis and membrane formation (Kiel et al., 2006); *SOD1*-3, superoxide dismutase, *CAT*, catalase (Biriukova et al., 2006); V-ATP, vacuolar ATPases, F-ATP mitochondrial ATPases (Li et al., 2011), and *pfa1, pfa2, pfa3,* and *ppt*, polyketide synthase-like enzyme complex composed of 17 subdomains to synthesize DHA (Gemperlein et al., 2019). Abbreviations: G6P – glucose 6-phosphate, F6P – fructose 6-phosphate, F1,6P – fructose 1,6-bisphosphate, GA3P – glyceraldehyde 3-phosphate, Gn6P – gluconate 6-phosphate, Ru5P – ribulose 5-phosphate, R5P – ribose 5-phosphate, RIB – ribose, X5P – xylulose 5-phosphate, S7P – sedoheptulose 7-phosphate, FUR6P – fructofuranose 6-phosphate, E4P – erythrose 4-phosphate, PEP – phosphoenolpyruvate, PYR – pyruvate, AcAL – acetaldehyde, ACE – acetate, OAA – oxaloacetate, α-KG – α-ketoglutarate, SUC – succinate, FUM – fumarate, MAL – malate, GLO – glyoxylate, 3PG – 3-phosphoglycerate, DHAP – dihydroxyacetone phosphate, G3P – glycerol-3-phosphate, LC-FA – long chain fatty acids, MAG-P – monoacylglycerol phosphate, DAG-P – diacylglycerol phosphate, DAG – diacylglycerol, TAG – triacylglycerol, ROS – reactive oxygen species.

4.4.2 Lipogenesis and lipid degradation

Temporal segregation of two antagonistic metabolic pathways, fatty acid synthesis (FAS) and PKS-like PUFA machinery, was observed on the global level (Metz et al., 2001). Highly energy demanding process of native fatty acid synthesis, along with subsequent elongation and desaturation steps, undergoes downregulation. Instead, previously synthesized fatty

acids are incorporated into lipid bodies through sequential enzymatic reactions involving 1-acylglycerol-3-phosphate O-acyltransferase (*AGPAT*) (Silverman et al., 2016), diacylglycerol diphosphate phosphatase (*DAGP*) (Fakas, 2017), and acyl-CoA: diacylglycerol acyltransferase (*DGAT*) (Gajdos et al., 2016). These reactions utilize glycerol-3-phosphate as a backbone and three acyl-CoAs and allow for the storage of synthesized fatty acids. Central carbon metabolism relies on glycerol transport, facilitated by *FPS1* and *FPS2* (Erian et al., 2022; Lubuta et al., 2019). The dihydroxyacetone-based pathway, the main route to catabolize external glycerol (Bellou et al., 2014) was downregulated, consistent with previous glycerol depletion (**Fig. 20**). The alternative G3P-based pathway was upregulated, likely to recycle G3P, formed during TAG degradation, back to DHAP (Beopoulos et al., 2008; Dulermo and Nicaud, 2011). Regarding lipid catabolism, genes encoding for TAG degradation (*TAGL1*, *TAGL2*, *TAGL3*, *TAGL4*) and peroxisomal β-oxidation were strongly upregulated, including the *POX* genes (**Fig. 20**).

The expression ratio between ATP-dependent citrate lyase (*ACL1, ACL2*) and aconitase (*ACO*) shifted in favor of the latter (Holz et al., 2009), presumably promoting the conversion of citrate into isocitrate instead of oxaloacetate and acetyl-CoA. The upregulation of *CTP1* during this phase, encoding for a mitochondrial citrate importer, matched this picture (**Fig. 20**). Isocitrate would then be available to fuel the peroxisomal glyoxylate shunt (Kamzolova et al., 2011; Lorenz and Fink, 2001), which was also found increased in expression, or to enter the mitochondrial TCA cycle (**Fig. 20**). Genes encoding mitochondrial TCA cycle enzymes revealed a mixed expression response. While most of them were downregulated, succinate dehydrogenase and citrate synthase (*CIT1*) were upregulated. Cytosolic acetyl-CoA synthetase (*ACS*) was found to be up regulated too, eventually linked to the re-use of acetate from the growth medium (**Fig. 15B**).

4.4.3 Acetyl-CoA as the central metabolic hub during the production phase

Overall, the expression changes indicated that the DHA-producing cells had fully adapted to the use of native lipids (Krivoruchko et al., 2015). The strongly reduced intracellular level of acetyl CoA during the stationary phase (**Fig. 16**) demonstrated that the intermediate (continuously formed from degraded lipids) was efficiently used up by other pathways, including the upregulated glyoxylate shunt as one route potentially involved. The further use of acetyl CoA could not be assigned to specific pathways given the complex transcriptional changes but as the CoA ester was the major catabolic intermediate at this point, a broad distribution within the metabolic network appeared likely. Upon glycerol consumption, *Y. lipolytica* exhibited typical environmental stress response, employing different enzymes such as succinate dehydrogenase (*SDH1-4*), NADH dehydrogenase (*NADH-DH1-12*), alcohol dehydrogenase (*ADH1-ADH5*) and others (Xu et al., 2017a). Other enzymes involved in oxidative phosphorylation showed similar scenario: mitochondrial and vacuolar ATP-ases were found to be down regulated and NADH-oxidoreductases upregulated. This suggests that the cells must cope with a significant increase in oxygen levels due to lipid oxidation (Li et al., 2011). Consequences of oxidative damage can be mitigated *via* two different types of enzymes, superoxide dismutase (*SOD1-3*) and catalase (*CAT1-3*): upregulation of genes that encode for these antioxidant enzymes indicate that the cell is fighting against reactive oxygen species (ROS), such as hydrogen peroxide (H_2O_2) which are a great threat to lipids, especially unsaturated fatty acids (Biriukova et al., 2006). Beneficially, the cells exhibited a strong upregulation of their defense system against oxidative stress (**Fig. 20**), important to protect the sensitive DHA molecule from oxidation (Xu et al., 2017b).

4.4.4 Insights into the nutritional impact on DHA production

Additionally, we explored different media with varied ratios between carbon, nitrogen, and phosphorous to produce DHA, as the availability of these elements has a crucial impact on growth and fatty acid metabolism in *Y. lipolytica* (Blazeck et al., 2014). The variation of the medium composition allowed to create different types of nutrient limitations (**Fig. 21**).

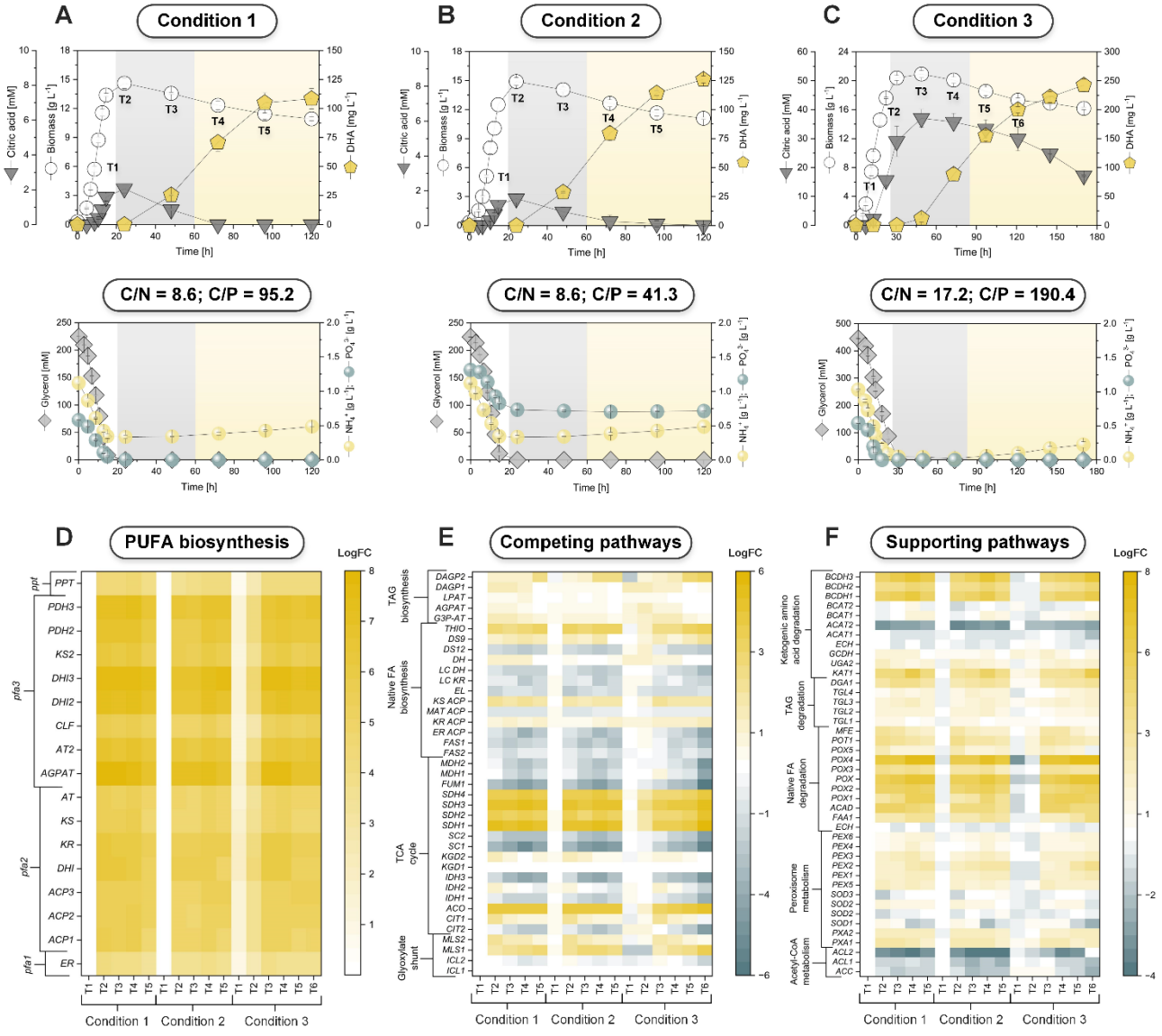

Figure 21. Impact of the supply of carbon, nitrogen, and phosphorous on the production of docosahexaenoic acid (DHA) in recombinant *Y. lipolytica* Af4. The data show the cultivation profiles from three set-ups using minimal medium with 20 g L^{-1} (220 mM) of glycerol, 5 L^{-1} of $(NH_4)_2SO_4$, 1 g L^{-1} KH_2PO_4 (A), 20 g L^{-1} (220 mM) of glycerol, 5 L^{-1} of $(NH_4)_2SO_4$, 2 g L^{-1} KH_2PO_4 (B), 40 g L^{-1} (440 mM) of glycerol, 5 L^{-1} of $(NH_4)_2SO_4$, 1 g L^{-1} KH_2PO_4 (C). The processes are divided into three phases of exponential growth, early DHA production, and late DHA production, indicated by the background color. Each of processes was additionally studied on the level of the transcriptome

at five time points (T1-T5) for the first two set-ups (A, B), and six time points (T1-T6) for the third one (C). All data are normalized to the gene expression levels of T1 in the reference process (A). They comprise DHA biosynthesis, i. e. all 17 subdomains of the four PKS-synthase complex, encoded by *pfa1*, *pfa2*, *pfa3*, and *ppt* D), genes encoding pathways that compete with DHA biosynthesis, including the glyoxylate shunt, the TCA cycle, native fatty acid biosynthesis including elongation and desaturation, and tri-acyl-glycerol biosynthesis (E), and genes encoding pathways that support DHA biosynthesis, including acetyl-CoA and malonyl CoA metabolism, peroxisomal β-oxidation, peroxisome assembly, triacyl-glycerol degradation, stress defense, and ketogenic acid amino catabolism (F). The data display means and standard errors from three biological replicates. The complete raw and processed transcriptome data sets are available at the Gene Expression Omnibus Database (GEO 224529). The encoded enzymes can be taken from the Appendix (**Appendix Table 13).**

Regarding production (**Fig. 21B**), doubling the amount of phosphate (condition 2) resulted in 25% more DHA (125 mg L^{-1}), while the double amount of carbon (condition 3) increased the DHA titer even by 100% (250 mg L^{-1}) (**Fig. 21C**). The latter set-up resulted in stronger citrate accumulation (up to 40 mM) and, also, a higher biomass concentration.

Therefore, increased amounts of glycerol displayed an efficient way to increase the production performance. Despite these differences in DHA production, however, transcriptional changes in pathways associated to PUFA synthesis and central carbon metabolism were found highly conserved between the different nutrient regimes (**Fig. 21**). In all cases, the levels of acetyl-CoA and malonyl-CoA collapsed with entry into the stationary phase (**Fig. 16**).

4.5 Deciphering the role of citrate in biosynthesis of DHA

Despite extensive efforts to elucidate the involvement of citrate in fatty acid metabolism in oleaginous organisms, its precise role remains a subject of ongoing debate. On one hand, some observation emphasized its beneficial role by facilitating the generation of cytoplasmic acetyl-CoA and, thereby promoting fatty acid biosynthesis (Goncalves et al., 2014), which was confirmed through higher lipid content in *Y. lipolytica* cultures supplemented with citric acid (Magdouli et al., 2020; Sabra et al., 2017). Nonetheless, other studies have presented

a contrasting perspective, suggesting that citrate biosynthesis may divert carbon from fatty acids, rendering it a by-product rather than a direct contributor to lipid production (Papanikolaou et al., 2002b; Qiao et al., 2017; Wang et al., 2013). Lastly, some profited from the dual nature of citrate and used it to produce both lipids and citric acid (Abghari and Chen, 2017).

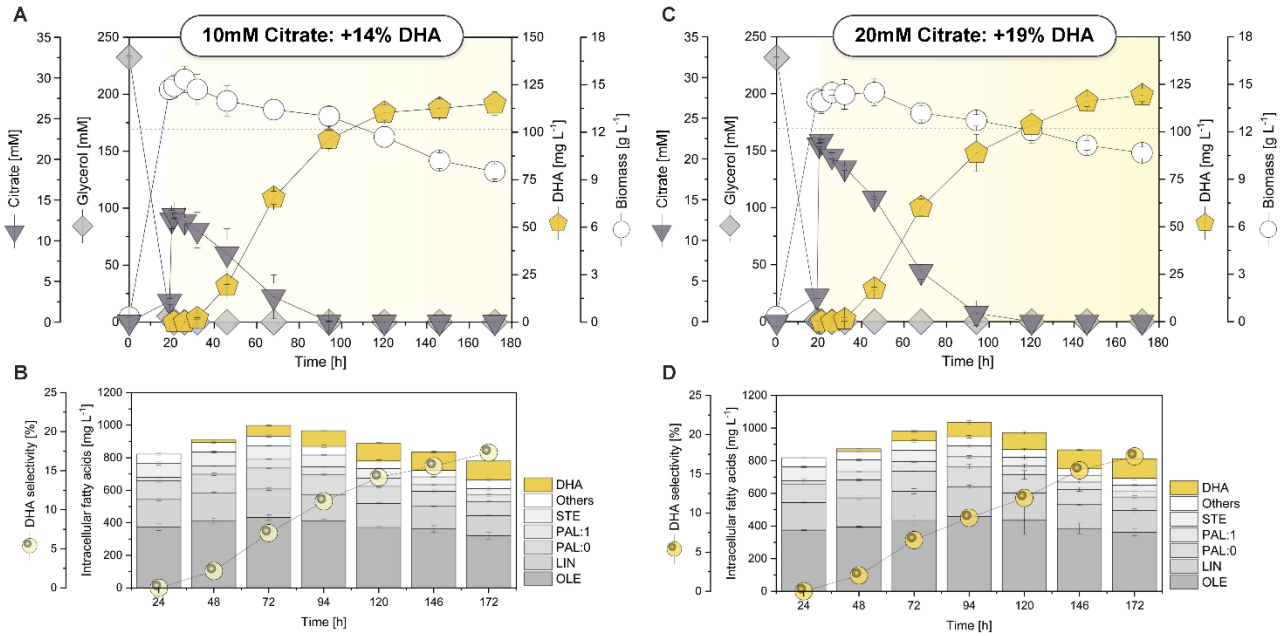

Figure 22. Enhanced DHA production in recombinant *Y. lipolytica* Af4 upon supplementation with 10 mM (AB) and 20 mM citrate (CD). The different concentrations of citrate were added at the end of the growth phase when glycerol was depleted. The data represent the cultivation profile using a minimal medium with 20 g L^{-1} (220 mM) of glycerol as the sole carbon source (A, C) and changes in the intracellular content of native fatty acids and DHA over time (B, D). PAL:0, palmitic acid (C16:0); PAL:1, palmitoleic acid (C16:1); STE, stearic acid (C18:0); OLE, oleic acid (C18:1); LIN, linoleic acid (C18:2); DHA, docosahexaenoic acid (C22:5). Other native fatty acids occurring in low amount such as docosanoic acid (C22:0), tetracosanoic acid (C24:0), and hexacosanoic acid (C26:0) are given as summed fraction. The data display means and standard errors from three biological replicates.

Citrate played an important role, given its re-utilization during the major DHA production observed here and before (Jia et al., 2022). To clarify its metabolism further, we separately spiked 10 mM and 20 mM of citrate to the medium at the beginning of the stationary phase (20 h, increasing the broth level to 13 mM and 23 mM, respectively) (**Fig. 22AC**). The pulse provided an extended phase of citrate excess. While upon-feeding, citrate was present up

to 100 h, the organic acid was depleted after 60 h in the control. It was interesting to note that citrate was consumed two times faster in the culture supplemented with 10 mM (2.8 mg g^{-1} h^{-1}) and three times (4.5 mg g^{-1} h^{-1}) as compared to the control (1.4 mg g^{-1} h^{-1}), eventually triggered by the increased availability. Favorably, supplementation increased the synthesis of DHA (**Fig. 22B**). The relative fraction of DHA among total fatty acids (17%) was, however, unchanged due to a simultaneously stimulated synthesis of native fatty acids (**Appendix Table 14**). The relative improvement of the DHA titer (15% and 19%) was slightly higher than the extra amount of supplemented carbon (10%), indicating a preferred use of citrate for DHA synthesis over other processes.

Strikingly, the addition of citrate impacted the levels of the CoA-esters (**Fig. 23AB**). The pool of succinyl-CoA was doubled, indicating that citrate was directed into the TCA cycle in the mitochondrion, the only pathway that can form this intermediate in *Y. lipolytica* (Cui et al., 2017). The doubled succinyl-CoA level coincided with the increased specific citrate uptake rate, suggesting that the flux into the TCA cycle was increased, likely to catabolize the extra carbon that entered the cell. In addition, the added (and faster consumed) citrate resulted in increased intracellular levels of acetyl-CoA and malonyl-CoA (**Fig. 23AB**). The 40 h longer period of citrate excess, furthermore, provided an extra benefit in later phases of the culture. Two days after the supplementation (when extracellular citrate was only left in the spiked culture), the abundance of acetyl-CoA and malonyl-CoA was still 2.3-fold and 2.9-fold higher in culture with 10 mM citrate, while in culture with 20 mM citrate, acetyl-CoA and malonyl-CoA 3-fold and 4.6-fold higher.

4.5.1 Tracing ^{13}C-enriched patterns upon citrate feeding

In a separate experiments, we fed 10 mM and 20 mM 99% [$^{13}C_6$] citrate as isotopic tracer after 20 h, which resulted in 13 mM 75% [$^{13}C_6$] citrate and 23 mM 87% [$^{13}C_6$] citrate (3 mM

of non-labelled citrate was present at this time point). We then monitored the ^{13}C enrichment in intracellular metabolites over time using GC/MS and LC-MS/MS. Notably, we detected prominent ^{13}C enrichment in CoA esters (**Fig. 23BD**).

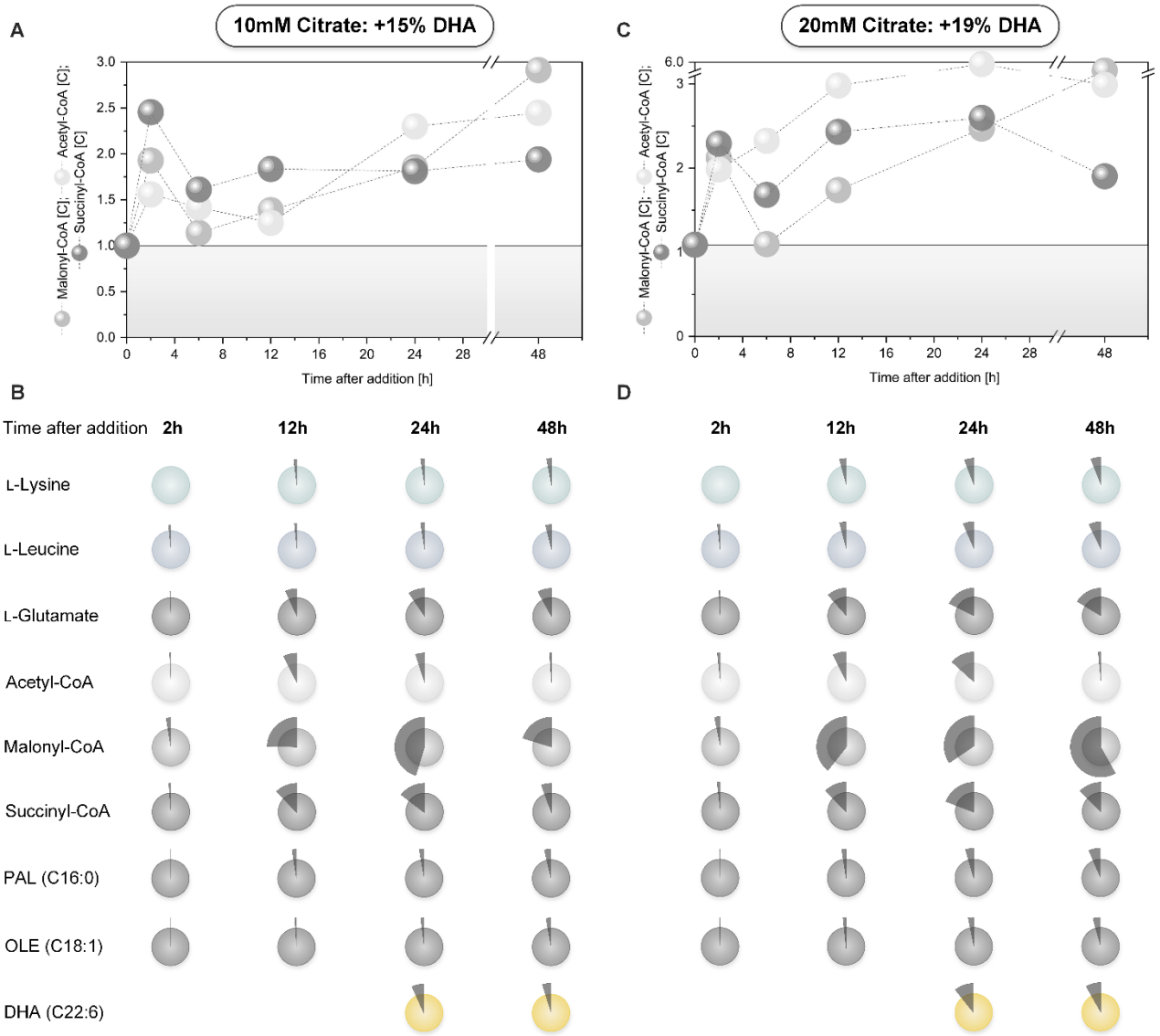

Figure 23. Metabolic pathway profiling in DHA-producing *Y. lipolytica* using ^{13}C-labelled isotopic tracers. In separate experiments, 10 mM and 20 mM of 99% [$^{13}C_6$] citrate (A, C) was spiked into the cultures at the end of the growth phase, when glycerol was depleted. This time point is given as 0 h here. The data comprise the dynamics of the intracellular pools of selected amino acids and CoA-esters (A, C), after addition of the corresponding tracer. The concentrations are given as relative values, as compared to the non-supplemented process [C]. In addition, the data show dynamic changes in the ^{13}C enrichment of intracellular amino acids, CoA-esters, native fatty acids, and DHA, assessed by LC-MS/MS and GC/MS, from the time point of addition of the ^{13}C-based tracer (B, D). From left to right the data represent measurements after 2 h, 12 h, 24 h, and 48 h. The data display means and standard errors from three biological replicates.

As example, in the first culture (10 mM of labeled tracer), malonyl-CoA exhibited 45% ^{13}C enrichment, 24 h after the tracer had been added, revealing that it originated to almost 60% from external citrate at this time point. The ^{13}C labelling of succinyl-CoA proved that citrate was (at least partially) metabolized *via* the TCA cycle in the mitochondrion, matching the increased succinyl-CoA abundance (Holz et al., 2011). Furthermore, amino acids such as L-glutamate (10%), L-glutamine (13%), and L-aspartate (11%) were significantly enriched in ^{13}C (**Fig. 23B**). These changes could not be attributed to a particular compartment due to the presence of various isoenzymes for isocitrate dehydrogenase and L-glutamate dehydrogenase in the cytosol, the mitochondrion, and the peroxisome (Li et al., 2013; Pomraning et al., 2016).

In fact, the occurrence of ^{13}C in all detected amino acids at later stages indicated a broad metabolic use of citrate (**Fig. 23B**). Strikingly, we could prove the incorporation of citrate-derived carbon into native fatty acids such as PAL, OLE, and into the heterologous product DHA (**Fig. 23B)**. The DHA ^{13}C-labelling went through a maximum (7% after 24 h), indicating a transient shift from the use of citrate to the use of fatty acids, related to the onset of lipid degradation and citrate depletion (**Appendix Fig. 32**). In the other supplemented culture (20 mM citrate), similar patterns were observed with slightly higher share of enriched molecules. Without doubt, the beneficial effects of supplementing citrate to increase precursor availability during the major phase of DHA production appeared valuable to be exploited further.

4.6 Catabolic breakdown of ketogenic and mixed amino acids

Acetyl-CoA sits at the crossroad of many metabolic pathways (Vorapreeda et al., 2012). Interestingly, the intermediate is formed during degradation of certain amino acids. The catabolization of the ketogenic amino acids L-lysine and L-leucine ultimately yields two and

even three molecules of acetyl-CoA, different to glucogenic amino acids that end up in other intermediates (Woolfson, 1983). L-isoleucine as example, belongs to a third group and exhibits a mixed type, forming one acetyl-CoA among other intermediates (D'Andrea, 2000). Given the previous findings, it appeared straightforward to study these catabolic pathways in more detail.

The transcriptome data of the DHA producer provided an interesting picture. When the cells entered the stationary phase at the onset of DHA production, they strongly upregulated genes encoding enzymes involved in degradation of acetyl-CoA-delivering amino acids, i. e. L-lysine (log2-fold up to 4.3), L-leucine (log2-fold up to 5.5), and L-isoleucine (log2-fold up to 5.5) (**Fig. 24ABC**). This picture indicated the activation of catabolic routes for ketogenic amino acids to replenish the acetyl-CoA pool during the stationary phase (Sabra et al., 2017). In contrast, degradation pathways for glucogenic amino acids (not yielding acetyl-CoA) were downregulated, exemplified for L-glutamate, glycine, L-serine, and L-aspartate (log2-fold up to -4.3) (**Fig. 24D, Appendix Table 15**).

It should be noted that the increased expression of genes encoding ketogenic amino acid pathways was observed for all tested nutrient conditions, suggesting a general response of the yeast to glycerol depletion (**Fig. 21DEF**).

Y. lipolytica uses lysine both as a nitrogen and as a carbon source, *via* the *N*-6-acetyllysine-5 aminovalerate pathway (Barth and Gaillardin, 1997). Previously, the *LYC1* gene encoding the first step of the pathway, *N*-6-lysine acetyl transferase (*LAT*), was cloned and sequenced and shown to be induced by L-lysine (Beckerich et al., 1994). For completion, the additionally encoded saccharopine pathway is shown (**Fig. 24A**). The degradation of L-isoleucine and L-leucine is catalyzed by same route, involving branched-chain amino acid aminotransferase (*BCAT1, BCAT2*), 2-oxoisovalerate dehydrogenase (*BCDH1, BCDH2*) and dihydrolipoyl transacylase (*BCDH3*) and several CoA-ester intermediates (Shao et al., 2018) (**Fig. 24BC**).

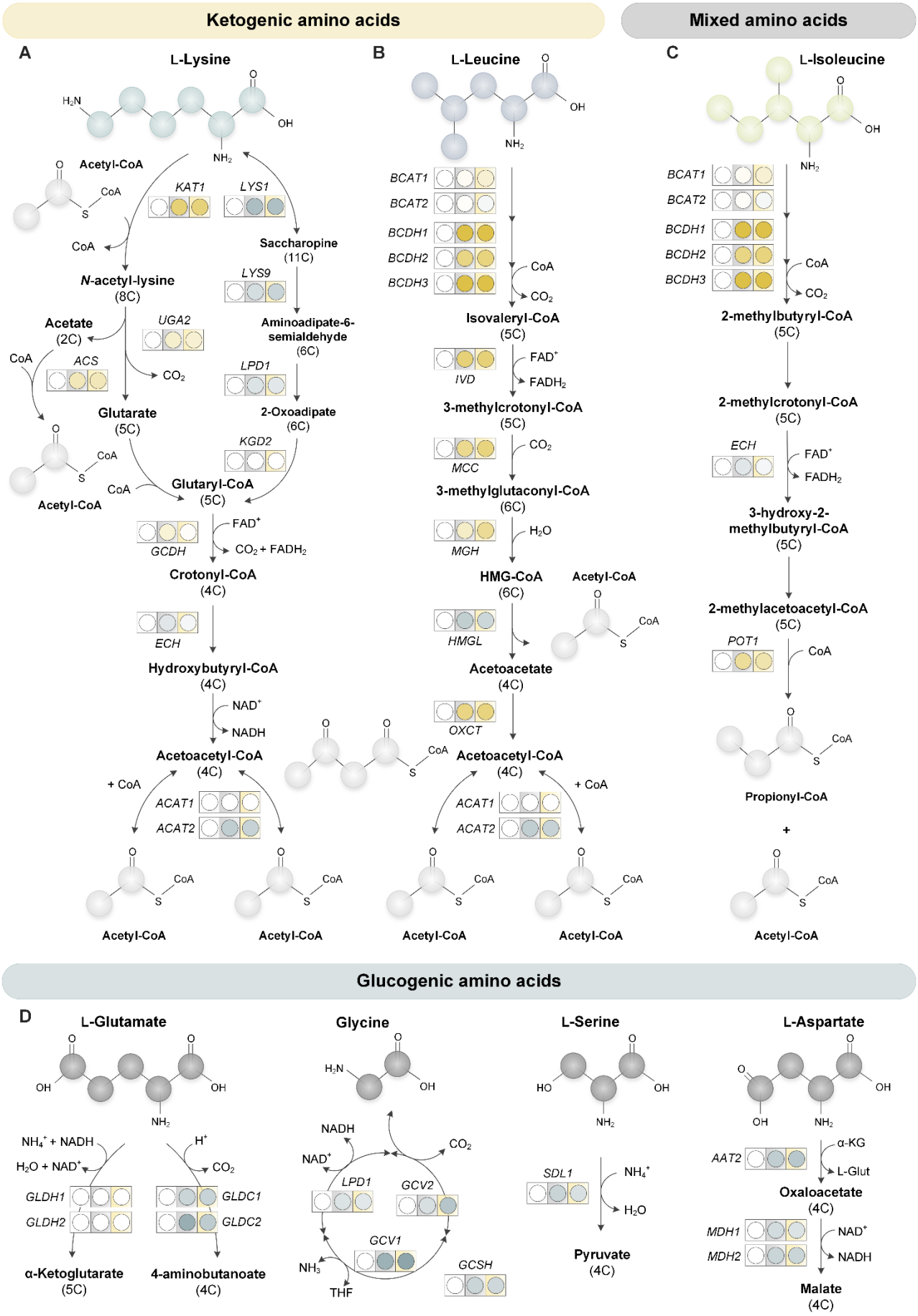

Figure 24. Transcriptional dynamics around the amino acid and CoA-ester metabolism in DHA-producing recombinant *Y. lipolytica* Af4.

The data comprise transcriptional changes in degradation pathways for the ketogenic amino acids L-lysine (A) and L-leucine (B), the mixed-type amino acid L-isoleucine (C), and the glucogenic amino acids L-glutamate, glycine, L-serine, and L-aspartate (D). The data refer to samples taken from a glycerol-based batch process (**Fig. 15B**) after 10 h, 48 h, and 96 h, respectively, and display means and standard errors from three biological replicates. Abbreviations: L-lysine-N-acetyltransferase (*KAT*), glutarate semialdehyde oxidoreductase (*UGA2*), acetyl-CoA synthetase (*ACS*), glutaryl-CoA dehydrogenase (*GCDH*), enoyl-CoA hydratase (*ECH*), acetyl-CoA acetyltransferase (*ACAT1*, *ACAT2*), branched chain amino acid aminotransferase (*BCAT1*, *BCAT2*), branched chain keto acid dehydrogenase (*BCDH*1, *BCDH2*, *BCDH3*), isovaleryl-CoA dehydrogenase (*IVD*), methyl-crotonyl-CoA carboxylase (*MCC*), methyl-glutaconyl-CoA hydratase (*MGH*), HMG-CoA lyase (*HMGL*), 3-oxoacid CoA-transferase (*OXCT*), 3-ketoacyl-CoA thiolase (*POT1*), L-glutamate:NADP dehydrogenase (*GLDH1, GLDH2*), L-glutamate decarboxylase (*GDC1, GDC2*), dihydrolipoamide dehydrogenase (*LPD1*), glycine decarboxylase (*GCV1, GCV2*), glycine cleavage system H protein (*GCSH*), L-serine dehydratase (*SDL1*), L-aspartate:2-oxoglutarate aminotransferase (*AAT2*), malate dehydrogenase (*MDH1, MDH2*).

The degradation of L-lysine, L-leucine, and L-isoleucine proceeds *via* HMG-CoA, isovaleryl-CoA, crotonyl-CoA, hydroxybutyryl-CoA, and propionyl-CoA, respectively (Park et al., 2020) (**Fig. 24ABC**), and we applied LC-MS/MS to study these intermediates. The analysis revealed *Y. lipolytica* exhibited a rich set of CoA esters with three to six carbon side chains in all growth stages (**Fig. 25, Appendix Table 16**), opposed to the rather limited short chain CoA ester repertoire found in *S. cerevisiae* (Krink-Koutsoubelis et al., 2018).

Strikingly, the pools of HMG-CoA, isovaleryl-CoA, and propionyl-CoA, displaying intermediates from L-leucine and L-isoleucine catabolism, respectively, were increased more than four-fold in stationary-phase cells, as compared to exponentially growing cells. In accordance with the transcriptome data, this accumulation indicated enhanced degradation of these amino acids (**Fig. 25**).

Interestingly, the intracellular levels of free L-lysine, L-leucine, and L-isoleucine remained rather constant (**Appendix Table 17**). Obviously, these pools were constantly fueled from degraded protein, matching the generally increased expression of genes encoding the protein degradation machinery (**Appendix Table 18**). Taken together, the yeast utilized different internal resources, including lipid-derived fatty acids and protein-derived (mainly ketogenic) amino acids to fuel its central carbon metabolism during the stationary phase. Acetyl CoA displayed the central hub, where the activated catabolic pathways merged.

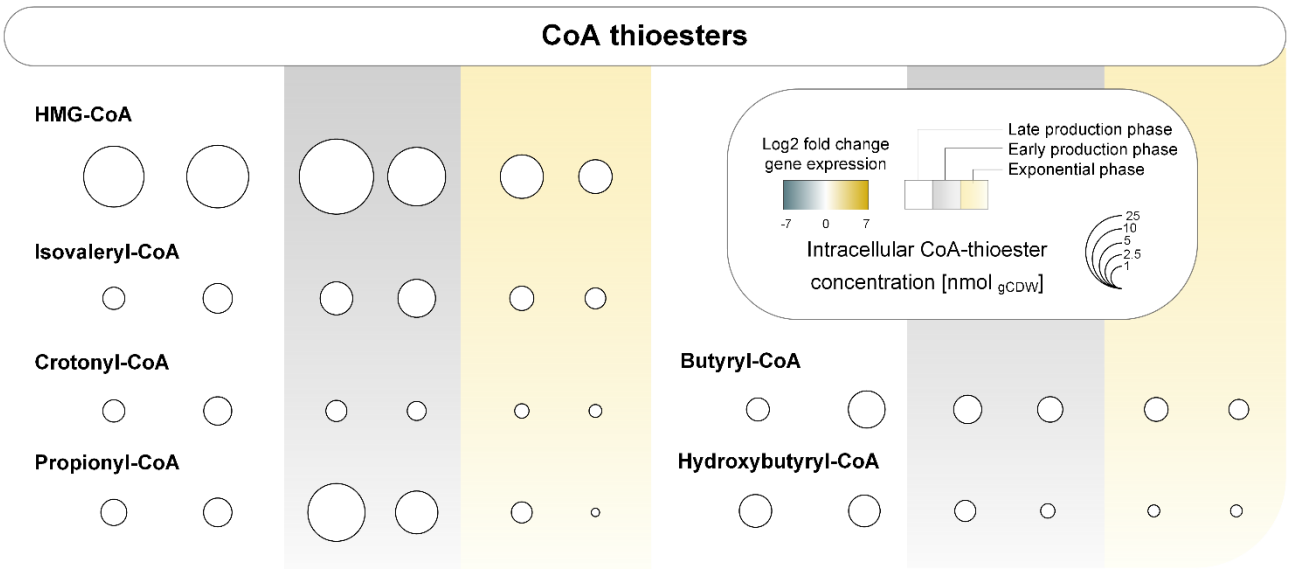

Figure 25. Metabolic dynamics around the amino acid and CoA-ester metabolism in DHA-producing recombinant *Y. lipolytica* Af4. The data comprise changes in intracellular CoA-esters. The concentrations were assessed at different time points during the cultivation: exponential growth phase (6h, 10h), early stationary phase (24h, 48h) and late stationary phase (72 h, 96 h) from a glycerol-based batch process (**Fig. 15B**) and display means from three biological replicates.

4.7 Time-resolved feeding strategy with L-Lysine, L-Leucine and L-Isoleucine

The obtained picture inspired us to explore individual amino acid feeding strategies. We therefore conducted additional *Y. lipolytica* cultures that were supplied with 10 mM of L-lysine, L-leucine, and L-isoleucine, respectively, when glycerol was depleted (**Fig. 26**). At this time point, ammonium (500 mg L^{-1}) was still available so that the supplementation did not recover the cells from nitrogen limitation (they were phosphate limited instead) (**Fig. 21A**). Supplementation enabled a remarkable increase in production (**Fig. 26CEG, Table 10**). The final DHA titer was increased by 30%, 33%, and even 38%, when adding a small amount of L-lysine, L-leucine, and L-isoleucine, respectively. Furthermore, the supplemented cultures achieved a far higher selectivity in production. As example, L-lysine-feeding yielded an almost 40% higher content of DHA among total fatty acids (**Fig. 26DFH**), resulting from an intensified degradation of native fatty acids in this process (**Appendix Table 14**).

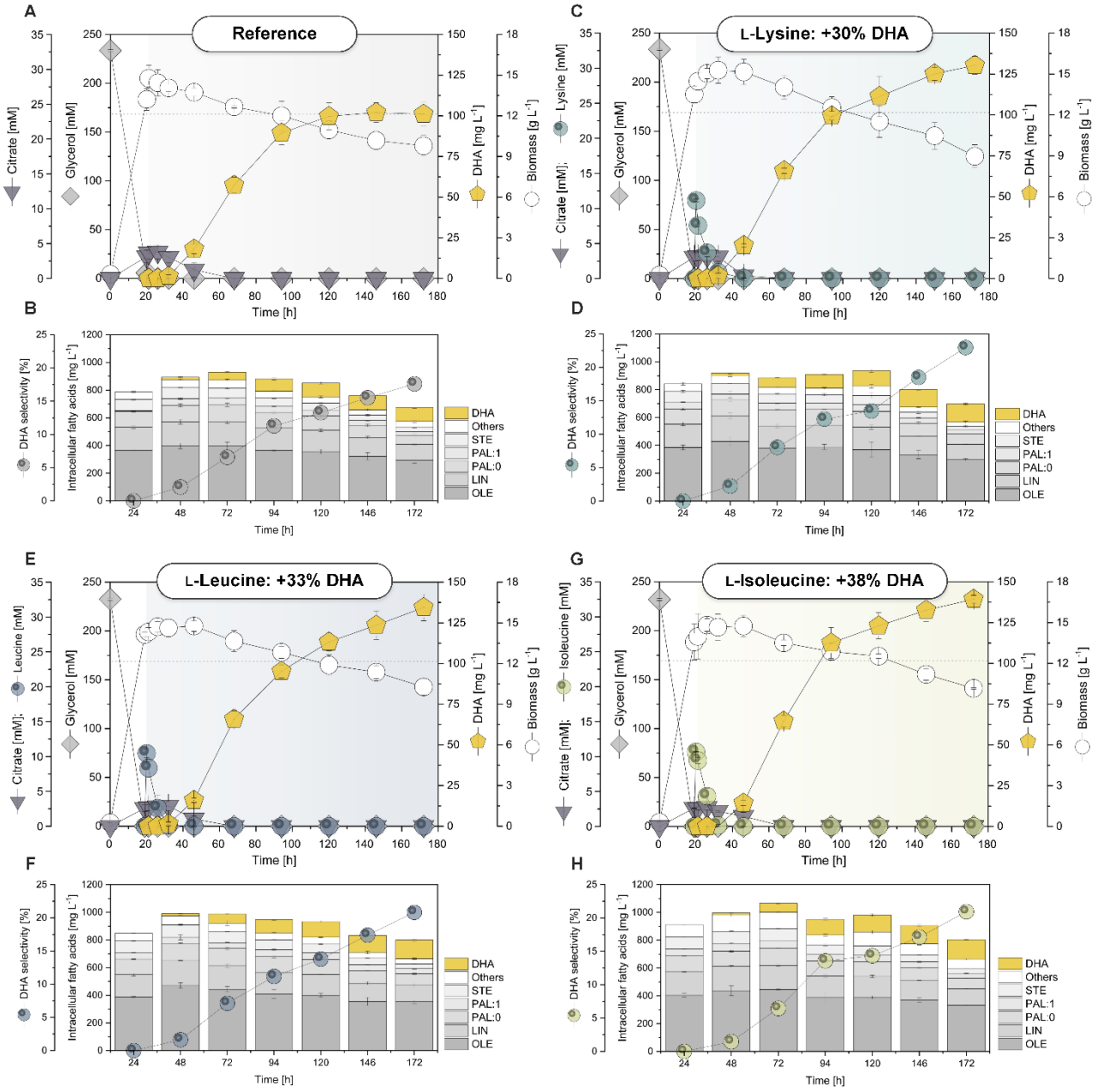

Figure 26. Enhanced DHA production in recombinant *Y. lipolytica* Af4 (reference condition - A, B) upon supplementation with L-lysine (C, D), L-leucine (E, F), and L-isoleucine (G, H). Different supplements (10 mM each) were added at the end of the growth phase, when glycerol was depleted. The data represent the cultivation profile using a minimal medium with 20 g L^{-1} (220 mM) of glycerol as the sole carbon source (A), additionally supplemented L-lysine (C), L-leucine (E), and L-isoleucine (G) and changes in the intracellular content of native fatty acids and DHA over time (B, D, F, H). PAL:0, palmitic acid (C16:0); PAL:1, palmitoleic acid (C16:1); STE, stearic acid (C18:0); OLE, oleic acid (C18:1); LIN, linoleic acid (C18:2); DHA, docosahexaenoic acid (C22:5). Other native fatty acids occurring in low amount such as docosanoic acid (C22:0), tetracosanoic acid (C24:0), and hexacosanoic acid (C26:0) are given as summed fraction. The data display means and standard errors from three biological replicates.

In this regard, supplementation with ketogenic and mixed-type amino acids emerged as smart way to boost heterologous PUFA synthesis in *Y. lipolytica*. In terms of production increase each of the amino acids was two- to three-fold more efficient than citrate and glycerol resulting only in 15% and 10% increase in DHA titer when adding the same amount of carbon, respectively. It was therefore interesting to study the underlying metabolic processes in more detail.

Table 10. The impact of supplementation on DHA production in recombinant *Y. lipolytica* Af4. Each supplement was added when the cells had depleted glycerol (**Fig. 22AC, Fig. 26CEG**). The given biomass concentrations are the maximum values, which were achieved at the end of the growth phase. The DHA titer and selectivity reflect the values at the process end, whereas the specific productivity represents the average over the entire process. The data displays the average values and standard errors from three biological replicates. CDM, cell dry mass; TFA, total fatty acids.

[a] significantly different from the reference

[b] significantly different from the supplementation with 10 mM citrate

Supplement	Growth [g_{CDM} L^{-1}]	DHA titer [mg L^{-1}]	DHA selectivity [% of TFAs]	DHA productivity [mg L^{-1} d^{-1}]
-	10 ± 1	101 ± 7 [b]	17 ± 1	17 ± 2 [b]
Citrate [10 mM]	10 ± 0	115 ± 6 [a]	17 ± 0	19 ± 1 [a]
Citrate [20 mM]	**11 ± 0**	120 ± 3 [a]	17 ± 1	20 ± 1 [a]
L-Lysine [10 mM]	9 ±1	**130 ± 6** [a,b]	**23 ± 1** [a,b]	**21 ± 1** [a]
L-Leucine [10 mM]	10 ± 0	**134 ± 8** [a]	**20 ± 0** [a,b]	**21 ± 2**
L-Isoleucine [10 mM]	10 ± 0	**139 ± 3** [a,b]	**21 ± 0** [a,b]	**25 ± 1** [a,b]

Upon addition, the amino acids were immediately consumed. Interestingly, they were each taken up at a similar rate: 4.0 mg g^{-1} h^{-1} for L-lysine, 3.5 mg g^{-1} h^{-1} for L-leucine and 3.6 mg g^{-1} h^{-1} for L-isoleucine, respectively. They were depleted from the medium within 12 hours (**Fig. 26CEG**). The production of DHA, however, was found still enhanced more than 100 hours later, which was surprising on a first glance. On the other hand, amino acid

supplements have been shown to trigger delayed metabolic effects in other microbes (Gläser et al., 2021).

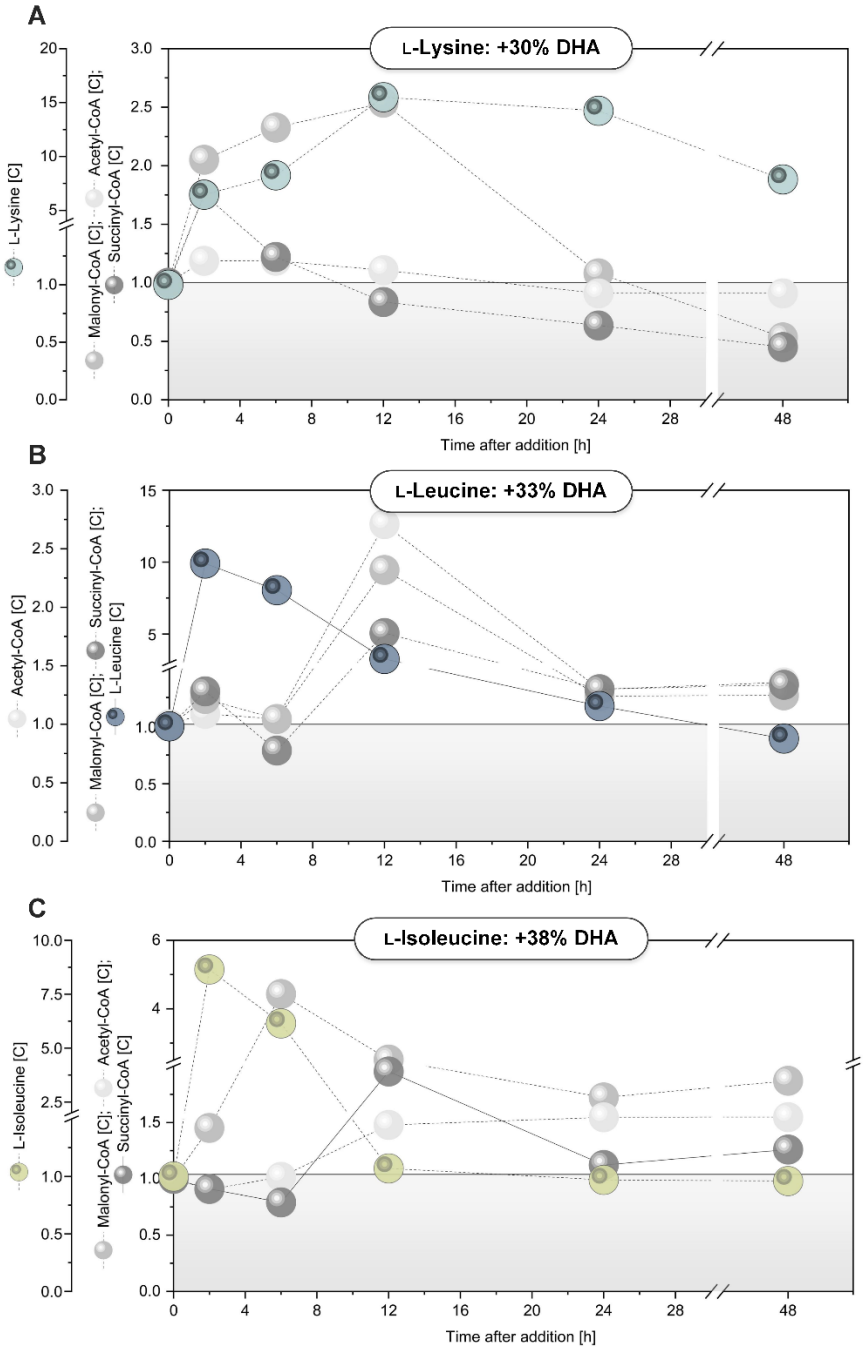

Figure 27. Supplementation effects of L-lysine (A), L-leucine (B) and L-isoleucine (C) on core metabolic compounds in DHA-producing *Y. lipolytica*. In separate experiments, L-lysine (A), L-isoleucine (B) and L-isoleucine (C), each at concentration of 10 mM were spiked into the cultures at the end of the growth phase, when glycerol was depleted. This time point is given as 0 h here. The data displays the dynamics of the intracellular pools of selected amino acids and CoA-esters, throughout the observed time points 2, 6, 12, 24 and 48h after addition of the corresponding tracer. The concentrations are given as relative values, as compared to the non-supplemented process. The data display means and standard errors from three biological replicates. The plot refers to the cultivation shown in **Fig. 26CEG.** Values are presented as relative changes in selected intracellular metabolites compared to the reference condition shown in **Fig. 26A.** [C] – correlation values between supplemented and non-supplemented cultures.

Indeed, the levels of intracellular CoA-esters were significantly increased by the supplementation, and these changes lasted for long time. We observed up to 2-fold higher levels of acetyl-CoA and malonyl-CoA (**Fig. 27ABC**). The level of catabolic CoA-ester intermediates from degradation of the added amino acids was increased up to almost 200-fold (**Appendix Fig. 33**). Notably, the CoA ester pools remained increased for a long time, after the amino acid had been depleted. As example, the pools of acetyl-CoA and malonyl-CoA were found to be two-fold increased 36 h after L-isoleucine had been depleted (the last time point analyzed) (**Appendix Fig. 33**).

4.7.1 Dynamic ^{13}C-based metabolic pathway profiling

An interesting picture was observed for the pools of free intracellular L-lysine, L-leucine, and L-isoleucine. The changes for L-leucine and L-isoleucine were strong but lasted only relatively short. Within a few hours, the corresponding intracellular level of the supplemented amino acid sharply rose in each of the two processes (up to ten-fold) (**Fig. 27BC**). Afterwards, it decreased and reached the level of non-supplemented cells within 12 h (L-isoleucine) and 24 h (L-leucine). In comparison, the intracellular pool of L-lysine was boosted the most upon supplementation (up to 15-fold), and the increased level was maintained for a longer time Cells contained ten-fold more L-lysine than non-supplemented cells, even 48 h after L-lysine had been added (**Fig. 27A**). Notably, *Y. lipolytica* strains can store L-lysine in the vacuole (Beckerich et al., 1986), which could well explain why the cells could maintain high L-lysine levels over several days. In this regard, the transiently stored ketogenic amino acid functioned as a reservoir of acetyl-CoA-based carbon, seemingly serving a similar purpose as a cellular lipid.

Isotopic tracer studies with 10 mM [$^{13}C_6$] L-lysine and 10 mM [$^{13}C_6$] L-leucine, respectively, could prove efficient use of the two amino acids to form DHA (**Fig. 28AB**). Based on ^{13}C

enrichment, the external amino acids were the dominant sources to synthetize intracellular acetyl-CoA (up to 60% and 64%) and malonyl-CoA (up to 55% and 55%). During the first day after supplementation, newly formed DHA contained 34% of L-lysine-derived carbon, based on ^{13}C enrichment (**Fig. 28A**), whereas supplemented L-leucine accounted for 19% (**Fig. 28B**). The tracer study further revealed that both amino acids entered the TCA cycle, as inferred from the rapid incorporation of ^{13}C in succinyl-CoA (**Fig. 28AB**). The slight incorporation of ^{13}C in PAL and OLE indicated that the native fatty acid synthesis was still on-going to some extent.

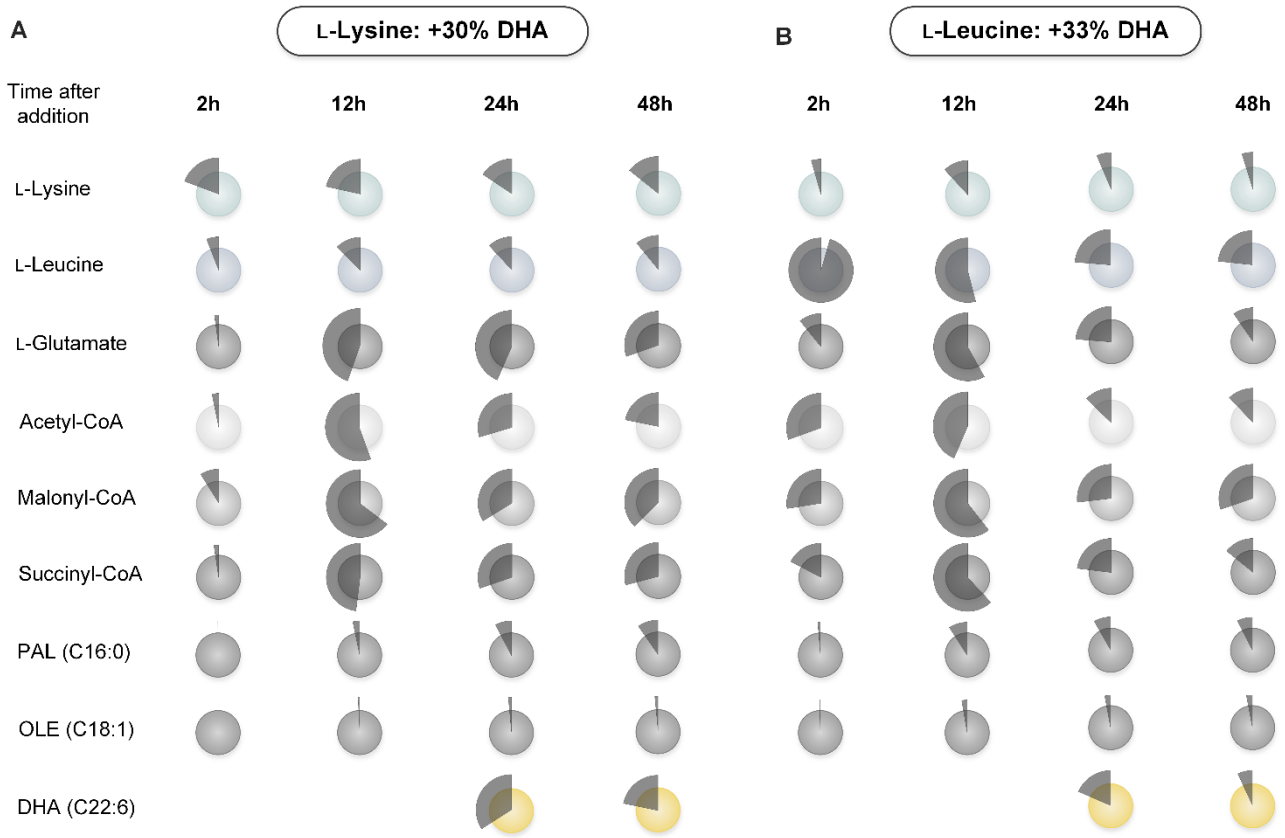

Figure 28. Metabolic pathway profiling in DHA-producing *Y. lipolytica* using 13C-labeled isotopic tracers (L-lysine – A, L-leucine – B). The data show dynamic changes in the ^{13}C enrichment of intracellular amino acids, CoA-esters, native fatty acids, and DHA, assessed by LC-MS/MS and GC/MS, from the time point of addition of the ^{13}C-based tracer. From left to right the data represent measurements after 2 h, 12 h, 24 h, and 48 h; changes in concentrations are presented on **Fig. 27AB**. The data display means and standard errors from three biological replicates.

Taken together, supplementation with ketogenic and mixed-type amino acids provided elevated levels of acetyl-CoA and malonyl-CoA, which, *inter alia,* boosted production of the PUFA. In terms of production, the dilution of ^{13}C in DHA in both tracer cultures (**Appendix Fig. 32**) indicated a diminishing contribution of the ketogenic amino acids during later stages of the process, suggesting sequential pulses for an intensified effect. Interesting differences between L-lysine and L-leucine resulted from the ^{13}C labelling of the intracellular amino acid pools. Shortly, after spiking [$^{13}C_6$] L-leucine into the culture, the intracellular L-leucine pool was found 95% ^{13}C-enriched, showing that it was almost completely composed of the externally added tracer. Different to that, the intracellular L-lysine pool revealed a substantially lower ^{13}C-enrichment) upon [$^{13}C_6$] L-lysine addition. A possible explanation could be the distribution of intracellular L-lysine between the cytoplasm and the vacuole (Beckerich et al., 1986) so that only the cytosolic fraction was subjected to fast replenishment by the isotopic tracer. Such a compartmentation of L-lysine would also explain the observation that L-glutamate (being a high-abundance cytosolic amino acid) and other metabolites became stronger enriched in ^{13}C than L-lysine itself (**Fig. 28A**).

4.8 Scaling up the DHA production process to lab-scale bioreactors

Next, we aimed to transfer the process to lab scale bioreactors. Previously, only one process configuration was applied to overproduce DHA in *Y. lipolytica* Af4 in a bioreactor (Gemperlein et al., 2019). The chosen strategy comprised a glycerol or glucose-based fed-batch with continuous feeding of the corresponding carbon source after depletion of the initially batched amount. When using glycerol, this set-up enabled the accumulation of 300 mg L^{-1} of DHA over 300 h at a selectivity of 7% of TFA, while cells reached a maximum biomass concentration of 30 g L^{-1} and piled up citrate up to 40 g L^{-1} during the glycerol-limited feed-phase. The selectivity of this process was much lower than that achieved in this

work using glycerol-grown batch cultures in shake flasks (17% of TFA) (**Fig. 15A, Table 7**), and the huge amount of unused citrate at the end of the process appeared as drawback too.

We therefore decided to test different process alternatives (**Table 4**). Given the positive effect of an increased glycerol level on the DHA titer, the first set-up comprised a batch process with 100 g L^{-1} of glycerol, 5 g L^{-1} of $(NH_4)_2SO_4$, and 1 g L^{-1} KH_2PO_4 (C-N-P) (**Fig. 29A**). The online recording of process parameter revealed that temperature and DO level were well controlled at the desired set-points, which was also found for all other processes. The final DHA titer (446 mg L^{-1}) was almost 50% higher than the value reported before, while the transiently accumulated citrate (58 mM) was re-used completely (Gemperlein et al., 2019).

Obviously, the set-up that had worked well in shake flasks could be successfully transferred to the bioreactor scale to overproduce DHA, and it was possible to increase the initial amount of carbon source to higher level towards higher titers. Different to the shake flask cultures, the accumulation of citrate was much higher, likely caused by the higher initial glycerol level and eventually the better aeration. The selectivity of DHA production (9% of TFA) was rather low, caused by the elevated formation of native fatty acids (**Table 11**). In a second set-up (C-N-2P), we reduced the C:P ratio and doubled the amount of phosphate, aiming at a higher biomass concentration (**Fig. 29B**). Indeed, cell growth lasted longer (even into the citrate consumption phase) and a significantly increased maximum biomass concentration (54 g L^{-1}) was reached after approximately 150 h. Despite the higher cell concentration, it took much longer to re-consume the accumulated citrate. DHA accumulated to a final titer of 574 mg L^{-1}. In comparison to the reference process, the increased production was largely due to the higher level of cells. The ratio between biomass and DHA concentration was almost identical between the two processes, and so was the DHA selectivity (8% of TFA) (**Table 11**). In a third set-up, we reduced the C:N ratio (C-2N-P) and doubled the amount of nitrogen in the medium (**Fig. 29C**).

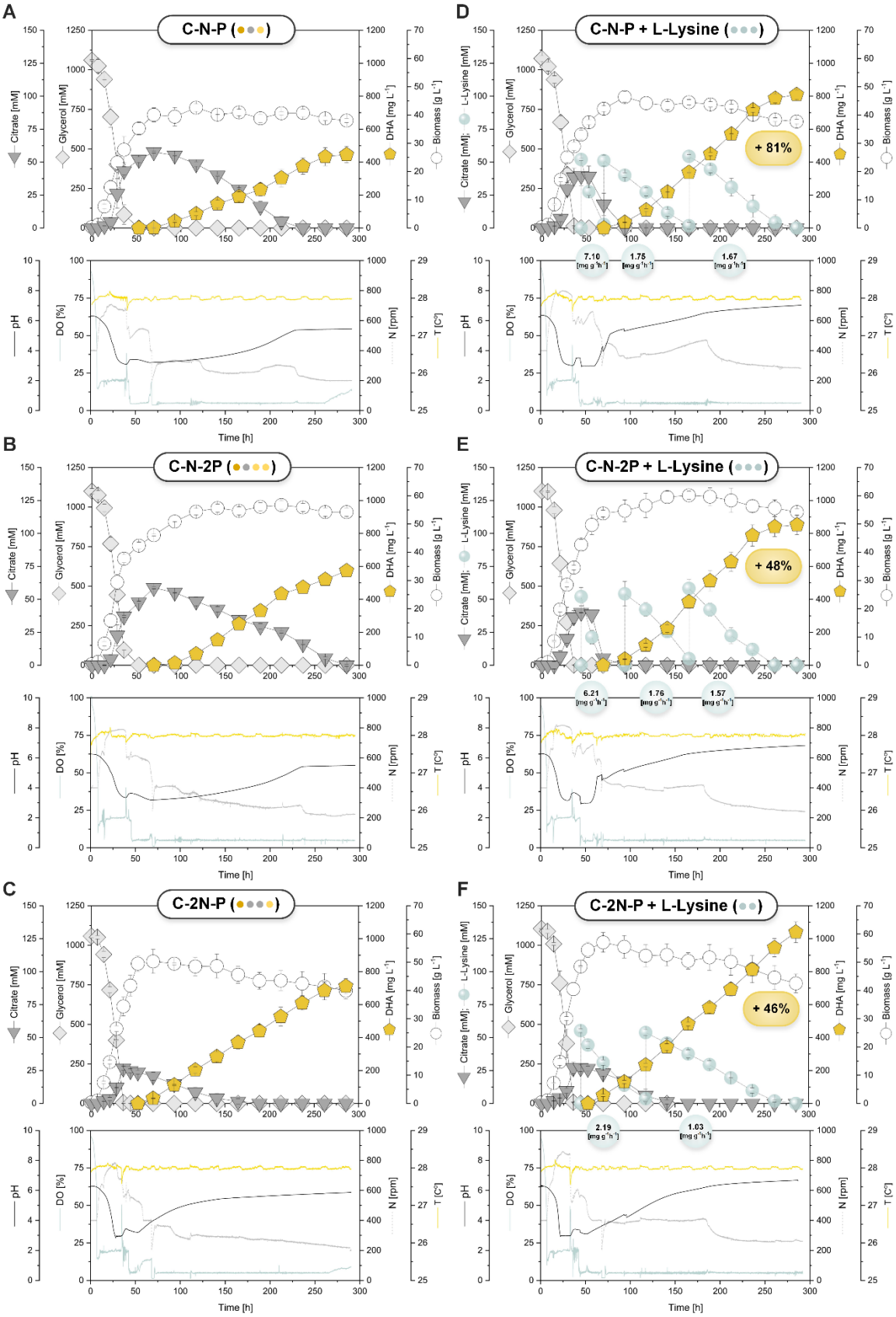

Figure 29. Benchmarking the production of docosahexaenoic acid (DHA) in recombinant *Y. lipolytica* Af4 in lab scale bioreactors. The processes were based on different nutrient regimes (**Table 4**) and partially received small shots of L-lysine during the DHA production phase (B, D, F). The data represent the fermentation profiles and online monitored process parameters. The data display means and deviations from two biological replicates.

This set-up was inspired by the fact that citrate, although promoting the supply of acetyl CoA, at the same stimulated the generation of native fatty acids (**Fig. 22**) (Magdouli et al., 2020; Sabra et al., 2017) that competed with the formation of DHA, thereby causing a low selectivity to produce DHA (**Table 10**). The excretion of citrate, *inter alia*, was known to be limited by a low C:N ratio (Goncalves et al., 2014). The chosen set-up met all expectations. Citrate accumulated to a much lower extent (**Fig. 29C**), while DHA titer (712 mg L^{-1}) and selectivity (16% of TFA) were found significantly increased (**Table 11**). Moreover, the cells grew much faster so that the maximum biomass concentration was reached one day earlier than in the other processes. The DHA production started about one day earlier as well than (**Fig. 29ABC**).

4.9 Benchmarking of the new L-lysine feeding strategy in a fed-batch process

Finally, all three production conditions (C-N-P, C-N-2P, C-2N-P) were used to benchmark the newly developed feeding strategy at the bioreactor scale (**Fig. 29BDF**). L-Lysine was chosen as the supplement, because it displayed a cheap industrial bulk product, widely available from renewable feedstocks through microbial fermentation (Becker et al., 2011; Hoffmann et al., 2021). After the depletion of glycerol (after around 48h), all cultures received a first shot of L-lysine. In the two nitrogen-limited cultures, the supplemented lysine was consumed at a high rate within only 24 h (**Fig. 29DE**). Surprisingly, its presence in the process immediately stopped the excretion of citrate (which continued to increase in the corresponding non-supplemented processes (**Fig. 29ABCD**). Over the next three days, Y. lipolytica Af4 co-consumed L-lysine (refilled in the culture *via* a second shot) with citrate, whereby the amino acid caused a massively increased citrate re-assimilation rate. A third shot of L-lysine was given in both cultures after about 135 h. On the contrary, the ammonium-enriched condition (C-2N-P), exhibited a more than three-fold lower L-lysine uptake rate

(**Fig. 29F**), so that, overall, only two pulses were given during the whole process. At the process end, the supplemented L-lysine was consumed in all three process set-ups.

Supplementation of the ketogenic amino acid boosted the DHA titer remarkably. The three supplemented cultures accumulated 809, 855, and 1039 mg L^{-1} of DHA, respectively, 81%, 48% and 46% more than in the corresponding non-supplemented processes (**Table 11**). Beneficially, the supplementation resulted in a significantly lower native fatty acid content which drastically improved DHA selectivity up to 27% of TFA (**Table 11**).

Table 11. Benchmarking of ketogenic feeding strategies for DHA production in recombinant *Y. lipolytica* Af4. The data summarizes the performance of batch and fed-batch processes in lab scale bioreactors (**Fig. 8**). The basic batch medium contained 100 g L^{-1} of glycerol, 5 g L^{-1} of $(NH_4)_2SO_4$, and 1 g L^{-1} of KH_2PO_4 as sources for carbon (●), nitrogen (●), and phosphorous (●). Additional setups comprised double amounts of nitrogen (●●●●) and phosphorous (●●●●). Each configuration was operated as batch process and as fed-batch process, additionally supplemented during the stationary phase with two (●●), or three (●●●) feed pulses from a concentrated L-lysine stock, each increasing the L-lysine level to 50 mM. The biomass concentration displays the maximum value achieved during the process. DHA titer, selectivity, and content reflect the maximum values at process end, whereas the specific productivity represents the average over the entire process. The data displays the average values and deviations from two biological replicates. CDM, cell dry mass; TFA, total fatty acids.

[a] significantly enhanced by lysine feeding

[b] significantly enhanced as compared to an assumed set-up that received the same amount of carbon in the form glycerol, considering that the extra glycerol would proportionally increase the DHA production

	DHA titer [mg L^{-1}]	DHA selectivity [% of TFAs]	DHA yield [mg g_{CDM}^{-1}]	Growth [g_{CDM} L^{-1}]	DHA productivity [mg L^{-1} d^{-1}]
C-N-P (●●●)	446 ± 49	9 ± 1	12 ± 1	38 ± 1	45 ± 6
C-N-P (●●●) L-lysine (●●●)	809 ± 22 [a,b]	22 ± 0 [a]	22 ± 0	38 ± 1	90 ± 2 [a]
C-N-2P (●●●●)	574 ± 48	8 ± 0	11 ± 0	**54 ± 1**	64 ± 2
C-N-2P (●●●●) L-lysine (●●●)	853 ± 54 [a,b]	21 ± 2 [a]	16 ± 1	**54 ± 1**	95 ± 6 [a]
C-2N-P (●●●●)	712 ± 46	16 ± 1	19 ± 3	40 ± 6	72 ± 5
C-2N-P (●●●●) L-lysine (●●)	**1039 ± 63** [a,b]	**27 ± 1**	**24 ± 0**	43 ± 4	**106 ± 7** [a]

It should be noted, L-lysine partially served as a carbon source for growth. Its addition slightly enhanced the biomass cell concentration as compared to the non-supplemented cultures (**Table 11**). However, even when assuming that one would have added the same extra amount of carbon in the form of glycerol and this would have resulted in a concomitantly improved DHA titer, the feeding of lysine still appeared superior (**Table 11**).

5 CONCLUSIONS AND OUTLOOK

PUFAs have entered the forefront of industrial biotechnology. The enormous impact of PUFAs on human health on one hand, supported by the recent U.S. FDA approval of health claims on DHA containing foods and dietary supplements, and the anticipated near future gap have created a market with highly lucrative opportunities for PUFA-rich superfoods, aquafeed, and medical formulations. At this stage, DHA producing microbes have a huge potential for industrial application. Considering recent trends, we can expect better performing strains that might even approach theoretical limits in near future. Synthetic biology and systems metabolic engineering, designing and optimizing cells on a global level, will be a strong driver for this development. Hereby, bioprocess operation must be further optimized to reduce cost and increase sustainability, e.g. by using waste streams and non-food renewables for the production (Becker and Wittmann, 2019; Kothri et al., 2020; Poblete-Castro et al., 2020; Tian-Yuan et al., 2019).

Over recent years, the oleaginous yeast *Y. lipolytica* has revealed a remarkable potential to synthetize PUFAs. Heterologous extension of native fatty acid biosynthesis through desaturases and elongases, the so-called aerobic route has provided a range of PUFAs between sixteen and twenty carbons. The first report on overproducing the twenty-two-carbon long DHA molecule in *Y. lipolytica* was based on a myxobacterial polyketide synthase (PKS)-like PUFA-cluster instead. This so-called anaerobic route utilizes only half (14 mol) of the NAD(P)H, as compared to the aerobic route (26 mol) (Jovanovic et al., 2021) and seems to exclusively exist in microorganisms, such as marine and terrestrial bacteria (Gemperlein et al., 2014; Gemperlein et al., 2018) and unicellular microalgae (Allemann and Allen, 2018).

Here, we provided a detailed picture of the metabolic and regulatory dynamics, linked to heterologous DHA production in *Y. lipolytica*. As shown, the shift from the growth to the

stationary phase at the onset of DHA production was associated to fundamental changes in the carbon core metabolic machinery of the yeast (**Fig. 20**). While cells switched from the use of glycerol to the use of native lipids and excreted citrate, both providing acetyl-CoA as the central intermediate, the level of acetyl-CoA and its derivative malonyl-CoA, dropped by up to 98% into the picomolar range (**Fig. 16**). The two CoA-metabolites displayed precursors to synthetize DHA, so their shortage suggested a bottleneck limiting production. Using global transcription profiling, we discovered that the cells activated the degradation of ketogenic amino acids, presumably to contribute to the supply of acetyl-CoA (**Fig. 24**). As shown, supplementation of the cultures with lysine, leucine, and isoleucine significantly increased the CoA-esters pools during the DHA production phase (**Fig. 26**) and resulted in strongly increased titers (**Table 10**), finally enabling DHA production at the gram scale in recombinant *Y. lipolytica* for the first time (**Fig. 29, Table 11**). Hereby, DHA was produced at high selectivity (27 % of TFA) which promises to facilitate its downstream purification for high-value medical applications that require the pure product (Li et al., 2021).

From the viewpoint of optimization strategies, the quantitative systems biology experiments were crucial to discover a limiting bottleneck within a complex metabolism, understand the overall physiology of the producing strain during the process, and use the gained knowledge to design a straightforward strategy for superior production. So far, we know only little about the abundance of intracellular CoA esters in *Y. lipolytica*. Therefore, we could encourage a stronger use of the recently LC-MS/MS based approach that allowed precise absolute quantification of even low abundance CoA esters, given the fact that these intermediates are important precursors for various products of interest to be produced in the yeast (Cordova and Alper, 2018; Ledesma-Amaro and Nicaud, 2016; Xie et al., 2015).

Inter alia, the newly developed feeding strategy appears not only useful for DHA production, as shown here, but could also promote the production of other valuable chemicals in *Y. lipolytica* also other (polyunsaturated) fatty acids (Cao et al., 2022; Jia et al., 2022), as well

as polyketides, terpenoids, flavonoids, and tetracyclines, respectively (Choi and Da Silva, 2014; Sun et al., 2018a). As example, heterologous expression of a polyketide synthase from *Schizochytrium* sp. in *Y. lipolytica* led to the accumulation of EPA and other 20-carbon long polyunsaturated fatty acids, displaying a very similar strategy as used here (Jia et al., 2023). Furthermore, feeding ketogenic precursors could nicely complement genetic strategies that aim at elevated acetyl-CoA supply through the overexpression of *acl ACL* (Wei et al., 2021) and *ACC* (Tai and Stephanopoulos, 2013). As shown, the feeding of different ketogenic amino acids increased various CoA-ester pools in addition to acetyl-CoA and malonyl-CoA (**Appendix Fig. 33**), which could promote the synthesis of compounds that require one of these intermediates as precursor (Kuhl et al., 2020; Kuhl et al., 2021).

Regarding DHA biosynthesis in *Y. lipolytica* there are still several unresolved issues that require further investigation. This study has highlighted the critical importance of intracellular availability and localization of DHA precursors, namely acetyl and malonyl-CoA (Harwood, 2019). This highly dynamic process could be effectively enhanced from carefully designed strategies, involving gene silencing and overexpression, specifically tailored for stationary phase (Shi et al., 2018b). For instance, simultaneous activation of genes responsible for increased production of acetyl and malonyl-CoA (Liu et al., 2019b), coupled with the deactivation of genes involved in competitive routes of DHA synthesis, may help overcome process limitations. Until today, the exact localization of enzymes, molecules and transport mechanisms in *Y. lipolytica* remains poorly understood. Therefore, it would be very interesting to resolve the underlying metabolism on the protein level and enhance the comprehensive multi-omics understanding obtained thus far. Innate potential of *Y. lipolytica* in utilizing diverse carbon sources, as previously demonstrated (Zeng SY et al., 2018) was not addressed in this study. Exploring the utilization of various waste materials for DHA synthesis, both in flask-scale experiments and in bioreactor systems, could hold significant biotechnological implications, justifying further investigation (Sinigaglia et al., 1994).

6 APPENDIX

6.1 Supplementary data figures

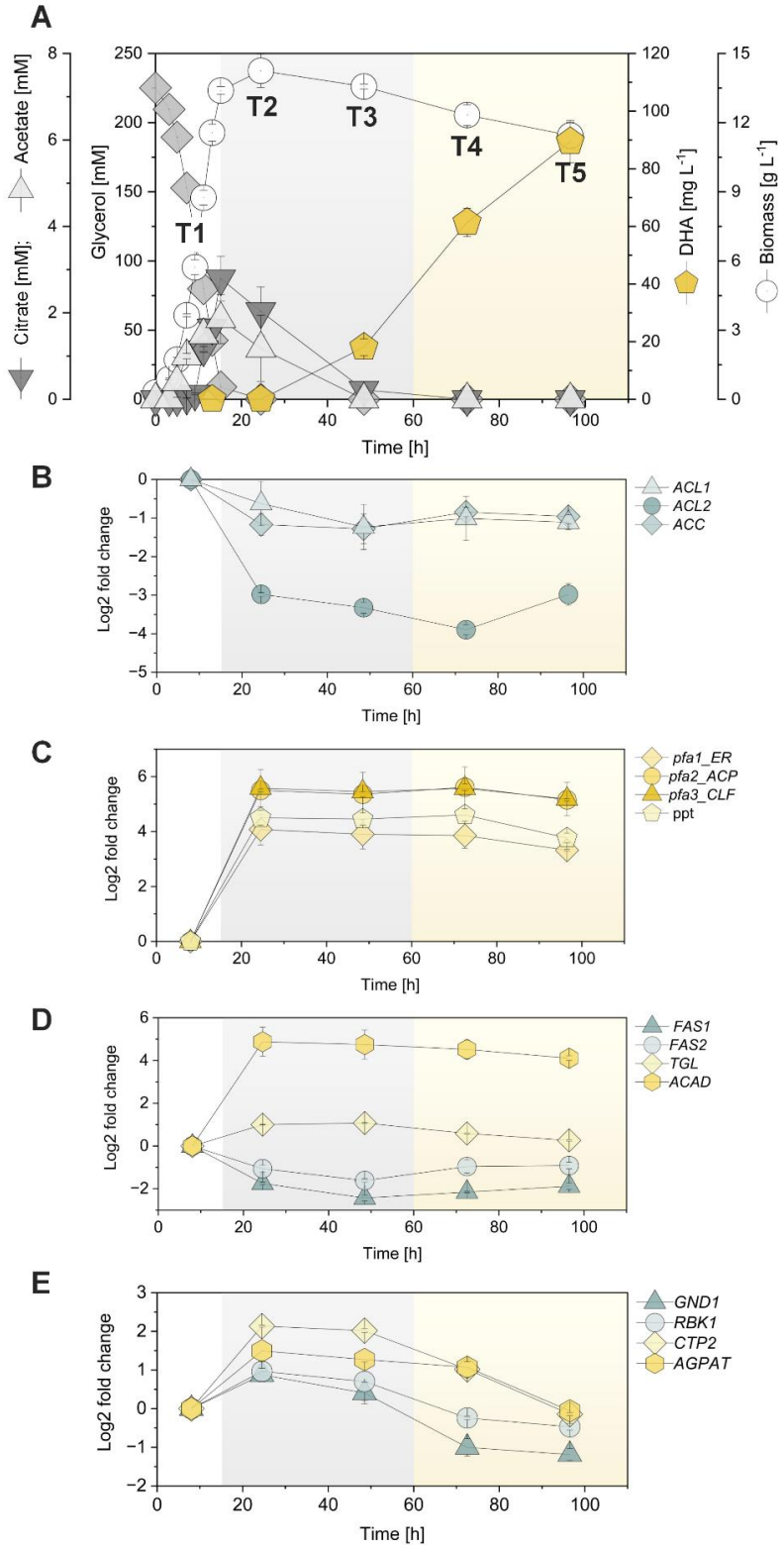

Figure 30. Dynamics in the expression of selected genes in DHA-producing *Y. lipolytica* grown on glycerol (Fig. 15B).

The expression levels were quantified at different time points (A) and are normalized to the expression value of the exponential phase. The selected genes comprised genes encoding proteins involved in the supply of DHA precursors from citrate (B), i.e. ATP-dependent citrate lyase (*ACL1*, *ACL2*) and acetyl-CoA carboxylase (*ACC*), encoded the PKS-like complex for DHA synthesis (C), i.e. PKS-like PUFA synthase/enoyl reductase (*pfa1_ER*), PKS-like PUFA synthase/acyl carrier protein (*pfa2_ACP*), and PKS-like PUFA synthase/chain length factor (*pfa3_CLF*), encoding proteins of the native fatty acid biosynthesis and degradation (D), i.e. fatty acid synthase (*FAS1*, *FAS2*), triacylglycerol lipase (*TAGL*), acyl-CoA dehydrogenase (*ACAD*), and genes encoding proteins with significant expressions changes between the early and the late production phase (E), i.e. 6-phosphogluconate dehydrogenase (*GND1*), ribokinase (*RBK1*), tricarboxylate transport protein (*CTP1*), and acylglycerol-3-phosphate acyltransferase (*AGPAT*). The data displays the average values and standard errors from three biological replicates.

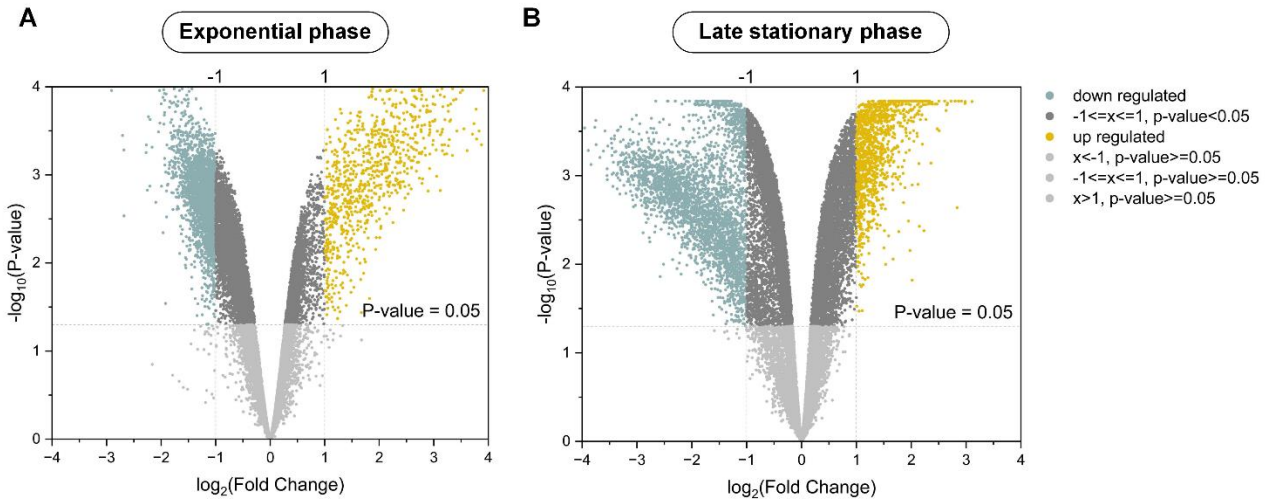

Figure 31. Differences in gene expression between the DHA-producing producer *Y. lipolytica* Af4 and the wild type Po1h during the exponential phase (10h) and the late stationary phase (72h). Timepoints refer to the cultivation profiles on **Fig. 15BD**. The data are visualized as volcano plots. Each sample was analyzed in biological triplicate.

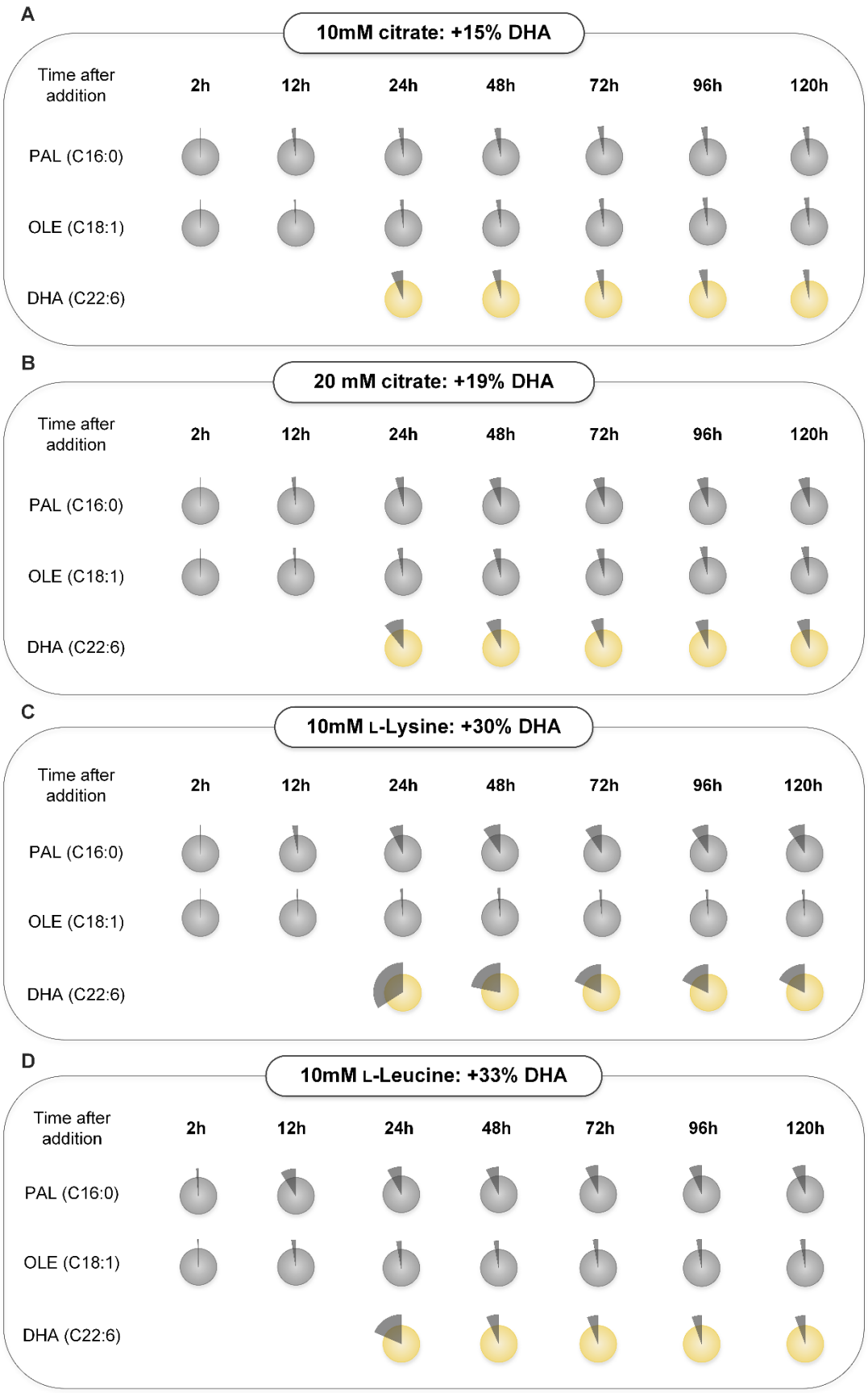

Figure 32. Metabolic pathway profiling in DHA-producing *Y. lipolytica* using ^{13}C-labeled isotopic tracers. In separate experiments, 99% [$^{13}C_6$] citrate (A, B), 99% [$^{13}C_6$] L-lysine (C) and 99% [$^{13}C_6$] L-leucine (D) were spiked into the cultures at the end of the growth phase, when glycerol was depleted. The data comprise the ^{13}C enrichment of the intracellular pools of selected fatty acids 2 h, 12 h, 24 h, 48 h, 72 h, 96 h and120 h after the addition of the corresponding tracer.

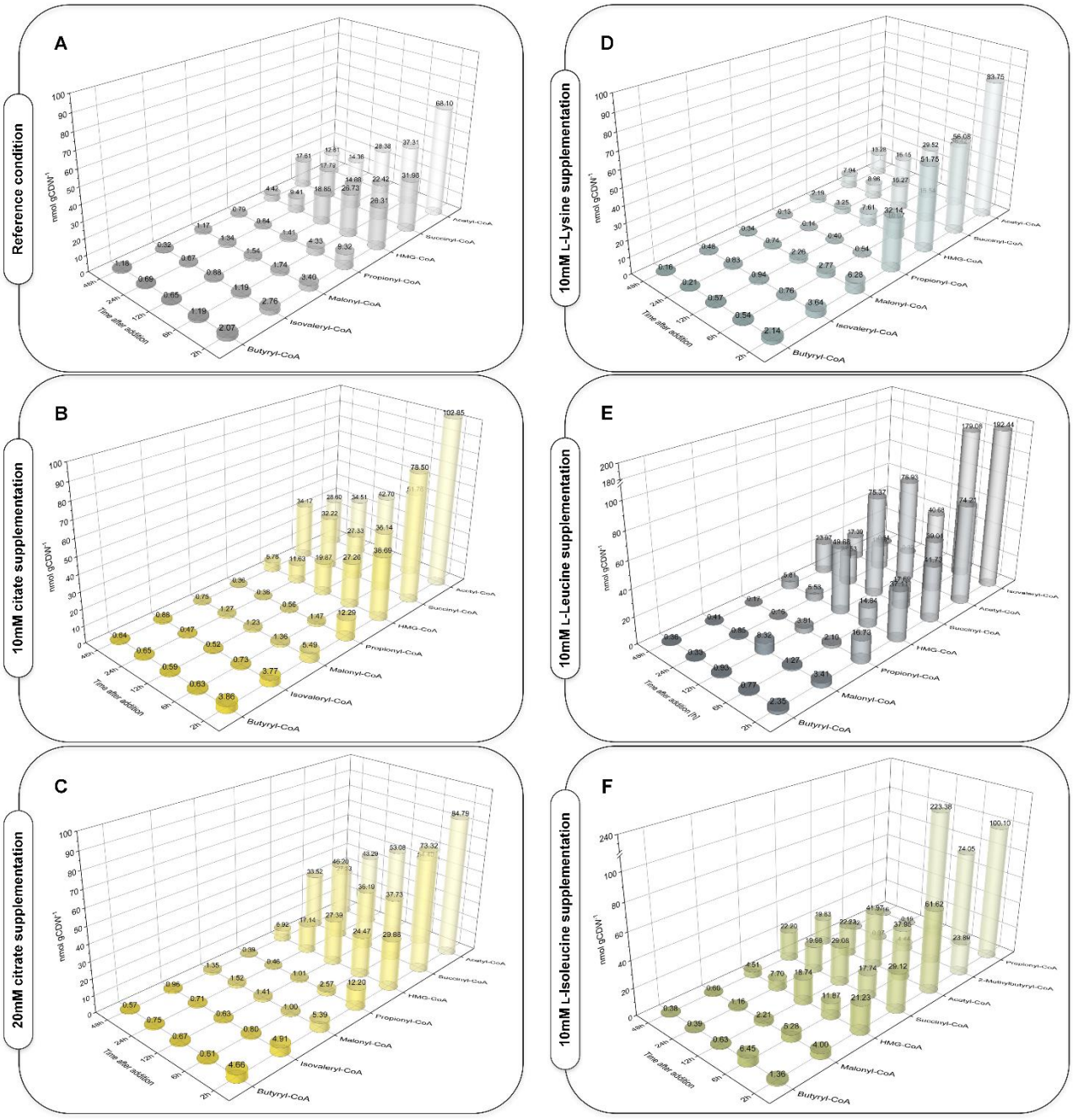

Figure 33. Dynamics of intracellular CoA-thioesters in DHA-producing *Y. lipolytica* Af4. The given time points refer to the time after supplementation (**Fig. 5**). Each sample was analyzed in biological triplicate.

6.2 Supplementary data tables

Table 12. Most significant differences in gene expression between 115 the DHA producer *Y. lipolytica* Af4 and the parent wild type in the late stationary phase (72 h, Fig. 1AB). The fold change cutoff and the *P* value were set to 2 and ≤ 0.05, respectively. Each sample was analyzed in biological triplicate. The data are shown as relative values to the expression level of the wild type. The data comprise the 50 most down regulated genes and the 50 most up regulated genes, respectively. The comparative expression levels of all genes are shown as volcano plot in **Fig. 31**. Each sample was analyzed in biological triplicate.

Gene ID	LogFC producer vs wild type	Function	Similarity
YALI0_C03091g	-3.58	Unknown	No similarity
YALI0_F03685g	-3.41	Unknown	No similarity
YALI0_C17281g	-3.38	Unknown	SEO1 sulfoxyde ethionine resistance
YALI0_F01078g	-3.32	Transporter	GABA-specific permease (GABA-specific transport protein)
YALI0_D18018g	-3.31	Signaling pathway	SST2 involved in desensitization to alpha-factor pheromone
YALI0_A14949g	-3.25	Ribonuclease	Ribonuclease H (RNase H)
YALI0_B01210g	-3.24	Unknown	No similarity
YALI0_E21560g	-3.21	Oxidoreductase	toxD gene
YALI0_B22264g	-3.17	Ribonuclease	Ribonuclease H (RNase H)
YALI0_B01914g	-3.14	Transporter	Probable transporter SEO1
YALI0_B00396g	-3.13	Transporter	Maltose permease
YALI0_A12265g	-3.11	Unknown	No similarity
YALI0_C14674g	-3.11	Unknown	No similarity
YALI0_D03696g	-3.11	Unknown	No similarity
YALI0_D09471g	-3.08	Unknown	No similarity
YALI0_E08932g	-3.05	Unknown	No similarity
YALI0_A15169g	-3.04	Unknown	No similarity
YALI0_B22990g	-3.04	Proteolisis	Alkaline extracellular protease precursor (AEP)
YALI0_D20108g	-3.01	Transporter	JEN1 carboxylic acid transporter protein singleton
YALI0_C16126g	-2.98	Unknown	No similarity
YALI0_B19844g	-2.98	Unknown	No similarity
YALI0_A18139g	-2.97	Unknown	No similarity
YALI0_F08129g	-2.97	Oxidoreductase	Oxidoreductase zinc-binding mitochondrial inner membrane protease
YALI0_E31262g	-2.97	Chromatin	HOS2 Histone deacetylase
YALI0_F31515g	-2.96	Unknown	No similarity
YALI0_A17666g	-2.96	Transporter	TNA1 similarity to allantoate transport protein
YALI0_E18161g	-2.93	Unknown	No similarity
YALI0_C02541g	-2.91	Transporter	MFS efflux transporter of unknown specificity

YALI0_E01012g	-2.90	Unknown	No similarity possibly noncoding
YALI0_C05236g	-2.90	Unknown	No similarity
YALI0_C08679g	-2.89	Unknown	No similarity
YALI0_A13937g	-2.87	Unknown	No similarity
YALI0_C04279g	-2.87	Proteolisis	Aspartyl protease YLR121C precursor
YALI0_B04202g	-2.86	Transporter	DUR3 urea transport protein
YALI0_D03311g	-2.86	Unknown	No similarity
YALI0_F20130g	-2.84	Unknown	No similarity
YALI0_E06875g	-2.84	Unknown	No similarity possibly noncoding
YALI0_A11759g	-2.84	Unknown	No similarity
YALI0_A15444g	-2.83	Transferase	Possible N-acetyltransferase activity
YALI0_F14971g	-2.83	Unknown	No similarity possibly noncoding
YALI0_B02310g	-2.83	Unknown	No similarity
YALI0_B02596g	-2.82	Unknown	No similarity
YALI0_C07546g	-2.81	Unknown	No similarity
YALI0_C17919g	-2.81	Unknown	No similarity
YALI0_A04279g	-2.79	Helicase	SEN1 positive effector of tRNA-splicing endonuclease
YALI0_A01848g	-2.78	Unknown	No similarity
YALI0_D06732g	-2.78	Unknown	No similarity
YALI0_A11891g	-2.78	Unknown	No similarity
YALI0_D18040g	-2.78	Unknown	No similarity
YALI0_B14487g	1.77	Chromatin	NAP1 nucleosome assembly protein I
YALI0_A10659g	1.78	Transporter	ADP/ATP translocase Aac1p
YALI0_F09163g	1.79	Hydrolase	GPI-anchored aspartyl protease 3 (yapsin 3)
YALI0_F11473g	1.79	Hydrolase	CCT2 chaperonin of the TCP1 ring complex
YALI0_F21659g	1.81	Transporter	Zinc ion transmembrane transporter activity
YALI0_F24167g	1.82	Unknown	No similarity
YALI0_A21098g	1.83	GTPase	GSP1-guanyl-nucleotide exchange factor
YALI0_F05940g	1.83	Hydrolase	Cysteine proteinase 1, mitochondrial
YALI0_B14146g	1.83	Structural	60S acidic ribosomal protein P0
YALI0_E14190g	1.83	Oxidoreductase	MDH1 malate dehydrogenase
YALI0_B21692g	1.84	Unknown	No similarity
YALI0_E19899g	1.84	Unknown	No similarity
YALI0_F11759g	1.86	Hydrolase	SAH1 Adenosylhomocysteinase
YALI0_A16566g	1.87	Unknown	No similarity
YALI0_F05544g	1.89	Structural	SUP46 small ribosomal protein RPS9B
YALI0_E02684g	1.89	Transferase	CIT2 citrate synthase transmembrane segment
YALI0_E29755g	1.90	Structural	STA1 extracellular alpha-1 4-glucan glucosidase
YALI0_C22000g	1.90	Lyase	Glutathione-independent glyoxalase HSP31

YALI0_E12485g	1.91	GTPase	Zinc-regulated GTPase metalloprotein activator 1
YALI0_C09328g	1.91	Transporter	SGT2 similarity to protein phosphatases
YALI0_B02728g	1.91	Isomerase	GPM1 Phosphoglycerate mutase 1
YALI0_D00429g	1.92	Transferase	SBA1 Hsp90 Associated co-chaperone
YALI0_F19140g	1.94	Unknown	No similarity
YALI0_D20570g	1.95	Hydrolase	CCT3 chaperonin of the TCP1 ring complex cytosolic
YALI0_B19976g	1.96	Oxidoreductase	NAD-dependent formate dehydrogenase (FDH)
YALI0_B19492g	1.98	Transporter	Gap1 General amino acid permease
YALI0_D06688g	2.00	Transporter	FTR1 Iron permease that mediates high-affinity iron uptake
YALI0_C17963g	2.03	Unknown	No similarity
YALI0_C14344g	2.04	Oxidoreductase	NAD-dependent formate dehydrogenase (FDH)
YALI0_E31559g	2.04	Unknown	No similarity
YALI0_F17974g	2.05	Hydrolase	Cysteine proteinase 1
YALI0_C05687g	2.06	Unknown	No similarity
YALI0_B08899g	2.07	Unknown	No similarity
YALI0_D08228g	2.07	Transporter	ADP/ATP translocase Aac1p
YALI0_E16346g	2.09	Transferase	Serine hydroxymethyltransferase (SHMT)
YALI0_D01375g	2.09	Unknown	No similarity
YALI0_F28765g	2.10	Oxidoreductase	NAD-dependent formate dehydrogenase (FDH)
YALI0_E23474g	2.11	Transporter	Alkane utilisation CYP52 family member
YALI0_D00363g	2.12	Transporter	Quinate permease
YALI0_B15125g	2.18	Oxidoreductase	TSA1 thiol-specific antioxidant
YALI0_A21307g	2.22	Transporter	PHO84 high-affinity inorganic phosphate/H+ symporter
YALI0_F26565g	2.22	Unknown	No similarity
YALI0_C22748g	2.24	Unknown	1,4-butanediol diacrylate esterase
YALI0_A17875g	2.26	Oxidoreductase	Aldehyde-dehydrogenase
YALI0_F13937g	2.27	Oxidoreductase	NAD-dependent formate dehydrogenase (FDH)
YALI0_D17248g	2.28	Unknown	No similarity
YALI0_F04095g	2.30	Oxidoreductase	IDP2 isocitrate dehydrogenase
YALI0_A12353g	2.36	Oxidoreductase	NAD-dependent formate dehydrogenase (FDH)
YALI0_C06424g	2.65	Transporter	SNF3 high-affinity glucose transporter/regulatory protein
YALI0_E14256g	2.86	Oxidoreductase	NAD-dependent formate dehydrogenase (FDH)
YALI0_F30437g	3.02	Unknown	No similarity

Table 13. Functional annotation and gene identifier (gene ID) of the genes shown in Figure 21DEF.

PUFA biosynthesis		
Gene	**Enzyme**	**Gene ID**
ER	PKS-like enoylreductase	pfa1
ACP1	PKS-like acyl carrier protein 1	pfa2_ACP1
ACP2	PKS-like acyl carrier protein 2	pfa2_ACP2
ACP3	PKS-like acyl carrier protein 3	pfa2_ACP3
DHI	PKS-like dehydratase/isomerase	pfa2_DH1
KR	PKS-like ketoreductase	pfa2_KR
KS	PKS-like ketosynthase 1	pfa2_KS1
AT	PKS-like acyltransferase	pfa2_MAT
AGPAT	PKS-like 1-acylglycerol-3-phospatate acyltransferase	pfa3_AGPAT
AT2	PKS-like acyltransferase	pfa3_AT
CLF	PKS-like chain length factor	pfa3_CLF
DHI2	PKS-like dehydratase/isomerase 2	pfa3_DH2
DHI3	PKS-like dehydratase/isomerase 3	pfa3_DH3
KS2	PKS-like ketosynthase	pfa3_KS2
PDH2	PKS-like pseudo dehydratase 2	pfa3_pseudo_DH2
PDH3	PKS-like pseudo dehydratase 3	pfa3_pseudo_DH3
PPT	PKS-like 4′-phosphopantetheinyl transferase	ppt

Competing pathways		
Gene	**Enzyme**	**Gene ID**
CIT1	Citrate synthase 1	YALI0_E00638g
CIT2	Citrate synthase 2	YALI0_E02684g
ACO	Aconitate hydratase (Aconitase)	YALI0_D09361g
IDH1	IDH2 isocitrate dehydrogenase	YALI0_D06303g
IDP2	IDP2 isocitrate dehydrogenase	YALI0_F04095g
IDH3	IDH1 isocitrate dehydrogenase (NAD+) subunit 1	YALI0_E05137g
KGD1	KGD1 2-oxoglutarate dehydrogenase complex E1	YALI0_E33517g
KGD2	KGD2 2-oxoglutarate dehydrogenase complex E2	YALI0_E16929g
SC1	Succinate-CoA ligase alpha subunit	YALI0_E24013g
SC2	Succinate-CoA ligase alpha subunit	YALI0_D04741g
SDH1	Succinate dehydrogenase subunit 1	YALI0_D23397g
SDH2	Succinate dehydrogenase subunit 2 mitochondrial	YALI0_D11374g
SDH3	Succinate dehydrogenase cytochrome b560 subunit	YALI0_E29667g
SDH4	Succinate dehydrogenase membrane	YALI0_A14784g
FUM1	Fumarate hydratase (Fumarase)	YALI0_C06776g

MDH1	Malate dehydrogenase 1	YALI0_E14190g
MDH2	Malate dehydrogenase 2	YALI0_D16753g
ICL1	Isocitrate lyase 1	YALI0_C16885g
ICL2	Isocitrate lyase 2	YALI0_F31999g
MLS1	Malate synthase 1	YALI0_D19140g
MLS2	Malate synthase 2	YALI0_E15708g
FAS1	Fatty acid synthase subunit alpha	YALI0_B15059g
FAS2	Fatty acid synthase subunit beta	YALI0_B19382g
ACC	Acetyl-CoA carboxylase	YALI0_C11407g
ER ACP	Acyl-carrier protein enoylreductase	YALI0_C19624g
KR ACP	Acyl-carrier protein ketoreductase	YALI0_C19965g
MAT ACP	Acyl-carrier protein malonyl-transferase	YALI0_E18590g
KS ACP	Acyl-carrier protein ketosynthase	YALI0_F30679g
EL	Fatty acid elongase	YALI0_B20196g
LC KR	Very-long-chain acyl-CoA reductase	YALI0_A06787g
LC DH	Very-long-chain acyl-CoA dehydratase	YALI0_F11935g
DH	Dehydrogenase	YALI0_A04983g
DS12	Delta-12 fatty acid desaturase	YALI0_B10153g
DS9	Delta-9 fatty acid desaturase	YALI0_C05951g
THIO	Palmitoyl-protein thioesterase	YALI0_F14135g
G3P-AT	Glycerol-3-phosphate acyltransferase	YALI0_C00209g
AGPAT	1-acylglycerol-3-phosphate acyltransferase	YALI0_C14014g
LPAT	Lysophosphatidate acyltransferase	YALI0_E18964g
DAGP1	Diacylglycerol diphosphate phosphatase 1	YALI0_B14531g
DAGP2	Diacylglycerol diphosphate phosphatase 2	YALI0_C11297g

Supporting pathways

Gene	Enzyme	Gene ID
PXA1	Peroxisomal long-chain fatty acid import protein 1	YALI0_A06655g
PXA2	Peroxisomal long-chain fatty acid import protein 2	YALI0_D04246g
SOD1	Superoxide dismutase 1	YALI0_B08921g
SOD2	Superoxide dismutase 2, alpha	YALI0_B16742g
SOD2	Superoxide dismutase 2, beta	YALI0_C16621g
SOD3	Superoxide dismutase 3	YALI0_B20086g
PEX1	Peroxisome assembly protein PEX1 (Peroxin-1)	YALI0_C15356g
PEX2	Peroxisome assembly protein PEX2 (Peroxin-2)	YALI0_F01012g
PEX3	Peroxisome assembly protein PEX3 (Peroxin-3)	YALI0_F22539g
PEX4	Peroxisome assembly protein PEX4 (Peroxin-4)	YALI0_B19624g
PEX5	Peroxisome assembly protein PEX5 (Peroxin-5)	YALI0_B22660g

PEX6	Peroxisome assembly protein PEX6 (Peroxin-6)	YALI0_C18689g
ECH	Enoyl-CoA hydratase	YALI0_B10406g
FAA1	Long-chain-fatty-acid-CoA synthase	YALI0_D17864g
ACAD	Acyl-CoA dehydrogenase	YALI0_C16797g
POX1	Peroxisomal acyl-CoA oxidase 1	YALI0_E32835g
POX2	Peroxisomal acyl-CoA oxidase 2	YALI0_F10857g
POX3	Peroxisomal acyl-CoA oxidase 3	YALI0_D24750g
POX4	Peroxisomal acyl-CoA oxidase 4	YALI0_E27654g
POX5	Peroxisomal acyl-CoA oxidase 5	YALI0_C23859g
POX6	Peroxisomal acyl-CoA oxidase 6	YALI0_E06567g
POT1	Peroxisomal acetyl-CoA acyltransferase	YALI0_E18568g
MFE	Multifunctional beta-oxidation enzyme	YALI0_E15378g
TAGL1	Triacylglycerol lipase 1	YALI0_E32035g
TAGL2	Triacylglycerol lipase 2	YALI0_F10010g
TAGL3	Triacylglycerol lipase 3	YALI0_D17534g
TAGL4	Triacylglycerol lipase 4	YALI0_E31515g
DGA1	Acyl-CoA: diacylglycerol acyltransferase	YALI0_E32769g
KAT1	Acetyl-CoA: lysine N6-acetyltransferase	YALI0_E05533g
UGA2	Glutarate-semialdehyde dehydrogenase	YALI0_F26191g
GCDH	Glutaryl-CoA dehydrogenase	YALI0_F23749g
ECH	Enoyl-CoA hydratase	YALI0_B10406g
ACAT1	Acetyl-CoA C-acetyltransferase 1	YALI0_E11099g
ACAT2	Acetyl-CoA C-acetyltransferase 2	YALI0_B08536g
BCAT1	Branched-chain amino acid aminotransferase 1	YALI0_D01265g
BCAT2	Branched-chain amino acid aminotransferase 2	YALI0_F19910g
BCDH1	2-Oxoisovalerate dehydrogenase E1 component alpha	YALI0_D08690g
BCDH2	2-Oxoisovalerate dehydrogenase E1 component beta	YALI0_F05038g
BCDH3	2-Oxoisovalerate dehydrogenase	YALI0_D23815g
ACC	Acetyl-CoA carboxylase	YALI0_C11407g
ACL1	ATP-dependent citrate lyase subunit 1	YALI0_E34793g
ACL2	ATP-dependent citrate lyase subunit 2	YALI0_D24431g

Table 14. Native fatty acid metabolism and DHA production in recombinant *Y. lipolytica* Af4 upon supplementation with citrate, L-lysine, L-leucine, and L-isoleucine, respectively. The different supplements were each added at the end of the growth phase after 20 h, when glycerol was depleted. The data represent the formation/degradation of native FAs during the exponential growth phase (0 – 20h h), the early stationary phase (20 – 72 h), and the late stationary phase (72 – 180 h), respectively, and the final values reached at the end of each phase. In addition, the selectivity of DHA production at the end of the process is shown. The native fatty acids comprised the lumped pools of palmitic acid (C16:0), palmitoleic acid (C16:1), stearic acid (C18:0), oleic acid (C18:1), linoleic acid (C18:2), docosanoic acid (C22:0), tetracosanoic acid (C24:0), and hexacosanoic acid (C26:0). The data displays the average values and standard errors from three biological replicates. FA: fatty acids, DHA: docosahexaenoic acid.

	Exponential phase		Early stationary phase		Late stationary phase		
Supplement	**Native FA produced [mg L^{-1}]**	**Native FA end conc. [mg L^{-1}]**	**Native FA produced [mg L^{-1}]**	**Native FA end conc. [mg L^{-1}]**	**Degraded FA [mg L^{-1}]**	**Native FA end conc. [mg L^{-1}]**	**DHA selectivity [%]**
-	876 ± 59	876 ± 59	0	876 ± 59	302	574 ± 34	17 ± 1
10mM citrate	822 ± 23	822 ± 23	111	933 ± 27	269	664 ± 31	17 ± 0
20mM citrate	819 ± 29	819 ± 29	128	947 ± 82	255	692 ± 43	17 ± 1
L-Lysine	843 ± 37	843 ± 37	58	901 ± 62	334	567 ± 9	**23 ± 1**
L-Leucine	850 ± 21	850 ± 21	125	975 ± 56	330	645 ± 23	**20 ± 0**
L-Isoleucine	899 ± 19	899 ± 19	102	1001 ± 15	336	665 ± 6	**21 ± 0**

Table 15. Dynamics of the expression of genes encoding proteins of amino acid degradation pathways in DHA-producing *Y. lipolytica*. The yeast culture was grown on glycerol and sampled after 12 h (exponential growth phase), 24h (early stationary phase), and 96 h (late stationary phase). (sampled at 96h) (**Fig. 15B**). The fold change cutoff and the *P* value were set to 2 and ≤ 0.05, respectively. Each sample was analyzed in biological triplicate. The data are shown as relative values to the expression level in the exponential phase. The amino acids are grouped into glucogenic, ketogenic, and mixed (D'Andrea, 2000). Branched-chain amino acids (BCAA) belonged to different groups (L-valine, glucogenic; L-isoleucine, mixed; acids L-leucine, ketogenic) but shared the first steps of the degradation routes (Brosnan and Brosnan, 2006).

Amino acid	Enzyme	Gene	Gene ID	LogFC early stat phase	LogFC late stat phase
Glucogenic amino acid degradation					
L-Asparagine	L-asparaginase	*ASG*	YALI0_F30723g	-2.67	-1.01
L-Asparagine	Nitrilase	*NIT3*	YALI0_B07359g	0.00	0.00
L-Aspartate	L-Aspartate:2-oxoglutarate aminotransferase	*AAT2*	YALI0_B02178g	-2.57	-2.93
L-Aspartate	Malate dehydrogenase	*MDH1*	YALI0_E14190g	-1.86	-1.44
L-Aspartate	Malate dehydrogenase	*MDH2*	YALI0_D16753g	-2.22	-2.25
L-Aspartate	Aspartate kinase HOM3 L-aspartate 4-P-transferase	*HOM3*	YALI0_D11704g	-2.50	-2.66
L-Aspartate	Aspartate-semialdehyde dehydrogenase	*HOM2*	YALI0_D13596g	-1.36	-1.61
L-Aspartate	Homoserine dehydrogenase	*HOM6*	YALI0_D01089g	-3.43	-3.63
L-Aspartate	Homoserine kinase	*THR1*	YALI0_F13453g	0.00	0.00
L-Aspartate	Threonine synthase / homoserine p-lyase	*THR4*	YALI0_F23221g	0.00	0.00
L-Glutamine	L-Glutamine amonia ligase	*GAL1*	YALI0_E09493g	-2.27	-2.51
L-Glutamine	L-Glutamine amonia ligase	*GAL2*	YALI0_D07370g	-2.05	-2.21
L-Glutamine	Glutaminase	*GLN*	YALI0_E20603g	-2.07	-1.59
L-Glutamate	Glutamate decarboxylase	*GLDC1*	YALI0_C16753g	-2.21	-2.30
L-Glutamate	Glutamate decarboxylase	*GLDC2*	YALI0_F08415g	-4.29	-2.70
L-Glutamate	L-Glutamate:NADP+ dehydrogenase	*GLDH1*	YALI0_F17820g	0.00	0.00
L-Glutamate	L-Glutamate:NADP+ dehydrogenase	*GLDH2*	YALI0_E09603g	0.00	0.00
L-Cysteine	Cystathionine gamma-lyase	*CYS3*	YALI0_F05874g	-2.53	-3.75
L-Cysteine	Cystathionine beta-lyase	*CYS2*	YALI0_D00605g	-1.29	-1.13
L-Cysteine	Cysteine dioxygenase	*CDO*	YALI0_F11627g	0.00	0.00
L-Cysteine	Thiosulfate sulfurtransferases	*THS*	YALI0_F23551g	-2.15	-2.21
L-Cysteine	Homocysteine methyltransferase	*MET6*	YALI0_E12683g	-4.69	-3.98
L-Methionine	S-adenosylmethionine synthetase	*SAM1*	YALI0_B14509g	-2.76	-3.38
L-Methionine	Adenosylhomocysteinase	*SAH1*	YALI0_F11759g	-3.70	-4.13
L-Methionine	Cystathionine beta-synthase	*CYS4*	YALI0_E09108g	-1.28	-1.84
L-Methionine	S-Adenosylmethionine decarboxylase	*SPE2*	YALI0_E20361g	-0.58	-1.15
L-Methionine	Spermidine synthase	*SPE3*	YALI0_E33143g	-1.22	-1.34
L-Methionine	5'-Methylthioadenosine phosphorylase	*MEU1*	YALI0_B13420g	-2.37	-2.00

Glycine	Glycine decarboxylase P/dehydrogenase	*GCV2*	YALI0_A09856g	-1.66	-3.04
Glycine	Glycine decarboxylase/ aminomethyltransferase	*GCV1*	YALI0_F02849g	-4.06	-4.72
Glycine	Dihydrolipoamide dehydrogenase	*LPD1*	YALI0_D20768g	-1.47	-1.17
Glycine	Glycine cleavage system H protein	*GCSH*	YALI0_E00242g	-2.20	-2.03
Glycine	Glycine hydroxymethyltransferase	*SHM1*	YALI0_D22484g	-1.56	-1.77
Glycine	Glycine hydroxymethyltransferase	*SHM2*	YALI0_E16346g	-3.35	-4.17
L-Serine	L-Serine dehydratase	*SDL1*	YALI0_E10307g	-2.26	-1.60
L-Alanine	Alanine-glyoxylate transaminase/serine-pyruvate transaminase	*AGX1*	YALI0_E16643g	-2.56	-3.02
L-Histidine	Carnosine N-methyltransferase	*CARMT*	YALI0_D07238g	-1.71	-0.80
L-Histidine	Hercynylcysteine S-oxide lyase	*HCOL1*	YALI0_B19162g	1.72	1.17
L-Histidine	Hercynylcysteine S-oxide lyase	*HCOL2*	YALI0_E09262g	-2.50	-1.55
L-Proline	Proline dehydrogenase	*PUT1*	YALI0_B09625g	1.92	1.59
L-Proline	Pyrroline-5-carboxylate reductase	*PRO3*	YALI0_B14399g	-1.16	-1.11
L-Proline	1-Pyrroline-5-carboxylate dehydrogenase	*PUT2*	YALI0_B09647g	1.11	-0.10
L-Arginine	Arginase	*CAR1*	YALI0_E07535g	0.00	0.00
L-Arginine	Ornithine decarboxylase	*SPE1*	YALI0_B11330g	0.00	0.00
L-Arginine	Ornithine-oxo-acid transaminase	*OOAT*	YALI0_C04433g	-0.38	-1.11
L-Arginine	Agmatinase	*CAR2*	YALI0_E04202g	-1.13	0.18
Mixed amino acid degradation					
L-Tyrosine	Pyruvate decarboxylase	*PDC1*	YALI0_D10131g	-1.52	-1.94
L-Tyrosine	Histidinol-phosphate aminotransferase	*HIS5*	YALI0_E01254g	-2.92	-3.11
L-Tyrosine	Aromatic amino acid aminotransferase II	*ARO9*	YALI0_C05258g	0.00	0.00
L-Tyrosine	Aromatic amino acid aminotransferase I	*ARO8*	YALI0_E20977g	0.00	0.00
L-Tryptophan	Indoleamine 2,3-dioxygenase	*BNA2*	YALI0_F26455g	0.71	0.60
L-Tryptophan	Kynurenine formamidase	*BNA3*	YALI0_E03806g	-2.35	-2.10
L-Tryptophan	Kynurenine 3-monooxygenase	*BNA4*	YALI0_D09867g	1.50	0.97
L-Tryptophan	Kynureninase	*BNA5*	YALI0_B22902g	-1.14	-0.86
L-Tryptophan	3-Hydroxyanthranilate 3,4-dioxygenase	*BNA1*	YALI0_B02852g	0.00	0.00
L-Phenylalanine	3-Hydroxybutyryl-CoA dehydrogenase	*BHBD*	YALI0_C08811g	-1.94	-2.05
L-Phenylalanine	Primary-amine oxidase	*AMO3*	YALI0_A16445g	2.49	2.68
L-Phenylalanine	Primary-amine oxidase	*AMO2*	YALI0_C18315g	2.34	1.83
L-Phenylalanine	Primary-amine oxidase	*AMO1*	YALI0_C22792g	1.25	1.18
L-Phenylalanine	Phenylacetate 2-hydroxylase	*PHAH*	YALI0_F03663g	2.11	3.12
L-Phenylalanine	Acetamidase	*ACMD*	YALI0_D22110g	0.43	-1.19
L-Phenylalanine	Amidase	*AMD1*	YALI0_E11847g	-5.20	-4.01
L-Phenylalanine	Amidase	*AMD2*	YALI0_E34771g	0.85	3.91
L-Threonine	L-Serine/L-Threonine ammonia-lyase	*CHA1*	YALI0_B16214g	-1.23	-1.16

L-Threonine	Serine/Threonine dehydratase	*ILV1*	YALI0_D02497g	0.00	0.00
L-Threonine	Threonine aldolase	*THA*	YALI0_A21417g	0.55	1.40

Branched chain amino acid degradation (glucogenic, ketogenic and mixed)					
BCAA	Branched-chain amino acid aminotransferase	*BCAT1*	YALI0_D01265g	0.40	1.40
BCAA	Branched-chain amino acid aminotransferase	*BCAT2*	YALI0_F19910g	0.21	-0.41
BCAA	2-Oxoisovalerate dehydrogenase E1 component alpha subunit	*BCDH1*	YALI0_D08690g	5.50	5.25
BCAA	2-Oxoisovalerate dehydrogenase E1 component beta subunit	*BCDH2*	YALI0_F05038g	3.87	4.10
BCAA	2-Oxoisovalerate dehydrogenase/ dihydrolipoyl transacylase	*BCDH3*	YALI0_D23815g	5.85	5.77
BCAA	Enoyl-CoA hydratase	*ECH*	YALI0_B10406g	-1.24	-0.44
L-Valine	3-Hydroxyisobutyryl-CoA hydrolase	*HIBCH*	YALI0_D06215g	0.00	0.00
L-Valine	3-Hydroxyisobutyrate/ 3-hydroxypropionate dehydrogenase	*HIBDH*	YALI0_F02607g	2.12	3.04
L-Valine	Methylmalonate-semialdehyde dehydrogenase	*MMSDH*	YALI0_C01859g	3.29	2.93
L-Valine	Aldehyde dehydrogenase	*ALDH1*	YALI0_F23793g	1.35	0.03
L-Valine	Aldehyde dehydrogenase	*ALDH2*	YALI0_F04444g	0.00	0.00
L-Valine	Aldehyde dehydrogenase	*ALDH3*	YALI0_E00264g	0.00	0.00
L-Isoleucine	3-Ketoacyl-CoA thiolase/ Acetyl-CoA acyltransferase 1	*POT1*	YALI0_E18568g	3.22	2.57

Ketogenic amino acid degradation					
L-Leucine	Isovaleryl-CoA dehydrogenase	*IVD*	YALI0_E12573g	4.28	4.29
L-Leucine	3-Methylcrotonyl-CoA carboxylase alpha subunit	*MCC*	YALI0_B14619g	3.57	4.06
L-Leucine	Methylglutaconyl-CoA hydratase	*MGH*	YALI0_F22121g	1.76	3.35
L-Leucine	3-Hydroxy-3-methylglutaryl-CoA acetoacetate-lyase	*HMGL*	YALI0_B22550g	-2.54	-2.11
L-Leucine	3-Oxoacid CoA-transferase	*OXCT*	YALI0_F26587g	3.92	4.08
L-Leucine	Acetoacetyl-CoA thiolase, acetyl-CoA C-acetyltransferase	*ACAT1*	YALI0_E11099g	0.00	0.00
L-Lysine	Acetyl-CoA: lysine N6-acetyltransferase	*KAT1*	YALI0_E05533g	4.33	4.17
L-Lysine	Glutarate-semialdehyde dehydrogenase	*UGA2*	YALI0_F26191g	1.55	1.45
L-Lysine	Glutaryl-CoA dehydrogenase	*GCDH*	YALI0_F23749g	1.28	0.21
L-Lysine	Enoyl-CoA hydratase	*ECH*	YALI0_B10406g	-1.24	-0.44
L-Lysine	Acetoacetyl-CoA thiolase, Acetyl-CoA C-acetyltransferase	*ACAT1*	YALI0_E11099g	0.00	0.00
L-Lysine	Acetyl-CoA C-acetyltransferase	*ACAT2*	YALI0_B08536g	-2.55	-2.36

L-Lysine	Saccharopine dehydrogenase (NAD+, L-lysine forming)	*LYS1*	YALI0_B15444g	-3.41	-3.31
L-Lysine	Saccharopine dehydrogenase (NADP+, L-glutamate forming)	*LYS9*	YALI0_D22891g	-1.76	-2.26
L-Lysine	Dihydrolipoamide dehydrogenase	*LPD1*	YALI0_D20768g	-1.47	-1.17
L-Lysine	2-Oxoglutarate dehydrogenase (dihydrolipoamide succinyl transferase)	*KGD2*	YALI0_E16929g	0.00	0.00

Table 16. Dynamics of intracellular CoA-thioesters in DHA-producing *Y. lipolytica*. The culture was grown on glycerol and samples at six different time points – exponential phase (6h, 10h), early stationary phase (24h, 48h), and late stationary phase (72 h, 96 h) (**Fig. 15B**). The data represent absolute intracellular concentrations and are given in nmol g_{CDM}^{-1} (**Fig. 25**). They display the average values and standard errors from three biological replicates.

	Exponential phase		Early stationary phase		Late stationary phase	
Crotonyl-CoA	0.8 ± 0.1	1.7 ± 0.2	0.7 ± 0.1	0.6 ± 0.1	0.4 ± 0.0	0.3 ± 0.1
Hydroxybutyryl-CoA	3.1 ± 1.2	2.3 ± 0.5	0.7 ± 0.2	0.4 ± 0.0	0.2 ± 0.0	0.2 ± 0.1
Butyryl-CoA	1.1 ± 0.1	3.4 ± 0.8	1.7 ± 0.3	1.3 ± 0.1	1.2 ± 0.3	0.9 ± 0.1
Propionyl-CoA	1.4 ± 0.2	1.9 ± 0.2	9 ± 1.7	4.3 ± 0.2	0.8 ± 0.0	0.07 ± 0.0
Isovaleryl-CoA	0.8 ± 0.3	1.5 ± 0.5	2.1 ± 0.4	2.7 ± 1.0	1.2 ± 0.8	0.7 ± 0.0
Hydroxy-methylglutaryl-CoA	11 ± 5.0	13 ± 2.1	26.7 ± 6.4	9.5 ± 3.2	4.4 ± 0.9	2.5 ± 0.2

Table 17. Dynamics of amino acid metabolism in DHA-producing *Y. lipolytica* Af4 upon supplementation with citrate, L-lysine, L-leucine, and L-isoleucine, respectively. The different supplements were each added at the end of the growth phase after 20 h, when glycerol was depleted (**Fig. 22, Fig. 26**). The data represent the absolute levels of free intracellular amino acids (µmol g_{CDM}^{-1}) at different time points (2, 6, 12, 24, 48 h) after supplementation. The data from the reference culture without supplementation are shown for comparison. They display the average values and standard errors from three biological replicates.

Intracellular amino acid concentration (reference)

		Asn	Asp	Glu	Gln	Met	Gly	Ser	Ala	Pro	Arg	Tyr	Phe	Thr	Val	Ile	Leu	Lys
2h	mean	1.5	29.2	84.6	14.7	0.9	4.4	3.5	19.0	7.6	11.8	0.6	1.3	4.6	3.3	1.7	1.5	6.4
	SD	1.0	7.5	29.0	3.6	0.2	1.4	1.0	13.8	1.9	3.6	0.2	0.3	2.2	1.1	0.4	0.4	2.8
6h	mean	2.9	33.2	72.6	15.2	0.8	4.2	3.3	12.0	8.9	10.1	0.7	1.5	3.4	3.3	1.6	1.3	6.4
	SD	1.2	10.1	17.1	4.1	0.0	1.0	0.8	4.1	3.5	2.4	0.3	0.6	1.0	1.1	0.3	0.3	2.7
12h	mean	4.1	37.7	71.6	15.7	0.7	4.2	3.2	9.6	10.3	8.8	0.8	1.8	2.8	3.3	1.4	1.2	7.3
	SD	1.6	6.6	19.3	4.3	0.1	0.7	0.9	2.1	2.0	1.4	0.1	0.4	0.3	0.5	0.3	0.2	1.2
24h	mean	3.5	24.4	59.0	12.9	0.6	3.6	2.4	8.8	9.0	6.1	0.7	1.6	2.2	2.1	1.2	1.0	6.2
	SD	2.1	6.6	17.0	3.6	0.0	0.8	0.4	2.4	2.3	1.4	0.2	0.3	0.5	0.7	0.2	0.1	1.9
48h	mean	4.7	25.6	68.7	13.4	0.5	4.1	2.8	11.1	8.0	5.0	0.9	1.7	2.1	1.8	1.0	1.0	6.2
	SD	3.8	15.4	30.9	3.7	0.1	1.8	0.9	5.7	0.7	0.4	0.4	0.5	0.8	0.5	0.1	0.2	1.9

Intracellular amino acid concentration (+ 10mM citrate supplementation)

		Asn	Asp	Glu	Gln	Met	Gly	Ser	Ala	Pro	Arg	Tyr	Phe	Thr	Val	Ile	Leu	Lys
2h	mean	1.8	29.6	76.2	15.5	0.7	2.7	3.0	11.6	6.9	8.3	0.5	1.1	3.4	2.2	1.3	1.3	5.0
	SD	1.5	9.5	19.6	5.6	0.1	2.0	0.5	2.2	1.8	7.2	0.2	0.2	0.5	0.6	0.3	0.2	1.3
6h	mean	3.4	44.7	81.2	18.1	0.7	3.7	3.3	11.2	8.2	11.1	0.6	1.2	3.4	2.6	1.5	1.3	5.9
	SD	1.5	7.6	8.3	3.1	0.1	0.6	0.2	2.1	2.3	1.3	0.2	0.1	0.4	0.5	0.0	0.2	1.7
12h	mean	4.2	43.5	70.7	17.4	0.6	3.7	2.8	10.3	9.5	8.5	0.7	1.3	2.5	1.9	1.3	1.0	6.5
	SD	0.7	7.9	5.5	2.6	0.1	0.5	0.4	1.3	1.1	1.8	0.1	0.1	0.5	0.2	0.3	0.1	1.0
24h	mean	1.7	18.1	41.9	10.0	0.5	2.2	1.7	6.1	6.6	4.2	0.4	0.9	1.4	1.1	0.9	0.8	3.3
	SD	2.0	18.0	26.1	6.3	0.1	1.0	0.9	3.7	2.0	2.8	0.3	0.3	0.7	0.6	0.2	0.3	2.4
48h	mean	0.2	9.4	26.9	5.7	0.4	1.6	1.1	4.1	4.6	1.8	0.3	0.7	0.8	0.7	0.7	0.5	1.7
	SD	0.3	5.8	9.9	2.0	0.1	0.5	0.2	1.5	0.4	0.7	0.1	0.1	0.2	0.2	0.2	0.1	0.8

Intracellular amino acid concentration (+ 20mM citrate supplementation)

		Asn	Asp	Glu	Gln	Met	Gly	Ser	Ala	Pro	Arg	Tyr	Phe	Thr	Val	Ile	Leu	Lys
2h	mean	1.8	29.8	81.8	15.9	0.8	3.8	3.2	12.7	7.9	10.9	0.5	1.1	3.8	2.8	1.5	1.3	5.7
	SD	1.2	6.8	7.9	4.2	0.1	0.3	0.2	3.4	1.6	1.4	0.1	0.1	0.1	0.3	0.1	0.1	0.8
6h	mean	3.2	46.2	83.3	17.9	0.7	3.9	3.4	10.4	9.3	10.3	0.7	1.3	3.5	3.2	1.5	1.3	6.4
	SD	1.9	13.6	3.4	2.0	0.1	0.4	0.6	0.4	1.8	1.6	0.1	0.3	0.7	0.4	0.3	0.1	1.3
12h	mean	4.8	44.1	77.5	19.3	0.6	3.9	3.1	10.1	10.7	8.1	0.8	1.6	2.6	2.7	1.2	1.2	7.3
	SD	0.5	2.5	6.0	0.9	0.1	0.4	0.2	1.3	0.8	1.1	0.0	0.3	0.2	0.8	0.0	0.0	0.9
24h	mean	4.5	27.1	72.0	17.4	0.6	3.7	2.8	10.2	9.8	6.2	0.8	1.4	2.2	1.8	1.2	1.1	6.3
	SD	0.9	12.1	9.1	2.1	0.0	0.3	0.4	1.2	1.1	0.8	0.0	0.1	0.2	0.1	0.1	0.1	0.8
48h	mean	2.9	20.9	55.3	12.5	0.4	3.1	2.1	8.0	6.4	4.1	0.6	1.0	1.6	1.3	0.8	0.7	4.7
	SD	1.2	4.8	17.4	4.7	0.2	0.9	0.6	2.3	3.2	2.1	0.2	0.4	0.5	0.6	0.3	0.3	2.1

Intracellular amino acid concentration (+ 10mM L-Lysine supplementation)

		Asn	Asp	Glu	Gln	Met	Gly	Ser	Ala	Pro	Arg	Tyr	Phe	Thr	Val	Ile	Leu	Lys
2h	mean	1.2	13.1	35.4	5.4	0.2	1.7	1.4	4.4	7.7	2.7	1.2	0.5	1.3	1.3	0.6	0.5	41.2
	SD	0.3	5.7	14.0	1.7	0.1	0.7	0.5	1.2	2.4	1.0	1.0	0.2	0.5	1.0	0.2	0.1	18.1
6h	mean	2.5	9.3	29.8	4.3	0.3	1.6	1.3	3.7	6.8	2.0	1.5	0.6	1.1	1.2	0.5	0.4	52.5
	SD	0.4	4.9	16.7	2.6	0.1	0.7	0.6	1.6	2.9	1.6	0.7	0.2	0.6	1.0	0.2	0.2	18.3
12h	mean	0.0	5.8	18.6	2.5	0.3	1.2	0.9	3.0	6.1	0.8	1.6	0.4	0.6	0.5	0.4	0.3	113.5
	SD	0.6	3.4	10.1	1.4	0.1	0.4	0.5	1.7	1.5	0.3	1.1	0.1	0.3	0.2	0.1	0.1	33.3
24h	mean	2.5	10.1	33.3	4.2	0.3	2.0	1.5	5.8	7.4	1.0	2.9	0.5	1.1	0.7	0.5	0.5	88.6
	SD	0.8	9.1	22.3	2.8	0.1	1.1	0.9	4.0	2.0	0.4	0.3	0.1	0.7	0.4	0.2	0.2	7.9
48h	mean	6.3	16.9	48.4	9.4	0.4	2.8	2.4	9.6	10.9	1.8	3.9	0.9	1.7	1.1	0.8	0.7	48.6
	SD	3.5	3.2	5.9	2.8	0.4	0.6	0.9	2.5	7.0	0.1	1.1	0.6	0.5	0.5	0.4	0.4	6.4

Intracellular amino acid concentration (+ 10mM L-Leucine supplementation)

		Asn	Asp	Glu	Gln	Met	Gly	Ser	Ala	Pro	Arg	Tyr	Phe	Thr	Val	Ile	Leu	Lys
2h	mean	0.9	5.6	20.2	3.3	0.2	1.2	0.8	2.3	4.4	2.5	0.1	0.4	0.8	0.9	0.4	14.7	1.4
	SD	0.2	3.5	8.9	2.0	0.1	0.4	0.4	1.4	0.6	1.6	0.1	0.1	0.5	0.6	0.1	2.0	0.9
6h	mean	0.7	4.7	22.0	2.9	0.4	1.4	1.0	2.0	5.0	2.7	0.2	0.4	0.9	0.9	0.3	10.7	1.7
	SD	0.3	2.2	7.0	1.1	0.2	0.3	0.2	0.6	0.4	0.9	0.0	0.0	0.3	0.5	0.1	1.4	0.4
12h	mean	0.9	3.1	24.1	2.7	0.3	1.4	1.2	2.1	5.8	2.2	0.2	0.4	0.8	0.6	0.4	3.8	1.8
	SD	0.4	2.3	8.2	1.9	0.2	0.8	0.8	1.4	0.5	1.6	0.2	0.1	0.5	0.3	0.3	1.3	1.2
24h	mean	7.9	8.5	39.8	9.1	0.7	2.4	3.1	3.5	10.6	3.3	0.5	0.9	1.4	1.1	0.9	1.1	2.8
	SD	6.9	3.5	11.8	5.1	0.3	0.5	1.3	0.8	4.1	1.3	0.1	0.3	0.3	0.2	0.2	0.3	1.0
48h	mean	12.3	16.4	29.4	10.8	0.8	2.1	2.3	4.5	12.3	2.3	0.4	1.1	1.2	1.1	1.0	0.9	2.1
	SD	1.3	9.2	9.3	4.5	0.0	0.3	0.5	1.7	1.3	0.7	0.1	0.2	0.2	0.2	0.1	0.3	0.6

Intracellular amino acid concentration (+ 10mM L-Isoleucine supplementation)

		Asn	Asp	Glu	Gln	Met	Gly	Ser	Ala	Pro	Arg	Tyr	Phe	Thr	Val	Ile	Leu	Lys
2h	mean	0.9	8.9	35.9	6.0	0.3	2.0	1.6	3.5	6.6	4.1	0.2	0.4	2.0	0.9	14.3	0.4	2.5
	SD	0.4	3.7	14.5	2.8	0.0	1.5	1.5	3.2	1.3	4.0	0.2	0.2	2.0	0.6	6.5	0.3	2.6
6h	mean	1.9	7.0	45.2	6.2	0.3	2.2	2.9	5.0	7.7	3.6	0.3	0.4	1.8	0.9	9.8	0.5	3.1
	SD	0.2	2.5	10.2	1.6	0.0	0.0	0.1	1.1	1.0	0.2	0.0	0.1	0.2	0.1	0.5	0.0	0.1
12h	mean	12.7	19.4	32.1	11.0	0.8	2.1	2.9	5.6	13.9	2.3	0.4	1.1	2.1	1.1	1.4	0.9	2.3
	SD	0.3	3.9	0.4	1.6	0.0	0.0	0.1	0.2	0.0	0.3	0.0	0.1	0.0	0.0	0.3	0.0	0.4
24h	mean	16.0	23.1	45.5	15.5	0.8	2.8	2.2	10.0	14.9	3.1	0.7	1.4	1.6	1.4	1.1	1.0	3.4
	SD	0.8	2.5	0.1	0.2	0.1	0.1	0.1	0.7	1.1	0.2	0.0	0.0	0.0	0.0	0.0	0.0	0.2
48h	mean	16.0	20.5	37.1	11.6	0.8	3.4	2.2	8.6	14.7	2.2	0.7	1.6	1.8	1.6	1.0	1.0	2.4
	SD	4.5	12.4	14.0	4.1	0.0	1.9	1.1	5.5	1.4	1.1	0.4	0.7	0.9	0.6	0.2	0.3	1.5

Table 18. Dynamics of the expression of genes encoding proteins involved in protein degradation in DHA-producing *Y. lipolytica*. The yeast culture was grown on glycerol and sampled after 12 h (exponential growth phase), 24h (early stationary phase), and 96 h (late stationary phase) (**Fig. 15B**). The fold change cutoff and the *P* value were set to 2 and ≤ 0.05, respectively. Each sample was analyzed in biological triplicate. The data are shown as relative values to the expression level in the exponential phase.

Gene ID	Pathway	LogFC early stat phase	LogFC late stat phase
YALI0_E18436g	Ubiquitin mediated proteolysis	2.50	1.74
YALI0_E18117g	Ubiquitin mediated proteolysis	2.27	-0.09
YALI0_C06149g	Ubiquitin mediated proteolysis	2.22	0.12
YALI0_D12452g	Ubiquitin mediated proteolysis	1.81	1.19
YALI0_E08844g	Ubiquitin mediated proteolysis	2.33	1.34
YALI0_B20911g	Ubiquitin mediated proteolysis	1.17	1.17
YALI0_E02134g	Ubiquitin mediated proteolysis	1.30	0.16
YALI0_F15367g	Ubiquitin mediated proteolysis	1.90	1.29
YALI0_A02871g	Ubiquitin mediated proteolysis	0.24	0.34
YALI0_B03718g	Ubiquitin mediated proteolysis	1.88	1.21
YALI0_B17072g	Ubiquitin mediated proteolysis	-1.97	-0.97
YALI0_D02871g	Ubiquitin mediated proteolysis	0.35	-1.33
YALI0_D03531g	Ubiquitin mediated proteolysis	1.36	-0.90
YALI0_D18194g	Ubiquitin mediated proteolysis	0.40	1.43
YALI0_D21120g	Ubiquitin mediated proteolysis	0.20	1.09
YALI0_B02794g	Ubiquitin mediated proteolysis	1.69	2.15
YALI0_F07667g	Ubiquitin mediated proteolysis	1.07	0.02
YALI0_F17974g	Ubiquitin mediated proteolysis	0.34	-0.71
YALI0_F19646g	Ubiquitin mediated proteolysis	2.36	2.49
YALI0_D15444g	Ubiquitin mediated proteolysis	1.01	1.60
YALI0_D27302g	Ubiquitin mediated proteolysis	1.63	0.69
YALI0_A02200g	Ubiquitin mediated proteolysis	0.48	1.38
YALI0_A03575g	Ubiquitin mediated proteolysis	1.81	0.81
YALI0_A09658g	Ubiquitin mediated proteolysis	0.85	1.60
YALI0_B03520g	Ubiquitin mediated proteolysis	1.71	1.19
YALI0_B05940g	Ubiquitin mediated proteolysis	1.55	1.08
YALI0_B09977g	Ubiquitin mediated proteolysis	1.82	0.92
YALI0_B12430g	Ubiquitin mediated proteolysis	1.44	1.35
YALI0_B17358g	Ubiquitin mediated proteolysis	1.21	0.89
YALI0_B22638g	Ubiquitin mediated proteolysis	1.09	0.62
YALI0_C00561g	Ubiquitin mediated proteolysis	-0.22	-1.12
YALI0_C14740g	Ubiquitin mediated proteolysis	1.33	1.41
YALI0_C18469g	Ubiquitin mediated proteolysis	1.85	0.87
YALI0_D11748g	Ubiquitin mediated proteolysis	1.43	0.95
YALI0_E05401g	Ubiquitin mediated proteolysis	2.96	1.81
YALI0_E06017g	Ubiquitin mediated proteolysis	1.15	-0.58
YALI0_E07117g	Ubiquitin mediated proteolysis	1.52	0.85
YALI0_E12081g	Ubiquitin mediated proteolysis	1.09	1.01
YALI0_E15290g	Ubiquitin mediated proteolysis	0.78	1.01
YALI0_E21439g	Ubiquitin mediated proteolysis	2.35	2.23
YALI0_E23342g	Ubiquitin mediated proteolysis	1.96	0.88
YALI0_E28182g	Ubiquitin mediated proteolysis	-1.01	-0.07
YALI0_F02563g	Ubiquitin mediated proteolysis	1.35	-0.03
YALI0_F02981g	Ubiquitin mediated proteolysis	1.08	1.23
YALI0_F04147g	Ubiquitin mediated proteolysis	1.59	0.60
YALI0_F05478g	Ubiquitin mediated proteolysis	1.46	0.72
YALI0_F05764g	Ubiquitin mediated proteolysis	-0.76	-1.79
YALI0_F16753g	Ubiquitin mediated proteolysis	0.63	1.08
YALI0_F31955g	Ubiquitin mediated proteolysis	1.19	0.27

7 REFERENCES

Abdel-Mawgoud, A. M., Markham, K. A., Palmer, C. M., Liu, N., Stephanopoulos, G., Alper, H. S., 2018. Metabolic engineering in the host *Yarrowia lipolytica*. Metab Eng. 50**,** 192-208.

Adarme-Vega, T. C., Lim, D. K., Timmins, M., Vernen, F., Li, Y., Schenk, P. M., 2012. Microalgal biofactories: a promising approach towards sustainable omega-3 fatty acid production. Microb Cell Fact. 11**,** 96.

Adili, R., Hawley, M., Holinstat, M., 2018. Regulation of platelet function and thrombosis by omega-3 and omega-6 polyunsaturated fatty acids. Prostaglandins Other Lipid Mediat. 139**,** 10-18.

Allemann, M. N., Allen, E. E., 2018. Characterization and application of marine microbial omega-3 polyunsaturated fatty acid synthesis. Methods Enzymol. 605**,** 3-32.

Allen, K. M., Habte-Tsion, H. M., Thompson, K. R., Filer, K., Tidwell, J. H., Kumar, V., 2019. Freshwater microalgae (*Schizochytrium* sp.) as a substitute to fish oil for shrimp feed. Sci Rep. 9.

Amiri-Jami, M., LaPointe, G., Griffiths, M. W., 2014. Engineering of EPA/DHA omega-3 fatty acid production by *Lactococcus lactis* subsp. *cremoris* MG1363. Appl Microbiol Biotechnol. 98**,** 3071-3080.

Aranda, P. S., LaJoie, D. M., Jorcyk, C. L., 2012. Bleach gel: a simple agarose gel for analyzing RNA quality. Electrophoresis. 33**,** 366-9.

Arbter, P., Sinha, A., Troesch, J., Utesch, T., Zeng, A. P., 2019. Redox governed electro-fermentation improves lipid production by the oleaginous yeast Rhodosporidium toruloides. Bioresour Technol. 294**,** 122122.

Aslan, C., Maralbashi, S., Kahroba, H., Asadi, M., Soltani-Zangbar, M. S., Javadian, M., Shanehbandi, D., Baradaran, B., Darabi, M., Kazemi, T., 2020. Docosahexaenoic acid (DHA) inhibits pro-angiogenic effects of breast cancer cells *via* down-regulating cellular and exosomal expression of angiogenic genes and microRNAs. Life Sci. 258.

Balamurugan, S., Wang, X., Wang, H. L., An, C. J., Li, H., Li, D. W., Yang, W. D., Liu, J. S., Li, H. Y., 2017. Occurrence of plastidial triacylglycerol synthesis and the potential regulatory role of AGPAT in the model diatom *Phaeodactylum tricornutum*. Biotechnol Biofuels. 10**,** 97.

Bankar, A. V., Kumar, A. R., Zinjarde, S. S., 2009. Environmental and industrial applications of *Yarrowia lipolytica*. Appl Microbiol Biotechnol. 84**,** 847-865.

Bao, W. J., Li, Z. F., Wang, X. M., Gao, R. L., Zhou, X. Q., Cheng, S. K., Men, Y., Zheng, L., 2021. Approaches to improve the lipid synthesis of oleaginous yeast *Yarrowia lipolytica*: A review. Renew Sust Energ Rev. 149.

Barth, G., Gaillardin, C., 1997. Physiology and genetics of the dimorphic fungus *Yarrowia lipolytica*. FEMS Microbiol Rev. 19**,** 219-237.

Bartosova, Z., Ertesvag, H., Nyflot, E. L., Kampe, K., Aasen, I. M., Bruheim, P., 2021. Combined metabolome and lipidome analyses for in-depth characterization of lipid accumulation in the DHA producing *Aurantiochytrium* sp. T66. Metabolites. 11.

Becker, J., Wittmann, C., 2019. A field of dreams: Lignin valorization into chemicals, materials, fuels, and health-care products. Biotechnol Adv. 37**,** 107360.

Becker, J., Zelder, O., Hafner, S., Schroder, H., Wittmann, C., 2011. From zero to hero-Design-based systems metabolic engineering of *Corynebacterium glutamicum* for L-lysine production. Metab Eng. 13**,** 159-168.

Beckerich, J. M., Lambert, M., Gaillardin, C., 1994. LYC1 is the structural gene for lysine N-6-acetyl transferase in yeast. Curr Genet. 25**,** 24-9.

Beckerich, J. M., Pommies, E., Faivre, C., Lambert, M., Heslot, H., 1986. Estimation of compartmentation of lysine inside the cells of *Yarrowia lipolytica*. Biochimie. 68**,** 517-529.

Bellou, S., Makri, A., Triantaphyllidou, I. E., Papanikolaou, S., Aggelis, G., 2014. Morphological and metabolic shifts of *Yarrowia lipolytica* induced by alteration of the dissolved oxygen concentration in the growth environment. Microbiol-Sgm. 160**,** 807-817.

Bellou, S., Triantaphyllidou, I. E., Aggeli, D., Elazzazy, A. M., Baeshen, M. N., Aggelis, G., 2016. Microbial oils as food additives: recent approaches for improving microbial oil production and its polyunsaturated fatty acid content. Curr Opin Biotechnol. 37**,** 24-35.

Bentsen, H., 2017. Dietary polyunsaturated fatty acids, brain function and mental health. Microb Ecol Health Dis. 28**,** 1281916.

Beopoulos, A., Cescut, J., Haddouche, R., Uribelarrea, J. L., Molina-Jouve, C., Nicaud, J. M., 2009. *Yarrowia lipolytica* as a model for bio-oil production. Prog Lipid Res. 48**,** 375-387.

Beopoulos, A., Haddouche, R., Kabran, P., Dulermo, T., Chardot, T., Nicaud, J. M., 2012. Identification and characterization of DGA2, an acyltransferase of the DGAT1 acyl-CoA:diacylglycerol acyltransferase family in the oleaginous yeast *Yarrowia lipolytica*. New insights into the storage lipid metabolism of oleaginous yeasts. Appl Microbiol Biotechnol. 93**,** 1523-37.

Beopoulos, A., Mrozova, Z., Thevenieau, F., Le Dall, M. T., Hapala, I., Papanikolaou, S., Chardot, T., Nicaud, J. M., 2008. Control of lipid accumulation in the yeast *Yarrowia lipolytica*. Appl Environ Microbiol. 74**,** 7779-7789.

Bian, M. J., Li, S., Wei, H. H., Huang, S. P., Zhou, F., Zhu, Y. M., Zhu, G. P., 2018. Heteroexpression and biochemical characterization of a glucose-6-phosphate dehydrogenase from oleaginous yeast *Yarrowia lipolytica*. Protein Expr Purif. 148**,** 1-8.

Biriukova, E. N., Medentsev, A. G., Arinbasarova, A., Akimenko, V. K., 2006. Tolerance of the yeast *Yarrowia lipolytica* to oxidative stress. Mikrobiologiia. 75**,** 293-8.

Blazeck, J., Hill, A., Liu, L. Q., Knight, R., Miller, J., Pan, A., Otoupal, P., Alper, H. S., 2014. Harnessing *Yarrowia lipolytica* lipogenesis to create a platform for lipid and biofuel production. Nat Commun. 5.

Bolten, C. J., Wittmann, C., 2008. Appropriate sampling for intracellular amino acid analysis in five phylogenetically different yeasts. Biotechnol Lett. 30**,** 1993-2000.

Bonfanti, C., Cardoso, C., Afonso, C., Matos, J., Garcia, T., Tanni, S., Bandarra, N. M., 2018. Potential of microalga *Isochrysis galbana*: Bioactivity and bioaccessibility. Algal Res. 29**,** 242-248.

Borkowska, M., Bialas, W., Celinska, E., 2020. A new set of reference genes for comparative gene expression analyses in *Yarrowia lipolytica*. Fems Yeast Res. 20.

Brosnan, J. T., Brosnan, M. E., 2006. Branched-chain amino acids: enzyme and substrate regulation. J Nutr. 136**,** 207S-11S.

Burns, J. L., Nakamura, M. T., Ma, D. W. L., 2018. Differentiating the biological effects of linoleic acid from arachidonic acid in health and disease. Prostaglandins Leukot Essent Fatty Acids. 135**,** 1-4.

Burr, G. O., Burr, M. M., 1929. A new deficiency disease produced by the rigid exclusion of fat from the diet. J Biol Chem. 82**,** 345–367.

Calder, P. C., 2018. Very long-chain n-3 fatty acids and human health: fact, fiction and the future. Proc Nutr Soc. 77**,** 52-72.

Cao, L., Yin, M., Shi, T. Q., Lin, L., Ledesma-Amaro, R., Ji, X. J., 2022. Engineering *Yarrowia lipolytica* to produce nutritional fatty acids: Current status and future perspectives. Synth Syst Biotechnol. 7**,** 1024-1033.

Cardoso, C., Afonso, C., Bandarra, N. M., 2016. Dietary DHA and health: cognitive function ageing. Nutr Res Rev. 29**,** 281-294.

Carsanba, E., Papanikolaou, S., Fickers, P., Erten, H., 2020. Lipids by *Yarrowia lipolytica* strains cultivated on glucose in batch cultures. Microorganisms. 8.

Castro, L. F., Tocher, D. R., Monroig, O., 2016. Long-chain polyunsaturated fatty acid biosynthesis in chordates: Insights into the evolution of Fads and Elovl gene repertoire. Prog Lipid Res. 62**,** 25-40.

Cavallo, E., Charreau, H., Cerrutti, P., Foresti, M. L., 2017. *Yarrowia lipolytica*: a model yeast for citric acid production. Fems Yeast Res. 17.

Celińska, E., Nicaud, J. M., 2019. Filamentous fungi-like secretory pathway strayed in a yeast system: peculiarities of *Yarrowia lipolytica* secretory pathway underlying its extraordinary performance. Appl Microbiol Biotechnol. 103**,** 39-52.

Cervenak, F., Jurikova, K., Devillers, H., Kaffe, B., Khatib, A., Bonnell, E., Sopkovicova, M., Wellinger, R. J., Nosek, J., Tzfati, Y., Neuveglise, C., Tomaska, L., 2019. Identification of telomerase RNAs in species of the *Yarrowia* clade provides insights into the co-evolution of telomerase, telomeric repeats and telomere-binding proteins. Sci Rep. 9.

Chalima, A., Taxeidis, G., Topakas, E., 2020. Optimization of the production of docosahexaenoic fatty acid by the heterotrophic microalga *Crypthecodinium cohnii* utilizing a dark fermentation effluent. Renew Energ. 152**,** 102-109.

Chen, C. Y., Lee, M. H., Dong, C. D., Leong, Y. K., Chang, J. S., 2020. Enhanced production of microalgal lipids using a heterotrophic marine microalga *Thraustochytrium* sp. BM2. Biochem Eng J. 154.

Chen, C. Y., Nagarajan, D., Cheah, W. Y., 2018. Eicosapentaenoic acid production from *Nannochloropsis oceanica* CY2 using deep sea water in outdoor plastic-bag type photobioreactors. Bioresour Technol. 253**,** 1-7.

Chen, H., He, X., Geng, H., Liu, H., 2014. Physiological characterization of ATP-citrate lyase in Aspergillus niger. J Ind Microbiol Biotechnol. 41**,** 721-31.

Choi, J. W., Da Silva, N. A., 2014. Improving polyketide and fatty acid synthesis by engineering of the yeast acetyl-CoA carboxylase. J Biotechnol. 187**,** 56-59.

Cholewski, M., Tomczykowa, M., Tomczyk, M., 2018. A comprehensive review of chemistry, sources and bioavailability of omega-3 fatty acids. Nutrients. 10.

Christmann, J., Cao, P., Becker, J., Desiderato, C. K., Goldbeck, O., Riedel, C. U., Kohlstedt, M., Wittmann, C., 2023. High-efficiency production of the antimicrobial peptide pediocin PA-1 in metabolically engineered Corynebacterium glutamicum using a microaerobic process at acidic pH and elevated levels of bivalent calcium ions. Microb Cell Fact. 22**,** 41.

Colombo, S. M., Rodgers, T. F. M., Diamond, M. L., Bazinet, R. P., Arts, M. T., 2020. Projected declines in global DHA availability for human consumption as a result of global warming. Ambio. 49**,** 865-880.

Cordova, L. T., Alper, H. S., 2018. Production of alpha-linolenic acid in *Yarrowia lipolytica* using low-temperature fermentation. Appl Microbiol Biotechnol. 102**,** 8809-8816.

Cortes-Maldonado, L., Marcial-Quino, J., Gomez-Manzo, S., Fierro, F., Tomasini, A., 2020. A method for the extraction of high quality fungal RNA suitable for RNA-seq. J Microbiol Methods. 170.

Cui, J., Diao, J., Sun, T., Shi, M., Liu, L., Wang, F., Chen, L., Zhang, W., 2018. 13C metabolic flux analysis of enhanced lipid accumulation modulated by ethanolamine in *Crypthecodinium cohnii*. Front Microbiol. 9**,** 956.

Cui, Z. Y., Gao, C. J., Li, J. J., Hou, J., Lin, C. S. K., Qi, Q. S., 2017. Engineering of unconventional yeast *Yarrowia lipolytica* for efficient succinic acid production from glycerol at low pH. Metab Eng. 42**,** 126-133.

D'Andrea, G., 2000. Classifying amino acids as gluco(glyco)genic, ketogenic, or both. Biochem Educ. 28**,** 27-28.

da Silva, L. V., Coelho, M. A. Z., da Silva, M. R. S., Amaral, P. F. F., 2020. Investigation of mitochondrial protein expression profiles of *Yarrowia lipolytica* in response to citric acid production. Bioprocess Biosyst Eng. 43**,** 1703-1715.

Darvishi, F., Fathi, Z., Ariana, M., Moradi, H., 2017. *Yarrowia lipolytica* as a workhorse for biofuel production. Biochemical Engineering Journal. 127**,** 87-96.

Diao, J., Li, X., Pei, G., Liu, L., Chen, L., 2018. Comparative metabolomic analysis of *Crypthecodinium cohnii* in response to different dissolved oxygen levels during docosahexaenoic acid fermentation. Biochem Biophys Res Commun. 499**,** 941-947.

Diao, J., Song, X., Cui, J., Liu, L., Shi, M., Wang, F., Zhang, W., 2019. Rewiring metabolic network by chemical modulator based laboratory evolution doubles lipid production in *Crypthecodinium cohnii*. Metab Eng. 51**,** 88-98.

Diao, J., Song, X., Guo, T., Wang, F., Chen, L., Zhang, W., 2020. Cellular engineering strategies toward sustainable omega-3 long chain polyunsaturated fatty acids production: State of the art and perspectives. Biotechnol Adv. 40**,** 107497.

DiNicolantonio, J. J., O'Keefe, J. H., 2018. Importance of maintaining a low omega-6/omega-3 ratio for reducing inflammation. Open Heart. 5**,** e000946.

Dobrowolski, A., Mironczuk, A. M., 2020. The influence of transketolase on lipid biosynthesis in the yeast *Yarrowia lipolytica*. Microb Cell Fact. 19**,** 138.

Donot, F., Fontana, A., Baccou, J. C., Strub, C., Schorr-Galindo, S., 2014. Single cell oils (SCOs) from oleaginous yeasts and moulds: Production and genetics. Biomass Bioenerg. 68**,** 135-150.

Du, Z. Y., Alvaro, J., Hyden, B., Zienkiewicz, K., Benning, N., Zienkiewicz, A., Bonito, G., Benning, C., 2018. Enhancing oil production and harvest by combining the marine alga *Nannochloropsis oceanica* and the oleaginous fungus *Mortierella elongata*. Biotechnol Biofuels. 11**,** 174.

Dujon, B., Sherman, D., Fischer, G., Durrens, P., Casaregola, S., Lafontaine, I., De Montigny, J., Marck, C., Neuveglise, C., Talla, E., Goffard, N., Frangeul, L., Aigle, M., Anthouard, V., Babour, A., Barbe, V., Barnay, S., Blanchin, S., Beckerich, J. M., Beyne, E., Bleykasten, C., Boisrame, A., Boyer, J., Cattolico, L., Confanioleri, F., De Daruvar, A., Despons, L., Fabre, E., Fairhead, C., Ferry-Dumazet, H., Groppi, A., Hantraye, F., Hennequin, C., Jauniaux, N., Joyet, P., Kachouri, R., Kerrest, A., Koszul, R., Lemaire, M., Lesur, I., Ma, L., Muller, H., Nicaud, J. M., Nikolski, M., Oztas, S., Ozier-Kalogeropoulos, O., Pellenz, S., Potier, S., Richard, G. F., Straub, M. L., Suleau, A., Swennen, D., Tekaia, F., Wesolowski-Louvel, M., Westhof, E., Wirth, B., Zeniou-Meyer, M., Zivanovic, I., Bolotin-Fukuhara, M., Thierry, A., Bouchier, C., Caudron, B., Scarpelli, C., Gaillardin, C., Weissenbach, J., Wincker, P., Souciet, J. L., 2004. Genome evolution in yeasts. Nature. 430**,** 35-44.

Dulermo, R., Gamboa-Melendez, H., Ledesma-Amaro, R., Thevenieau, F., Nicaud, J. M., 2015. Unraveling fatty acid transport and activation mechanisms in *Yarrowia lipolytica*. Biochim Biophys Acta. 1851**,** 1202-17.

Dulermo, T., Nicaud, J. M., 2011. Involvement of the G3P shuttle and beta-oxidation pathway in the control of TAG synthesis and lipid accumulation in *Yarrowia lipolytica*. Metab Eng. 13**,** 482-91.

Dyerberg, J., Bang, H. O., Hjorne, N., 1975. Fatty acid composition of the plasma lipids in Greenland Eskimos. Am J Clin Nutr. 28**,** 958-66.

Erian, A. M., Egermeier, M., Marx, H., Sauer, M., 2022. Insights into the glycerol transport of *Yarrowia lipolytica*. Yeast. 39**,** 323-336.

Eroshin, V. K., Krylova, N. I., 1983. Efficiency of lipid-synthesis by yeasts. Biotechnol Bioeng. 25**,** 1693-1700.

Evans, C. T., Scragg, A. H., Ratledge, C., 1983. A comparative-study of citrate efflux from mitochondria of oleaginous and non-oleaginous yeasts. Eur J Biochem. 130**,** 195-204.

Fakas, S., 2017. Lipid biosynthesis in yeasts: A comparison of the lipid biosynthetic pathway between the model nonoleaginous yeast *Saccharomyces cerevisiae* and the model oleaginous yeast *Yarrowia lipolytica*. Eng Life Sci. 17**,** 292-302.

FAO, 2020. http://www.fao.org/state-of-fisheries-aquaculture. The State of World Fisheries and Aquaculture 2020. Food and Agricultural Organization, Food and Agricultural Organization.

Ferreira, I., Rauter, A. P., Bandarra, N. M., 2022. Marine sources of DHA-rich phospholipids with anti-Alzheimer effect. Mar Drugs. 20.

Fickers, P., Benetti, P. H., Wache, Y., Marty, A., Mauersberger, S., Smit, M. S., Nicaud, J. M., 2005. Hydrophobic substrate utilisation by the yeast *Yarrowia lipolytica*, and its potential applications. Fems Yeast Res. 5**,** 527-543.

Finco, A. M. O., Mamani, L. D. G., Carvalho, J. C., de Melo Pereira, G. V., Thomaz-Soccol, V., Soccol, C. R., 2017. Technological trends and market perspectives for production of microbial oils rich in omega-3. Crit Rev Biotechnol. 37**,** 656-671.

Fleige, S., Pfaffl, M. W., 2006. RNA integrity and the effect on the real-time qRT-PCR performance. Mol Aspects Med. 27**,** 126-39.

Frick, O., Wittmann, C., 2005. Characterization of the metabolic shift between oxidative and fermentative growth in *Saccharomyces cerevisiae* by comparative ^{13}C flux analysis. Microb Cell Fact. 4.

Gaden, E. L., 1959. Fermentation Process Kinetics. J Biochem Microbiol. 1**,** 413-429.

Gajdos, P., Ledesma-Amaro, R., Nicaud, J. M., Certik, M., Rossignol, T., 2016. Overexpression of diacylglycerol acyltransferase in *Yarrowia lipolytica* affects lipid body size, number and distribution. Fems Yeast Res. 16.

Ganger, M. T., Dietz, G. D., Ewing, S. J., 2017. A common base method for analysis of qPCR data and the application of simple blocking in qPCR experiments. Bmc Bioinformatics. 18.

Garcia, R., Stadler, M., Gemperlein, K., Muller, R., 2016. *Aetherobacter fasciculatus* gen. nov., sp. nov. and *Aetherobacter rufus* sp. nov., novel myxobacteria with promising biotechnological applications. Int J Syst Evol Microbiol. 66**,** 928-938.

Garcia, R. O., Reichenbach, H., Ring, M. W., Muller, R., 2009. *Phaselicystis flava* gen. nov., sp. nov., an arachidonic acid-containing soil myxobacterium, and the description of *Phaselicystidaceae* fam. nov. Int J Syst Evol Microbiol. 59**,** 1524-30.

Gatter, M., Ottlik, S., Kovesi, Z., Bauer, B., Matthaus, F., Barth, G., 2016. Three alcohol dehydrogenase genes and one acetyl-CoA synthetase gene are responsible for ethanol utilization in *Yarrowia lipolytica*. Fungal Genet Biol. 95**,** 30-38.

Ge, C., Chen, H., Mei, T., Tang, X., Chang, L., Gu, Z., Zhang, H., Chen, W., Chen, Y. Q., 2017. Application of a ω-3 desaturase with an arachidonic acid preference to eicosapentaenoic acid production in *Mortierella alpina*. Front Bioeng Biotechnol. 5**,** 89.

Gemperlein, K., Dietrich, D., Kohlstedt, M., Zipf, G., Bernauer, H. S., Wittmann, C., Wenzel, S. C., Müller, R., 2019. Polyunsaturated fatty acid production by *Yarrowia lipolytica* employing designed myxobacterial PUFA synthases. Nat Commun. 10**,** 4055.

Gemperlein, K., Rachid, S., Garcia, R. O., Wenzel, S. C., Müller, R., 2014. Polyunsaturated fatty acid biosynthesis in myxobacteria: different PUFA synthases and their product diversity. Chem Sci. 5**,** 1733-1741.

Gemperlein, K., Zaburannyi, N., Garcia, R., La Clair, J. J., Müller, R., 2018. Metabolic and biosynthetic diversity in marine myxobacteria. Mar Drugs. 16.

Gemperlein, K., Zipf, G., Bernauer, H. S., Muller, R., Wenzel, S. C., 2016. Metabolic engineering of *Pseudomonas putida* for production of docosahexaenoic acid based on a myxobacterial PUFA synthase. Metab Eng. 33**,** 98-108.

Geng, L., Chen, S., Sun, X., Hu, X., Ji, X., Huang, H., Ren, L., 2019. Fermentation performance and metabolomic analysis of an engineered high-yield PUFA-producing strain of *Schizochytrium* sp. Bioprocess Biosyst Eng. 42**,** 71-81.

Giner-Robles, L., Lazaro, B., de la Cruz, F., Moncalian, G., 2018. *fabH* deletion increases DHA production in *Escherichia coli* expressing *Pfa* genes. Microb Cell Fact. 17**,** 88.

Gläser, L., Kuhl, M., Jovanovic, S., Fritz, M., Vögeli, B., Erb, T. J., Becker, J., Wittmann, C., 2020. A common approach for absolute quantification of short chain CoA thioesters in prokaryotic and eukaryotic microbes. Microb Cell Fact. 19**,** 160.

Gläser, L., Kuhl, M., Stegmüller, J., Rückert, C., Myronovskyi, M., Kalinowski, J., Luzhetskyy, A., Wittmann, C., 2021. Superior production of heavy pamamycin derivatives using a bkdR deletion mutant of *Streptomyces albus* J1074/R2. Microb Cell Fact. 20**,** 111.

Goncalves, F. A., Colen, G., Takahashi, J. A., 2014. *Yarrowia lipolytica* and its multiple applications in the biotechnological industry. ScientificWorldJournal. 2014**,** 476207.

Gong, Y. M., Wan, X., Jiang, M. L., Hu, C. J., Hu, H. H., Huang, F. H., 2014a. Metabolic engineering of microorganisms to produce omega-3 very long-chain polyunsaturated fatty acids. Prog Lipid Res. 56**,** 19-35.

Gong, Z. W., Shen, H. W., Yang, X. B., Wang, Q., Xie, H. B., Zhao, Z. B. K., 2014b. Lipid production from corn stover by the oleaginous yeast *Cryptococcus curvatus*. Biotechnol Biofuels. 7.

Grigoriev, I. V., Nikitin, R., Haridas, S., Kuo, A., Ohm, R., Otillar, R., Riley, R., Salamov, A., Zhao, X. L., Korzeniewski, F., Smirnova, T., Nordberg, H., Dubchak, I., Shabalov, I., 2014. MycoCosm portal: gearing up for 1000 fungal genomes. Nucleic Acids Res. 42**,** D699-D704.

Groenewald, M., Boekhout, T., Neuveglise, C., Gaillardin, C., van Dijck, P. W. M., Wyss, M., 2014. *Yarrowia lipolytica*: Safety assessment of an oleaginous yeast with a great industrial potential. Crit Rev Microbiol. 40**,** 187-206.

Gunstone, F. D., 2001. Oilseed crops with modified fatty acid composition. J Oleo Sci. 50**,** 269-279.

Guo, D. S., Ji, X. J., Ren, L. J., Yin, F. W., Sun, X. M., Huang, H., Zhen, G., 2018. Development of a multi-stage continuous fermentation strategy for docosahexaenoic acid production by *Schizochytrium* sp. Bioresour Technol. 269**,** 32-39.

Guo, H. W., Madzak, C., Du, G. C., Zhou, J. W., Chen, J., 2014. Effects of pyruvate dehydrogenase subunits overexpression on the α-ketoglutarate production in *Yarrowia lipolytica* WSH-Z06. Appl Microbiol Biotechnol. 98**,** 7003-7012.

Guo, M. R., Chen, G. G., Chen, J. L., Zheng, M. G., 2019. Identification of a long-chain fatty acid elongase from *Nannochloropsis* sp. involved in the biosynthesis of fatty acids by heterologous expression in *Saccharomyces cerevisiae*. J Ocean U China. 18**,** 1199-1206.

Haddouche, R., Poirier, Y., Delessert, S., Sabirova, J., Pagot, Y., Neuveglise, C., Nicaud, J. M., 2011. Engineering polyhydroxyalkanoate content and monomer composition in the

oleaginous yeast *Yarrowia lipolytica* by modifying the ss-oxidation multifunctional protein. Appl Microbiol Biotechnol. 91**,** 1327-40.

Hamilton, M. L., Powers, S., Napier, J. A., Sayanova, O., 2016. Heterotrophic production of omega-3 long-chain polyunsaturated fatty acids by trophically converted marine diatom *Phaeodactylum tricornutum*. Mar Drugs. 14.

Harauma, A., Yasuda, H., Hatanaka, E., Nakamura, M. T., Salem, N., Jr., Moriguchi, T., 2017. The essentiality of arachidonic acid in addition to docosahexaenoic acid for brain growth and function. Prostaglandins Leukot Essent Fatty Acids. 116**,** 9-18.

Harris, W. S., 2018. The Omega-6:Omega-3 ratio: A critical appraisal and possible successor. Prostaglandins Leukot Essent Fatty Acids. 132**,** 34-40.

Harwood, J. L., 2019. Algae: critical sources of very long-chain polyunsaturated fatty acids. Biomolecules. 9.

Hayashi, S., Satoh, Y., Ogasawara, Y., Dairi, T., 2020. Recent advances in functional analysis of polyunsaturated fatty acid synthases. Curr Opin Chem Biol. 59**,** 30-36.

Heggeset, T. M. B., Ertesvag, H., Liu, B., Ellingsen, T. E., Vadstein, O., Aasen, I. M., 2019. Lipid and DHA-production in *Aurantiochytrium* sp. - Responses to nitrogen starvation and oxygen limitation revealed by analyses of production kinetics and global transcriptomes. Sci Rep. 9**,** 19470.

Hicks, C. C., Cohen, P. J., Graham, N. A. J., Nash, K. L., Allison, E. H., D'Lima, C., Mills, D. J., Roscher, M., Thilsted, S. H., Thorne-Lyman, A. L., MacNeil, M. A., 2019. Harnessing global fisheries to tackle micronutrient deficiencies. Nature. 574**,** 95-98.

Hixson, S. M., Arts, M. T., 2016. Climate warming is predicted to reduce omega-3, long-chain, polyunsaturated fatty acid production in phytoplankton. Glob Chang Biol. 22**,** 2744-55.

Hoffmann, S. L., Kohlstedt, M., Jungmann, L., Hutter, M., Poblete-Castro, I., Becker, J., Wittmann, C., 2021. Cascaded valorization of brown seaweed to produce l-lysine and value-added products using Corynebacterium glutamicum streamlined by systems metabolic engineering. Metab Eng. 67**,** 293-307.

Holz, M., Forster, A., Mauersberger, S., Barth, G., 2009. Aconitase overexpression changes the product ratio of citric acid production by *Yarrowia lipolytica*. Appl Microbiol Biotechnol. 81**,** 1087-96.

Holz, M., Otto, C., Kretzschmar, A., Yovkova, V., Aurich, A., Potter, M., Marx, A., Barth, G., 2011. Overexpression of alpha-ketoglutarate dehydrogenase in *Yarrowia lipolytica* and its effect on production of organic acids. Appl Microbiol Biotechnol. 89**,** 1519-1526.

Hussain, S. A., Sarker, M. I., Yosief, H. O., Yadav, M. P., 2021. Evaluation of diverse biochemical stimulants to enhance growth, lipid and docosahexaenoic acid (DHA) production of *Aurantiochytrium* Sp. ATCC PRA-276. Biocatal Agr Biotech. 36.

Imatoukene, N., Verbeke, J., Beopoulos, A., Taghki, A. I., Thomasset, B., Sarde, C. O., Nonus, M., Nicaud, J. M., 2017. A metabolic engineering strategy for producing conjugated linoleic acids using the oleaginous yeast *Yarrowia lipolytica*. Appl Microbiol Biotechnol. 101**,** 4605-4616.

Innes, J. K., Calder, P. C., 2018. Omega-6 fatty acids and inflammation. Prostaglandins Leukot Essent Fatty Acids. 132**,** 41-48.

Innes, J. K., Calder, P. C., 2020. Marine omega-3 (N-3) fatty acids for cardiovascular health: An update for 2020. Int J Mol Sci. 21.

Jacob, F., Guertler, R., Naim, S., Nixdorf, S., Fedier, A., Hacker, N. F., Heinzelmann-Schwarz, V., 2013. Careful selection of reference genes is required for reliable performance of RT-qPCR in human normal and cancer cell lines. PLoS One. 8.

Jia, Y. L., Du, F., Nong, F. T., Li, J., Huang, P. W., Ma, W., Gu, Y., Sun, X. M., 2023. Function of the polyketide synthase domains of *Schizochytrium* sp. on fatty acid synthesis in *Yarrowia lipolytica*. J Agric Food Chem. 2446-2454.

Jia, Y. L., Wang, L. R., Zhang, Z. X., Gu, Y., Sun, X. M., 2022. Recent advances in biotechnological production of polyunsaturated fatty acids by *Yarrowia lipolytica*. Crit Rev Food Sci Nutr. 62**,** 8920-8934.

Johansson, M., Chen, X., Milanova, S., Santos, C., Petranovic, D., 2016. PUFA-induced cell death is mediated by Yca1p-dependent and -independent pathways, and is reduced by vitamin C in yeast. Fems Yeast Res. 16.

Johnson, M. T. J., Carpenter, E. J., Tian, Z. J., Bruskiewich, R., Burris, J. N., Carrigan, C. T., Chase, M. W., Clarke, N. D., Covshoff, S., dePamphilis, C. W., Edger, P. P., Goh, F., Graham, S.,

Greiner, S., Hibberd, J. M., Jordon-Thaden, I., Kutchan, T. M., Leebens-Mack, J., Melkonian, M., Miles, N., Myburg, H., Patterson, J., Pires, J. C., Ralph, P., Rolf, M., Sage, R. F., Soltis, D., Soltis, P., Stevenson, D., Stewart, C. N., Surek, B., Thomsen, C. J. M., Villarreal, J. C., Wu, X. L., Zhang, Y., Deyholos, M. K., Wong, G. K. S., 2012. Evaluating methods for isolating total RNA and predicting the success of sequencing phylogenetically diverse plant transcriptomes. PLoS One. 7.

Jovanovic, S., Dietrich, D., Becker, J., Kohlstedt, M., Wittmann, C., 2021. Microbial production of polyunsaturated fatty acids - high-value ingredients for aquafeed, superfoods, and pharmaceuticals. Curr Opin Biotechnol. 69**,** 199-211.

Kabeya, N., Fonseca, M. M., Ferrier, D. E. K., Navarro, J. C., Bay, L. K., Francis, D. S., Tocher, D. R., Castro, L. F. C., Monroig, O., 2018. Genes for *de novo* biosynthesis of omega-3 polyunsaturated fatty acids are widespread in animals. Sci Adv. 4**,** eaar6849.

Kamineni, A., Chen, S. Y., Chifamba, G., Tsakraklides, V., 2020. Promoters for lipogenesis-specific downregulation in *Yarrowia lipolytica*. Fems Yeast Res. 20.

Kamzolova, S. V., Lunina, J. N., Morgunov, I. G., 2011. Biochemistry of citric acid production from rapeseed oil by *Yarrowia lipolytica* yeast. J Am Oil Chem Soc. 88**,** 1965-1976.

Khan, M. A. K., Yang, J., Hussain, S. A., Zhang, H., Liang, L., Garre, V., Song, Y., 2019. Construction of DGLA producing cell factory by genetic modification of *Mucor circinelloides*. Microb Cell Fact. 18**,** 64.

Khozin-Goldberg, I., Leu, S., Boussiba, S., 2016. Microalgae as a source for VLC- PUFA production. Subcell Biochem. 86**,** 471-510.

Kiel, J. A., Veenhuis, M., van der Klei, I. J., 2006. *PEX* genes in fungal genomes: common, rare or redundant. Traffic. 7**,** 1291-303.

Kohlstedt, M., Weimer, A., Weiland, F., Stolzenberger, J., Selzer, M., Sanz, M., Kramps, L., Wittmann, C., 2022. Biobased PET from lignin using an engineered cis, cis-muconate-producing *Pseudomonas putida* strain with superior robustness, energy and redox properties. Metab Eng. 72**,** 337-352.

Kohlstedt, M., Wittmann, C., 2019. GC-MS-based (13)C metabolic flux analysis resolves the parallel and cyclic glucose metabolism of Pseudomonas putida KT2440 and Pseudomonas aeruginosa PAO1. Metab Eng. 54**,** 35-53.

Kolouchova, I., Mat'atkova, O., Sigler, K., Masak, J., Rezanka, T., 2016a. Lipid accumulation by oleaginous and non-oleaginous yeast strains in nitrogen and phosphate limitation. Folia Microbiol (Praha). 61**,** 431-438.

Kolouchova, I., Matatkova, O., Sigler, K., Masak, J., Rezanka, T., 2016b. Production of palmitoleic and linoleic acid in oleaginous and nonoleaginous yeast biomass. Int J Anal Chem. 2016**,** 7583684.

Korpys-Wozniak, P., Kubiak, P., Celinska, E., 2021. Secretory helpers for enhanced production of heterologous proteins in *Yarrowia lipolytica*. Biotechnol Rep (Amst). 32**,** e00669.

Kot, A. M., Blazejak, S., Kurcz, A., Gientka, I., Kieliszek, M., 2016. *Rhodotorula glutinis*-potential source of lipids, carotenoids, and enzymes for use in industries. Appl Microbiol Biotechnol. 100**,** 6103-6117.

Kothri, M., Mavrommati, M., Elazzazy, A. M., Baeshen, M. N., Moussa, T. A. A., Aggelis, G., 2020. Microbial sources of polyunsaturated fatty acids (PUFAs) and the prospect of organic residues and wastes as growth media for PUFA-producing microorganisms. FEMS Microbiol Lett. 367.

Krebs, S., Fischaleck, M., Blum, H., 2009. A simple and loss-free method to remove TRIzol contaminations from minute RNA samples. Anal Biochem. 387**,** 136-138.

Krink-Koutsoubelis, N., Loechner, A. C., Lechner, A., Link, H., Denby, C. M., Vogeli, B., Erb, T. J., Yuzawa, S., Jakociunas, T., Katz, L., Jensen, M. K., Sourjik, V., Keasling, J. D., 2018. Engineered production of short-chain acyl-Coenzyme A esters in *Saccharomyces cerevisiae*. ACS Synth Biol. 7**,** 1105-1115.

Krivoruchko, A., Zhang, Y. M., Siewers, V., Chen, Y., Nielsen, J., 2015. Microbial acetyl-CoA metabolism and metabolic engineering. Metab Eng. 28**,** 28-42.

Krömer, J. O., Fritz, M., Heinzle, E., Wittmann, C., 2005. *In vivo* quantification of intracellular amino acids and intermediates of the methionine pathway in *Corynebacterium glutamicum*. Anal Biochem. 340**,** 171-3.

Kubiak, M., Borkowska, M., Bialas, W., Korpys, P., Celinska, E., 2019. Feeding strategy impacts heterologous protein production in *Yarrowia lipolytica* fed-batch cultures-Insight into the role of osmolarity. Yeast. 36**,** 305-318.

Kuhl, M., Glaser, L., Rebets, Y., Ruckert, C., Sarkar, N., Hartsch, T., Kalinowski, J., Luzhetskyy, A., Wittmann, C., 2020. Microparticles globally reprogram Streptomyces albus toward accelerated morphogenesis, streamlined carbon core metabolism, and enhanced production of the antituberculosis polyketide pamamycin. Biotechnol Bioeng. 117**,** 3858-3875.

Kuhl, M., Ruckert, C., Glaser, L., Beganovic, S., Luzhetskyy, A., Kalinowski, J., Wittmann, C., 2021. Microparticles enhance the formation of seven major classes of natural products in native and metabolically engineered actinobacteria through accelerated morphological development. Biotechnol Bioeng. 118**,** 3076-3093.

Kujawska, N., Talbierz, S., Debowski, M., Kazimierowicz, J., Zielinski, M., 2021. Cultivation Method Effect on *Schizochytrium* sp. Biomass Growth and Docosahexaenoic Acid (DHA) Production with the Use of Waste Glycerol as a Source of Organic Carbon. Energies. 14.

Kusube, M., Kyaw, T. S., Tanikawa, K., Chastain, R. A., Hardy, K. M., Cameron, J., Bartlett, D. H., 2017. *Colwellia marinimaniae* sp. nov., a hyperpiezophilic species isolated from an amphipod within the Challenger Deep, Mariana Trench. Int J Syst Evol Microbiol. 67**,** 824-831.

Lamers, D., van Biezen, N., Martens, D., Peters, L., van de Zilver, E., Jacobs-van Dreume, N., Wijffels, R. H., Lokman, C., 2016. Selection of oleaginous yeasts for fatty acid production. BMC Biotechnol. 16.

Lange, A., Becker, J., Schulze, D., Cahoreau, E., Portais, J. C., Haefner, S., Schroder, H., Krawczyk, J., Zelder, O., Wittmann, C., 2017. Bio-based succinate from sucrose: High-resolution ^{13}-C metabolic flux analysis and metabolic engineering of the rumen bacterium *Basfia succiniciproducens*. Metab Eng. 44**,** 198-212.

Ledesma-Amaro, R., Jimenez, A., Revuelta, J. L., 2018. Pathway grafting for polyunsaturated fatty acids production in *Ashbya gossypii* through golden gate rapid assembly. ACS Synth Biol. 7**,** 2340-2347.

Ledesma-Amaro, R., Nicaud, J. M., 2016. *Yarrowia lipolytica* as a biotechnological chassis to produce usual and unusual fatty acids. Prog Lipid Res. 61**,** 40-50.

Li-Beisson, Y., Thelen, J. J., Fedosejevs, E., Harwood, J. L., 2019. The lipid biochemistry of eukaryotic algae. Prog Lipid Res. 74**,** 31-68.

Li, J., Pora, B. L. R., Dong, K., Hasjim, J., 2021. Health benefits of docosahexaenoic acid and its bioavailability: A review. Food Sci Nutr. 9**,** 5229-5243.

Li, Q., Bai, Z., O'Donnell, A., Harvey, L. M., Hoskisson, P. A., McNeil, B., 2011. Oxidative stress in fungal fermentation processes: the roles of alternative respiration. Biotechnol Lett. 33**,** 457-467.

Li, X., Wang, P., Ge, Y. D., Wang, W., Abbas, A., Zhu, G. P., 2013. $NADP^+$-specific isocitrate dehydrogenase from oleaginous yeast *Yarrowia lipolytica* CLIB122: Biochemical characterization and coenzyme sites evaluation. Appl Biochem Biotechnol. 171**,** 403-416.

Li, Z., Meng, T., Ling, X., Li, J., Zheng, C., Shi, Y., Chen, Z., Li, Q., Lu, Y., He, N., 2018. Overexpression of malonyl-CoA: ACP transacylase in *Schizochytrium* sp. to improve polyunsaturated fatty acid production. J Agric Food Chem. 66**,** 5382-5391.

Lien, E. L., Richard, C., Hoffman, D. R., 2018. DHA and ARA addition to infant formula: Current status and future research directions. Prostaglandins Leukot Essent Fatty Acids. 128**,** 26-40.

Liu, H., Marsafari, M., Deng, L., Xu, P., 2019a. Understanding lipogenesis by dynamically profiling transcriptional activity of lipogenic promoters in *Yarrowia lipolytica*. Appl Microbiol Biotechnol. 103**,** 3167-3179.

Liu, H., Marsafari, M., Wang, F., Deng, L., Xu, P., 2019b. Engineering acetyl-CoA metabolic shortcut for eco-friendly production of polyketides triacetic acid lactone in *Yarrowia lipolytica*. Metab Eng. 56**,** 60-68.

Liu, H., Song, Y., Fan, X., Wang, C., Lu, X., Tian, Y., 2020. *Yarrowia lipolytica* as an oleaginous platform for the production of value-added fatty acid-based bioproducts. Front Microbiol. 11**,** 608662.

Liu, H. H., Madzak, C., Sun, M. L., Ren, L. J., Song, P., Huang, H., Ji, X. J., 2017. Engineering *Yarrowia lipolytica* for arachidonic acid production through rapid assembly of metabolic pathway. Biochem Eng J. 119**,** 52-58.

Liu, H. H., Wang, C., Lu, X. Y., Huang, H., Tian, Y., Ji, X. J., 2019c. Improved production of arachidonic acid by combined pathway engineering and synthetic enzyme fusion in *Yarrowia lipolytica*. J Agric Food Chem. 67**,** 9851-9857.

Liu, L., Wang, F., Yang, J., Li, X., Cui, J., Liu, J., Shi, M., Wang, K., Chen, L., Zhang, W., 2018. Nitrogen feeding strategies and metabolomic analysis to alleviate high-nitrogen inhibition on docosahexaenoic acid production in *Crypthecodinium cohnii*. J Agric Food Chem. 66**,** 10640-10650.

Liu, N., Qiao, K., Stephanopoulos, G., 2016. ^{13}C Metabolic flux analysis of acetate conversion to lipids by *Yarrowia lipolytica*. Metab Eng. 38**,** 86-97.

Liu, Y. J., Ren, X., Fan, C., Wu, W. Z., Zhang, W., Wang, Y. W., 2022. Health benefits, food applications, and sustainability of microalgae-derived n-3 PUFA. Foods. 11.

Liu, Y. Y., Tian, Y. Y., Cai, W. Z., Guo, Y., Xue, C. H., Wang, J. F., 2021. DHA/EPA-Enriched phosphatidylcholine suppresses tumor growth and metastasis *via* activating peroxisome proliferator-activated receptor gamma in Lewis lung cancer mice. J Agric Food Chem. 69**,** 676-685.

Lorenz, M. C., Fink, G. R., 2001. The glyoxylate cycle is required for fungal virulence. Nature. 412**,** 83-86.

Lu, R., Cao, L. Z., Wang, K. F., Ledesma-Amaro, R., Ji, X. J., 2021. Engineering *Yarrowia lipolytica* to produce advanced biofuels: Current status and perspectives. Bioresour Technol. 341.

Lubuta, P., Workman, M., Kerkhoven, E. J., Workman, C. T., 2019. Investigating the Influence of Glycerol on the Utilization of Glucose in *Yarrowia lipolytica* Using RNA-Seq-Based Transcriptomics. G3 (Bethesda). 9**,** 4059-4071.

Luevano, L. A., Moyano, E., de Lacoba, M. G., Rial, E., Uribe-Carvajal, S., 2010. Identification of the mitochondrial carrier that provides *Yarrowia lipolytica* with a fatty acid- induced and nucleotides-sensitive uncoupling protein-like activity. Biophys J. 98**,** 736a-736a.

Ma, Z., Tan, Y., Cui, G., Feng, Y., Cui, Q., Song, X., 2015. Transcriptome and gene expression analysis of DHA producer *Aurantiochytrium* under low temperature conditions. Sci Rep. 5**,** 14446.

Madore, C., Leyrolle, Q., Morel, L., Rossitto, M., Greenhalgh, A. D., Delpech, J. C., Martinat, M., Bosch-Bouju, C., Bourel, J., Rani, B., Lacabanne, C., Thomazeau, A., Hopperton, K. E., Beccari, S., Sere, A., Aubert, A., De Smedt-Peyrusse, V., Lecours, C., Bisht, K., Fourgeaud, L., Gregoire, S., Bretillon, L., Acar, N., Grant, N. J., Badaut, J., Gressens, P., Sierra, A., Butovsky, O., Tremblay, M. E., Bazinet, R. P., Joffre, C., Nadjar, A., Laye, S., 2020. Essential omega-3 fatty acids tune microglial phagocytosis of synaptic elements in the mouse developing brain. Nat Commun. 11.

Madzak, C., 2021. *Yarrowia lipolytica* strains and their biotechnological applications: How natural biodiversity and metabolic engineering could contribute to cell factories improvement. J Fungi. 7.

Magdouli, S., Guedri, T., Rouissi, T., Brar, S. K., Blais, J. F., 2020. Sync between leucine, biotin and citric acid to improve lipid production by *Yarrowia lipolytica* on crude glycerol-based media. Biomass Bioenerg. 142.

Mamaev, D., Zvyagilskaya, R., 2021. *Yarrowia lipolytica*: a multitalented yeast species of ecological significance. Fems Yeast Res. 21.

Mao, X., Liu, Z., Sun, J., Lee, S. Y., 2017. Metabolic engineering for the microbial production of marine bioactive compounds. Biotechnol Adv. 35**,** 1004-1021.

Meesters, P. A. E. P., Huijberts, G. N. M., Eggink, G., 1996. High cell density cultivation of the lipid accumulating yeast *Cryptococcus curvatus* using glycerol as a carbon source. Appl Microbiol Biotechnol. 45**,** 575-579.

Mendes, A., Reis, A., Vasconcelos, R., Guerra, P., da Silva, T. L., 2009. *Crypthecodinium cohnii* with emphasis on DHA production: a review. J Appl Phycol. 21**,** 199-214.

Metz, J. G., Roessler, P., Facciotti, D., Levering, C., Dittrich, F., Lassner, M., Valentine, R., Lardizabal, K., Domergue, F., Yamada, A., Yazawa, K., Knauf, V., Browse, J., 2001. Production of polyunsaturated fatty acids by polyketide synthases in both prokaryotes and eukaryotes. Science. 293**,** 290-3.

Miller, K. K., Alper, H. S., 2019. *Yarrowia lipolytica*: more than an oleaginous workhorse. Appl Microbiol Biotechnol. 103**,** 9251-9262.

Mlickova, K., Luo, Y., d'Andrea, S., Pec, P., Chardot, T., Nicaud, J. M., 2004. Acyl-CoA oxidase, a key step for lipid accumulation in the yeast *Yarrowia lipolytica*. J Mol Catal B-Enzym. 28**,** 81-85.

Moi, I. M., Leow, A. T. C., Ali, M. S. M., Rahman, R., Salleh, A. B., Sabri, S., 2018. Polyunsaturated fatty acids in marine bacteria and strategies to enhance their production. Appl Microbiol Biotechnol. 102**,** 5811-5826.

Monroig, O., Kabeya, N., 2018. Desaturases and elongases involved in polyunsaturated fatty acid biosynthesis in aquatic invertebrates: a comprehensive review. Fisheries Sci. 84**,** 911-928.

Morabito, C., Bournaud, C., Maes, C., Schuler, M., Aiese Cigliano, R., Dellero, Y., Marechal, E., Amato, A., Rebeille, F., 2019. The lipid metabolism in thraustochytrids. Prog Lipid Res. 76**,** 101007.

Morales-Vargas, A. T., Dominguez, A., Ruiz-Herrera, J., 2012. Identification of dimorphism-involved genes of *Yarrowia lipolytica* by means of microarray analysis. Res Microbiol. 163**,** 378-87.

Moreira, J. D., Jolicoeur, M., Schwartz, L., Peres, S., 2021. Fine-tuning mitochondrial activity in *Yarrowia lipolytica* for citrate overproduction. Sci Rep. 11.

Morgunov, I. G., Solodovnikova, N. Y., Sharyshev, A. A., Kamzolova, S. V., Finogenova, T. V., 2004. Regulation of NAD^+-Dependent isocitrate dehydrogenase in the citrate producing yeast *Yarrowia lipolytica*. Biochemistry-Moscow+. 69**,** 1391-1398.

Morin, M., Monteoliva, L., Insenser, M., Gil, C., Dominguez, A., 2007. Proteomic analysis reveals metabolic changes during yeast to hypha transition in *Yarrowia lipolytica*. J Mass Spectrom. 42**,** 1453-62.

Morin, N., Cescut, J., Beopoulos, A., Lelandais, G., Le Berre, V., Uribelarrea, J. L., Molina-Jouve, C., Nicaud, J. M., 2011. Transcriptomic analyses during the transition from biomass production to lipid accumulation in the oleaginous yeast *Yarrowia lipolytica*. PLoS One. 6**,** e27966.

Mun, J. G., Legette, L. L., Ikonte, C. J., Mitmesser, S. H., 2019. Choline and DHA in Maternal and Infant Nutrition: Synergistic Implications in Brain and Eye Health. Nutrients. 11.

Nazir, Y., Shuib, S., Kalil, M. S., Song, Y., Hamid, A. A., 2018. Optimization of culture conditions for enhanced growth, lipid and docosahexaenoic acid (DHA) production of *Aurantiochytrium* SW1 by response surface methodology. Sci Rep. 8**,** 8909.

Nishshanka, G. K. S. H., Anthonio, R. A. D. P., Nimarshana, P. H. V., Ariyadasa, T. U., Chang, J. S., 2022. Marine microalgae as sustainable feedstock for multi-product biorefineries. Biochemical Engineering Journal. 187.

Norashikin, M. N., Loh, S. H., Aziz, A., Cha, T. S., 2018. Metabolic engineering of fatty acid biosynthesis in *Chlorella vulgaris* using an endogenous omega-3 fatty acid desaturase gene with its promoter. Algal Res. 31**,** 262-275.

Papanikolaou, S., Chatzifragkou, A., Fakas, S., Galiotou-Panayotou, M., Komaitis, M., Nicaud, J. M., Aggelis, G., 2009. Biosynthesis of lipids and organic acids by *Yarrowia lipolytica* strains cultivated on glucose. European Journal of Lipid Science and Technology. 111**,** 1221-1232.

Papanikolaou, S., Muniglia, L., Chevalot, I., Aggelis, G., Marc, I., 2002a. *Yarrowia lipolytica* as a potential producer of citric acid from raw glycerol. J Appl Microbiol. 92**,** 737-44.

Papanikolaou, S., Muniglia, L., Chevalot, I., Aggelis, G., Marc, I., 2002b. *Yarrowia lipolytica* as a potential producer of citric acid from raw glycerol. J Appl Microbiol. 92**,** 737-744.

Park, Y. K., Ledesma-Amaro, R., Nicaud, J. M., 2020. *De novo* biosynthesis of odd-chain fatty acids in *Yarrowia lipolytica* enabled by modular pathway engineering. Front Bioeng Biotechnol. 7.

Parrou, J. L., Enjalbert, B., Plourde, L., Bauche, A., Gonzalez, B., Francois, J., 1999. Dynamic responses of reserve carbohydrate metabolism under carbon and nitrogen limitations in *Saccharomyces cerevisiae*. Yeast. 15**,** 191-203.

Pauli, S., Kohlstedt, M., Lamber, J., Weiland, F., Becker, J., Wittmann, C., 2023. Systems metabolic engineering upgrades *Corynebacterium glutamicum* for selective high-level production of the chiral drug precursor and cell-protective extremolyte L-pipecolic acid. Metab Eng. 77**,** 100-117.

Pei, G. S., Li, X. R., Liu, L. S., Liu, J., Wang, F. Z., Chen, L., Zhang, W. W., 2017. *De novo* transcriptomic and metabolomic analysis of docosahexaenoic acid (DHA)-producing *Crypthecodinium cohnii* during fed-batch fermentation. Algal Res. 26**,** 380-391.

Peng, Y. F., Chen, W. C., Xiao, K., Xu, L., Wang, L., Wan, X., 2016. DHA production in *Escherichia coli* by expressing reconstituted key genes of polyketide synthase pathway from marine bacteria. PLoS One. 11**,** e0162861.

Poblete-Castro, I., Hoffmann, S. L., Becker, J., Wittmann, C., 2020. Cascaded valorization of seaweed using microbial cell factories. Curr Opin Biotechnol. 65**,** 102-113.

Pomraning, K. R., Bredeweg, E. L., Kerkhoven, E. J., Barry, K., Haridas, S., Hundley, H., LaButti, K., Lipzen, A., Yan, M., Magnuson, J. K., Simmons, B. A., Grigoriev, I. V., Nielsen, J., Baker, S. E., 2018. Regulation of Yeast-to-Hyphae Transition in *Yarrowia lipolytica*. mSphere. 3.

Pomraning, K. R., Kim, Y. M., Nicora, C. D., Chu, R. K., Bredeweg, E. L., Purvine, S. O., Hu, D., Metz, T. O., Baker, S. E., 2016. Multi-omics analysis reveals regulators of the response to nitrogen limitation in *Yarrowia lipolytica*. BMC Genomics. 17**,** 138.

Poole, L. B., Parsonage, D., Sergeant, S., Miller, L. R., Lee, J., Furdui, C. M., Chilton, F. H., 2020. Acyl-lipid desaturases and *Vipp1* cooperate in cyanobacteria to produce novel omega-3 PUFA-containing glycolipids. Biotechnol Biofuels. 13**,** 83.

Pudney, A., Gandini, C., Economou, C. K., Smith, R., Goddard, P., Napier, J. A., Spicer, A., Sayanova, O., 2019. Multifunctionalizing the marine diatom *Phaeodactylum tricornutum* for sustainable co-production of omega-3 long chain polyunsaturated fatty acids and recombinant phytase. Sci Rep. 9**,** 11444.

Qiao, K. J., Wasylenko, T. M., Zhou, K., Xu, P., Stephanopoulos, G., 2017. Lipid production in *Yarrowia lipolytica* is maximized by engineering cytosolic redox metabolism. Nature Biotechnology. 35**,** 173-177.

Qiu, X., Xie, X., Meesapyodsuk, D., 2020. Molecular mechanisms for biosynthesis and assembly of nutritionally important very long chain polyunsaturated fatty acids in microorganisms. Prog Lipid Res. 79**,** 101047.

Racey, M., MacFarlane, A., Carlson, S. E., Stark, K. D., Plourde, M., Field, C. J., Yates, A. A., Wells, G., Grantham, A., Bazinet, R. P., Ma, D. W. L., 2021. Dietary reference intakes based on chronic disease endpoints: outcomes from a case study workshop for omega-3's EPA and DHA. Appl Physiol Nutr Metab. 46**,** 530-539.

Ratledge, C., 2004. Fatty acid biosynthesis in microorganisms being used for Single Cell Oil production. Biochimie. 86**,** 807-815.

Ratledge, C., Hopkins, S., 2006. Modifying Lipids for Use in Food. Woodhead Publishing, Cambrige, UK.

Ratledge, C., Wynn, J. P., 2002. The biochemistry and molecular biology of lipid accumulation in oleaginous microorganisms. Adv Appl Microbiol. 51**,** 1-51.

Ren, L. J., Chen, S. L., Geng, L. J., Ji, X. J., Xu, X., Song, P., Gao, S., Huang, H., 2018. Exploring the function of acyltransferase and domain replacement in order to change the polyunsaturated fatty acid profile of *Schizochytrium* sp. Algal Res. 29**,** 193-201.

Ren, L. J., Sun, X. M., Ji, X. J., Chen, S. L., Guo, D. S., Huang, H., 2017. Enhancement of docosahexaenoic acid synthesis by manipulation of antioxidant capacity and prevention of oxidative damage in *Schizochytrium* sp. Bioresour Technol. 223**,** 141-148.

Rey, C., Delpech, J. C., Madore, C., Nadjar, A., Greenhalgh, A. D., Amadieu, C., Aubert, A., Pallet, V., Vaysse, C., Laye, S., Joffre, C., 2019. Dietary n-3 long chain PUFA supplementation promotes a pro-resolving oxylipin profile in the brain. Brain Behav Immun. 76**,** 17-27.

Rodriguez, G. M., Hussain, M. S., Gambill, L., Gao, D., Yaguchi, A., Blenner, M., 2016. Engineering xylose utilization in *Yarrowia lipolytica* by understanding its cryptic xylose pathway. Biotechnol Biofuels. 9**,** 149.

Rohles, C., Pauli, S., Giesselmann, G., Kohlstedt, M., Becker, J., Wittmann, C., 2022. Systems metabolic engineering of *Corynebacterium glutamicum* eliminates all by-products for selective and high-yield production of the platform chemical 5-aminovalerate. Metab Eng. 73**,** 168-181.

Rohles, C. M., Glaser, L., Kohlstedt, M., Giesselmann, G., Pearson, S., del Campo, A., Becker, J., Wittmann, C., 2018a. A bio-based route to the carbon-5 chemical glutaric acid and to bionylon-6,5 using metabolically engineered *Corynebacterium glutamicum*. Green Chemistry. 20**,** 4662-4674.

Rohles, C. M., Gläser, L., Kohlstedt, M., Gießelmann, G., Pearson, S., del Campo, A., Becker, J., Wittmann, C., 2018b. A bio-based route to the carbon-5 chemical glutaric acid and to

bionylon-6,5 using metabolically engineered *Corynebacterium glutamicum*. Green Chem. 20**,** 4662-4674.

Ryu, S., Trinh, C. T., 2018. Understanding functional roles of native pentose-specific transporters for activating dormant pentose metabolism in *Yarrowia lipolytica*. Appl Environ Microbiol. 84.

Sabra, W., Bommareddy, R. R., Maheshwari, G., Papanikolaou, S., Zeng, A. P., 2017. Substrates and oxygen dependent citric acid production by *Yarrowia lipolytica*: insights through transcriptome and fluxome analyses. Microb Cell Fact. 16**,** 78.

Sahin, D., Tas, E., Altindag, U. H., 2018. Enhancement of docosahexaenoic acid (DHA) production from *Schizochytrium* sp. S31 using different growth medium conditions. AMB Express. 8**,** 7.

Saini, R. K., Keum, Y. S., 2018. Omega-3 and omega-6 polyunsaturated fatty acids: Dietary sources, metabolism, and significance - A review. Life Sci. 203**,** 255-267.

Salem, N., Eggersdorfer, M., 2015. Is the world supply of omega-3 fatty acids adequate for optimal human nutrition? Curr Opin Clin Nutr Metab Care. 18**,** 147-154.

Santin, O., Moncalian, G., 2018. Loading of malonyl-CoA onto tandem acyl carrier protein domains of polyunsaturated fatty acid synthases. J Biol Chem. 293**,** 12491-12501.

Santos-Merino, M., Garcillan-Barcia, M. P., de la Cruz, F., 2018. Engineering the fatty acid synthesis pathway in *Synechococcus elongatus* PCC 7942 improves omega-3 fatty acid production. Biotechnol Biofuels. 11**,** 239.

Sasidharan, K., Amariei, C., Tomita, M., Murray, D. B., 2012. Rapid DNA, RNA and protein extraction protocols optimized for slow continuously growing yeast cultures. Yeast. 29**,** 311-322.

Sathasivam, R., Radhakrishnan, R., Hashem, A., Abd Allah, E. F., 2019. Microalgae metabolites: A rich source for food and medicine. Saudi J Biol Sci. 26**,** 709-722.

Schroeder, A., Mueller, O., Stocker, S., Salowsky, R., Leiber, M., Gassmann, M., Lightfoot, S., Menzel, W., Granzow, M., Ragg, T., 2006. The RIN: an RNA integrity number for assigning integrity values to RNA measurements. Bmc Mol Biol. 7.

Schwechheimer, S. K., Becker, J., Peyriga, L., Portais, J. C., Sauer, D., Müller, R., Hoff, B., Haefner, S., Schröder, H., Zelder, O., Wittmann, C., 2018a. Improved riboflavin production with *Ashbya gossypii* from vegetable oil based on ^{13}C metabolic network analysis with combined labeling analysis by GC/MS, LC/MS, 1D, and 2D NMR. Metab Eng. 47**,** 357-373.

Schwechheimer, S. K., Becker, J., Peyriga, L., Portais, J. C., Wittmann, C., 2018b. Metabolic flux analysis in *Ashbya gossypii* using ^{13}C-labeled yeast extract: industrial riboflavin production under complex nutrient conditions. Microb Cell Fact. 17.

Shahidi, F., Ambigaipalan, P., 2018. Omega-3 polyunsaturated fatty acids and their health benefits. Annu Rev Food Sci Technol. 9**,** 345-381.

Shaigani, P., Awad, D., Redai, V., Fuchs, M., Haack, M., Mehlmer, N., Brueck, T., 2021. Oleaginous yeasts- substrate preference and lipid productivity: a view on the performance of microbial lipid producers. Microb Cell Fact. 20**,** 220.

Shao, D., Villet, O., Zhang, Z., Choi, S. W., Yan, J., Ritterhoff, J., Gu, H. W., Djukovic, D., Christodoulou, D., Kolwicz, S. C., Raftery, D., Tian, R., 2018. Glucose promotes cell growth by suppressing branched-chain amino acid degradation. Nat Commun. 9.

Shi, H., Luo, X., Wu, R., Yue, X., 2018a. Production of eicosapentaenoic acid by application of a delta-6 desaturase with the highest ALA catalytic activity in algae. Microb Cell Fact. 17**,** 7.

Shi, T. Q., Huang, H., Kerkhoven, E. J., Ji, X. J., 2018b. Advancing metabolic engineering of *Yarrowia lipolytica* using the CRISPR/Cas system. Appl Microbiol Biotechnol. 102**,** 9541-9548.

Silverman, A. M., Qiao, K. J., Xu, P., Stephanopoulos, G., 2016. Functional overexpression and characterization of lipogenesis-related genes in the oleaginous yeast *Yarrowia lipolytica*. Appl Microbiol Biotechnol. 100**,** 3781-3798.

Sinigaglia, M., Lanciotti, R., Guerzoni, M. E., 1994. Biochemical and physiological characteristics of *Yarrowia lipolytica* strains in relation to isolation source. Can J Microbiol. 40**,** 54-59.

Sirisuk, P., Sunwoo, I., Kim, S. H., Awah, C. C., Hun Ra, C., Kim, J. M., Jeong, G. T., Kim, S. K., 2018. Enhancement of biomass, lipids, and polyunsaturated fatty acid (PUFA) production in *Nannochloropsis oceanica* with a combination of single wavelength light emitting diodes (LEDs) and low temperature in a three-phase culture system. Bioresour Technol. 270**,** 504-511.

Smith, S., Witkowski, A., Joshi, A. K., 2003. Structural and functional organization of the animal fatty acid synthase. Prog Lipid Res. 42**,** 289-317.

Soong, Y. H. V., Liu, N., Yoon, S., Lawton, C., Xie, D. M., 2019. Cellular and metabolic engineering of oleaginous yeast *Yarrowia lipolytica* for bioconversion of hydrophobic substrates into high-value products. Eng Life Sci. 19**,** 423-443.

Steinrucken, P., Prestegard, S. K., de Vree, J. H., Storesund, J. E., Pree, B., Mjos, S. A., Erga, S. R., 2018. Comparing EPA production and fatty acid profiles of three *Phaeodactylum tricornutum* strains under western Norwegian climate conditions. Algal Res. 30**,** 11-22.

Sun, M. L., Madzak, C., Liu, H. H., Song, P., Ren, L. J., Huang, H., Ji, X. J., 2017. Engineering *Yarrowia lipolytica* for efficient gamma-linolenic acid production. Biochem Eng J. 117**,** 172-180.

Sun, T., Li, S. B., Song, X. Y., Pei, G. S., Diao, J. J., Cui, J. Y., Shi, M. L., Chen, L., Zhang, W. W., 2018a. Re-direction of carbon flux to key precursor malonyl-CoA via artificial small RNAs in photosynthetic *Synechocystis* sp. PCC 6803. Biotechnol Biofuels. 11.

Sun, X. M., Ren, L. J., Bi, Z. Q., Ji, X. J., Zhao, Q. Y., Jiang, L., Huang, H., 2018b. Development of a cooperative two-factor adaptive-evolution method to enhance lipid production and prevent lipid peroxidation in *Schizochytrium* sp. Biotechnol Biofuels. 11**,** 65.

Swanson, D., Block, R., Mousa, S. A., 2012. Omega-3 fatty acids EPA and DHA: health benefits throughout life. Adv Nutr. 3**,** 1-7.

Tai, M., Stephanopoulos, G., 2013. Engineering the push and pull of lipid biosynthesis in oleaginous yeast *Yarrowia lipolytica* for biofuel production. Metab Eng. 15**,** 1-9.

Tallima, H., El Ridi, R., 2018. Arachidonic acid: Physiological roles and potential health benefits - A review. J Adv Res. 11**,** 33-41.

Techtmann, S. M., Fitzgerald, K. S., Stelling, S. C., Joyner, D. C., Uttukar, S. M., Harris, A. P., Alshibli, N. K., Brown, S. D., Hazen, T. C., 2016. *Colwellia psychrerythraea* strains from distant deep sea basins show adaptation to local conditions. Front Env Sci-Switz. 4.

Theron, C. W., Vandermies, M., Telek, S., Steels, S., Fickers, P., 2020. Comprehensive comparison of *Yarrowia lipolytica* and *Pichia pastoris* for production of *Candida antarctica* lipase B. Sci Rep. 10**,** 1741.

Thorpe, R. F., Ratledge, C., 1972. Fatty-acid distribution in triglycerides of yeasts grown on glucose or alkanes. J Gen Microbiol. 72**,** 151-&.

Tian-Yuan, Z., Yin-Hu, W., Jing-Han, W., Xiao-Xiong, W., Deantes-Espinosa, V. M., Guo-Hua, D., Xin, T., Hong-Ying, H., 2019. Heterotrophic cultivation of microalgae in straw lignocellulose hydrolysate for production of high-value biomass rich in polyunsaturated fatty acids (PUFA). Chem Eng J. 367**,** 37-44.

Tocher, D. R., Betancor, M. B., Sprague, M., Olsen, R. E., Napier, J. A., 2019. Omega-3 long-chain polyunsaturated fatty acids, EPA and DHA: bridging the gap between supply and demand. Nutrients. 11.

USDA, USDA National Nutrient Database for Standard Reference, release 28. Agricultural Research, 2015.

Valenzuela, A., Nieto, M. S., 2001. Docosahexaenoic acid (DHA) in fetal development and in infant nutrition. Rev Med Chil. 129**,** 1203-11.

van Winden, W. A., Wittmann, C., Heinzle, E., Heijnen, J. J., 2002. Correcting mass isotopomer distributions for naturally occurring isotopes. Biotechnol Bioeng. 80**,** 477-9.

Vorapreeda, T., Thammarongtham, C., Cheevadhanarak, S., Laoteng, K., 2012. Alternative routes of acetyl-CoA synthesis identified by comparative genomic analysis: involvement in the lipid production of oleaginous yeast and fungi. Microbiology. 158**,** 217-228.

Wan, X., Peng, Y. F., Zhou, X. R., Gong, Y. M., Huang, F. H., Moncalian, G., 2016. Effect of cerulenin on fatty acid composition and gene expression pattern of DHA-producing strain *Colwellia psychrerythraea* strain 34H. Microb Cell Fact. 15**,** 30.

Wang, F., Bi, Y., Diao, J., Lv, M., Cui, J., Chen, L., Zhang, W., 2019a. Metabolic engineering to enhance biosynthesis of both docosahexaenoic acid and odd-chain fatty acids in *Schizochytrium* sp. S31. Biotechnol Biofuels. 12**,** 141.

Wang, K. F., Shi, T. Q., Lin, L., Wei, P., Ledesma-Amaro, R., Ji, X. J., 2022. Engineering *Yarrowia lipolytica* to produce tailored chain-length fatty acids and their derivatives. ACS Synth Biol. 11**,** 2564-2577.

Wang, Q., Han, W., Jin, W. B., Gao, S. H., Zhou, X., 2021. Docosahexaenoic acid production by *Schizochytrium* sp.: review and prospect. Food Biotechnol. 35**,** 111-135.

Wang, Z., Wang, D. H., Park, H. G., Tobias, H. J., Kothapalli, K. S. D., Brenna, J. T., 2019b. Structural Identification of Monounsaturated Branched Chain Fatty Acid Methyl Esters by Combination of Electron Ionization and Covalent Adduct Chemical Ionization Tandem Mass Spectrometry. Anal Chem. 91**,** 15147-15154.

Wang, Z. P., Xu, H. M., Wang, G. Y., Chi, Z., Chi, Z. M., 2013. Disruption of the *MIG1* gene enhances lipid biosynthesis in the oleaginous yeast *Yarrowia lipolytica* ACA-DC 50109. Bba-Mol Cell Biol L. 1831**,** 675-682.

Wasylenko, T. M., Ahn, W. S., Stephanopoulos, G., 2015. The oxidative pentose phosphate pathway is the primary source of NADPH for lipid overproduction from glucose in *Yarrowia lipolytica*. Metab Eng. 30**,** 27-39.

Wei, H., Wang, W., Knoshaug, E. P., Chen, X. W., Van Wychen, S., Bomble, Y. J., Himmel, M. E., Zhang, M., 2021. Disruption of the *Snf1* gene enhances cell growth and reduces the metabolic burden in cellulase-expressing and lipid-accumulating *Yarrowia lipolytica*. Front Microbiol. 12.

Wiktorowska-Owczarek, A., Berezinska, M., Nowak, J. Z., 2015. PUFAs: Structures, Metabolism and Functions. Adv Clin Exp Med. 24**,** 931-41.

Wittmann, C., 2007. Fluxome analysis using GC-MS. Microb Cell Fact. 6**,** 6.

Wittmann, C., Krömer, J. O., Kiefer, P., Binz, T., Heinzle, E., 2004. Impact of the cold shock phenomenon on quantification of intracellular metabolites in bacteria. Anal Biochem. 327**,** 135-9.

Woolfson, A. M. J., 1983. Amino acids - Their role as an energy-source. P Nutr Soc. 42**,** 489-495.

Workman, M., Holt, P., Thykaer, J., 2013. Comparing cellular performance of *Yarrowia lipolytica* during growth on glucose and glycerol in submerged cultivations. AMB Express. 3**,** 58.

Wu, W. J., Zhang, A. H., Peng, C., Ren, L. J., Song, P., Yu, Y. D., Huang, H., Ji, X. J., 2017. An efficient multi-stage fermentation strategy for the production of microbial oil rich in arachidonic acid in *Mortierella alpina*. Bioresour Bioprocess. 4**,** 8.

Xie, D., Miller, E., Sharpe, P., Jackson, E., Zhu, Q., 2017. Omega-3 production by fermentation of *Yarrowia lipolytica*: From fed-batch to continuous. Biotechnol Bioeng. 114**,** 798-812.

Xie, D. M., Jackson, E. N., Zhu, Q., 2015. Sustainable source of omega-3 eicosapentaenoic acid from metabolically engineered *Yarrowia lipolytica*: from fundamental research to commercial production. Appl Microbiol Biotechnol. 99**,** 1599-1610.

Xu, P., Qiao, K., Stephanopoulos, G., 2017a. Engineering oxidative stress defense pathways to build a robust lipid production platform in *Yarrowia lipolytica*. Biotechnol Bioeng. 114**,** 1521-1530.

Xu, P., Qiao, K. J., Stephanopoulos, G., 2017b. Engineering oxidative stress defense pathways to build a robust lipid production platform in *Yarrowia lipolytica*. Biotechnol Bioeng. 114**,** 1521-1530.

Xue, Z., Sharpe, P. L., Hong, S. P., Yadav, N. S., Xie, D., Short, D. R., Damude, H. G., Rupert, R. A., Seip, J. E., Wang, J., Pollak, D. W., Bostick, M. W., Bosak, M. D., Macool, D. J., Hollerbach, D. H., Zhang, H., Arcilla, D. M., Bledsoe, S. A., Croker, K., McCord, E. F., Tyreus, B. D., Jackson, E. N., Zhu, Q., 2013. Production of omega-3 eicosapentaenoic acid by metabolic engineering of *Yarrowia lipolytica*. Nature Biotechnology. 31**,** 734-40.

Yanai, H., Masui, Y., Katsuyama, H., Adachi, H., Kawaguchi, A., Hakoshima, M., Waragai, Y., Harigae, T., Sako, A., 2018. An improvement of cardiovascular risk factors by omega-3 polyunsaturated fatty acids. J Clin Med Res. 10**,** 281-289.

Yang, S. Z., Wei, D. Z., Mu, B. Z., 2007. Determination of the structure of the fatty acid chain in a cyclic lipopeptide using GC-MS. J Biochem Biophys Methods. 70**,** 519-23.

Yazawa, K., 1996. Production of eicosapentaenoic acid from marine bacteria. Lipids. 31 Suppl**,** S297-300.

Ye, C., Qiao, W. H., Yu, X. B., Ji, X. J., Huang, H., Collier, J. L., Liu, L. M., 2015. Reconstruction and analysis of the genome-scale metabolic model of *Schizochytrium limacinum* SR21 for docosahexaenoic acid production. BMC Genomics. 16.

Yoshida, K., Hashimoto, M., Hori, R., Adachi, T., Okuyama, H., Orikasa, Y., Nagamine, T., Shimizu, S., Ueno, A., Morita, N., 2016. Bacterial long-chain polyunsaturated fatty acids: Their biosynthetic genes, functions, and practical use. Mar Drugs. 14.

Yoshino, T., Kakunaka, N., Liang, Y., Ito, Y., Maeda, Y., Nomaguchi, T., Matsunaga, T., Tanaka, T., 2017. Production of omega-3 fatty acids in marine cyanobacterium *Synechococcus* sp. strain NKBG 15041c via genetic engineering. Appl Microbiol Biotechnol. 101**,** 6899-6905.

Yuzbasheva, E. Y., Agrimi, G., Yuzbashev, T. V., Scarcia, P., Vinogradova, E. B., Palmieri, L., Shutov, A. V., Kosikhina, I. M., Palmieri, F., Sineoky, S. P., 2019. The mitochondrial citrate carrier in *Yarrowia lipolytica*: Its identification, characterization and functional significance for the production of citric acid. Metab Eng. 54**,** 264-274.

Yuzbasheva, E. Y., Mostova, E. B., Andreeva, N. I., Yuzbashev, T. V., Laptev, I. A., Sobolevskaya, T. I., Sineoky, S. P., 2017. Co-expression of glucose-6-phosphate dehydrogenase and acyl-CoA binding protein enhances lipid accumulation in the yeast *Yarrowia lipolytica*. New Biotechnol. 39**,** 18-21.

Zarate, R., El Jaber-Vazdekis, N., Tejera, N., Perez, J. A., Rodriguez, C., 2017. Significance of long chain polyunsaturated fatty acids in human health. Clin Transl Med. 6**,** 25.

Zeng SY, Liu HH, Shi TQ, Song P, Ren LJ, Huang H, XJ, J., 2018. Recent advances in metabolic engineering of *Yarrowia lipolytica* for lipid overproduction. Eur J Lipid Sci Technol. 120**,** 1700352.

Zhang, H. Y., Zhang, L. N., Chen, H. Q., Chen, Y. Q., Ratledge, C., Song, Y. D., Chen, W., 2013. Regulatory properties of malic enzyme in the oleaginous yeast, Yarrowia lipolytica, and its non-involvement in lipid accumulation. Biotechnol Lett. 35**,** 2091-2098.

Zhang, S., He, Y., Sen, B., Chen, X., Xie, Y., Keasling, J. D., Wang, G., 2018. Alleviation of reactive oxygen species enhances PUFA accumulation in *Schizochytrium* sp. through regulating genes involved in lipid metabolism. Metab Eng Commun. 6**,** 39-48.

Zhang, T. T., Xu, J., Wang, Y. M., Xue, C. H., 2019. Health benefits of dietary marine DHA/EPA-enriched glycerophospholipids. Prog Lipid Res. 75**,** 100997.

Zhang, Y., Luan, X., Zhang, H., Garre, V., Song, Y., Ratledge, C., 2017. Improved gamma-linolenic acid production in *Mucor circinelloides* by homologous overexpressing of delta-12 and delta-6 desaturases. Microb Cell Fact. 16**,** 113.

Zhao, B., Li, Y., Li, C., Yang, H., Wang, W., 2018. Enhancement of *Schizochytrium* DHA synthesis by plasma mutagenesis aided with malonic acid and zeocin screening. Appl Microbiol Biotechnol. 102**,** 2351-2361.

Zhao, X., Qiu, X., 2018. Analysis of the biosynthetic process of fatty acids in *Thraustochytrium*. Biochimie. 144**,** 108-114.

Zhao, X. M., Qiu, X., 2019. Very long chain polyunsaturated fatty acids accumulated in triacylglycerol are channeled from phosphatidylcholine in *Thraustochytrium*. Front Microbiol. 10.

Zhu, B. H., Tu, C. C., Shi, H. P., Yang, G. P., Pan, K. H., 2017. Overexpression of endogenous delta-6 fatty acid desaturase gene enhances eicosapentaenoic acid accumulation in *Phaeodactylum tricornutum*. Process Biochem. 57**,** 43-49.

Zhuang, P., Wang, W., Wang, J., Zhang, Y., Jiao, J., 2019. Polyunsaturated fatty acids intake, omega-6/omega-3 ratio and mortality: Findings from two independent nationwide cohorts. Clin Nutr. 38**,** 848-855.